Zebrafish Mutagenesis Study of Host Determinants of Mycobacterial Infection Outcome

Constantinos Alexandros Televantos

Clare College

December 2019

This thesis is submitted for the degree of Doctor of Philosophy

This thesis is the result of my own work and includes nothing which is the outcome of work done in collaboration except as declared in the Preface and specified in the text. It is not substantially the same as any that I have submitted, or, is being concurrently submitted for a degree or diploma or other qualification at the University of Cambridge or any other University or similar institution except as declared in the Preface and specified in the text. I further state that no substantial part of my thesis has already been submitted, or, is being concurrently submitted for any such degree, diploma or other qualification at the University of Cambridge or any other University or similar institution except as declared in the Preface and specified in the text. It does not exceed the prescribed word limit for the relevant Degree Committee.

Name: Constantinos Televantos

Thesis Title: Zebrafish Mutagenesis Study of Host Determinants of Mycobacterial Infection Outcome

Summary

This thesis describes a large-scale forward genetic screen in zebrafish for host determinants of mycobacterial infection outcome that I participated in. Zebrafish larvae from families randomly mutagenized with N-ethyl-N-nitrosourea were infected with *Mycobacterium marinum* and monitored over time. Larvae with increased susceptibility to infection were identified by the presence of mycobacterial cording, a phenotypic proxy for failure of immunity. 279 unrelated families have so far been screened with isolation of phenotypic larvae from 31 families. Genetic mapping has been carried out on phenotype sorted larvae from 5 families to identify genomic regions harbouring causative mutations. Positional cloning has been completed on one such mutant, *Guaguancó* which was found to map to a nonsense mutation in the gene *ubiquitously expressed transcript (uxt),* a poorly characterised gene not previously associated with anti-mycobacterial immunity. Subsequent cellular characterisation demonstrated that *uxt* mutants manifest a normal immune response in the early stages of infection, but then show accelerated macrophage death resulting in granuloma failure. Pharmacological inhibition of cell death pathways associated with mycobacterial infection did not influence *uxt* mutant susceptibility to infection, suggesting that *uxt* deficiency results in a novel form of death in mycobacterium-infected macrophages.

Preface

The forward genetic screen described in this study was a collaborative effort with aspects performed by several individuals:

My contribution to forward genetic screen involved infecting and screening larvae from 115 mutant families. Additionally, I isolated 12 phenotypic families, 9 of which were had mutant phenotypes confirmed in a subsequent generation (*Kalamatianos, Carpaea, Syrtos, Sirtaki, Hasapiko, Antichristos, Kartzilamas, Morris* and *Zeibekiko*)

Antonio Pagán (Research Associate): Initial identification of *Guaguancó*, *Montuno, Yambu*, *Pachanga*, and *Guajira* mutant families in addition to screening of 161 mutant families.

Richard White (Research Associate): Application of MMAPPR analysis pipeline on exome sequencing data to generate initial mapping intervals

Ian Sealy (Research Associate): RNA-seq analysis to generate DeSeq2 lists

Neha Wali (Research Technician): Nucleic acid extraction and genotyping for RNA-seq and exome sequencing.

Ione Smallwood (Research Technician): Screening and genotyping mutant families under supervision.

Bingnan Liu (PhD Student): Fine mapping of *Kalamatianos* mutant family under supervision

Benno Simmons (Post-Doctoral Fellow): Assistance in producing volcano plots of RNA-seq data

Acknowledgements

As well as thanking everyone mentioned in the preface who contributed to this study, I would I would like to thank the following people for their help and guidance during my PhD. Firstly, I would like to thank my supervisor Lalita Ramakrishnan for not only her scientific supervision but for her unerring kindness and understanding throughout the PhD. I would also like to thank Elisabeth Busch-Nentwich for her continuous support and guidance on the genetic mapping.

I would like to thank Antonio Pagán, who taught me most of what I know about zebrafish and was always willing to offer guidance and listen to my (often stupid) questions whether at 2pm on a Tuesday or 10pm on a Saturday. I would also like to thank Francisco Roca for his guidance on cell death.

I would also like to acknowledge the tireless efforts of the aquarium staff especially Nicola Goodwin and Rosie Keeble for their support and enabling all the zebrafish work described in this manuscript to be possible. Lastly, I would like to thank Jon Shanahan, Morwan Osman and the Clarevid-19 group.

Contents

Chapter 1

Introduction to Tuberculosis

1.1 A brief history of tuberculosis

Tuberculosis is a disease caused by infection with bacteria in the *Mycobacterium tuberculosis* complex, principally *Mycobacterium tuberculosis*[1]. Tuberculosis is most commonly a respiratory disease, though can affect any part of the body[1]. Tuberculosis can present with a wide variety of symptoms, but is commonly associated with pyrexia, weight loss, pallor as well as respiratory symptoms such as persistent cough and haemoptysis[1,2]. Tuberculosis infection is associated with significant morbidity and has an estimated mortality of 70% if left untreated[3] .

Tuberculosis is an ancient disease with archaeological evidence of the sequelae of infection found in skeletons dating to the Neolithic era[4]. Detailed accounts from the physicians of Classical Greece describe the symptoms of tuberculosis which they recognised as a distinct pathological entity they termed '*phthisis*', meaning 'to waste away', in reference to the often profound weight loss seen in tuberculosis patients[5,6]. By the end of the 18th century rapid urbanisation leading to increasingly cramped, unsanitary conditions potentiated a tuberculosis epidemic in Europe[7] in which around a quarter of deaths in urban areas were attributed to tuberculosis [8,9], then known as 'the great white plague' or the 'white death'[10]. Despite a plethora of proposed interventions throughout history from a monarch's touch to sea voyages, there was a dearth of effective tuberculosis interventions until the mid 19th century when sanitoria were introduced, which served to isolate and provide adequate nutrition to tuberculosis patients [7,11]. In 1882, the discovery of the bacterium *Mycobacterium tuberculosis* as the cause of tuberculosis by Robert Koch represented a major breakthrough in understanding the diesease[12].

This facilitated the production of the anti-tuberculosis Bacille Calmette–Guérin vaccine (BCG), developed by the repeated passage of *Mycobacterium bovis* in vitro, leading to a loss of virulence[13,14]. This was followed by the discovery of streptomycin, the first antibiotic cure for tuberculosis[15]. The combination of chemotherapy, improved diagnosis and public health measures served to greatly reduce the burden of tuberculosis during the 20th century[16]. In spite of this, tuberculosis remains the leading infectious cause of death and one of the top ten causes of death globally, causing approximately 1.7 million deaths per year [17].

Even in uncomplicated cases of tuberculosis, clinical management is complex and the most widely used treatment regimen requires treatment with a combination of four antibiotics (typically rifampicin, isoniazid, pyrazinamide and ethambutol) for six months to eradicate the disease[1], with shorter treatment times associated with temporary improvement followed by relapse[18]. Whilst current antibiotic regimens are generally effective when followed, poor compliance can result in relapse and has precipitated the emergence of drug resistant strains of *M. tuberculosis* [1,19,20]. Drug resistant tuberculosis represents a burgeoning epidemic with around 558,000 cases of rifampicin resistant tuberculosis (RR TB) annually[17]. 82% of RR TB cases also showed resistance to isoniazid, termed 'multi-drug resistant tuberculosis' (MDR TB) and 8.5% of MDR TB also showed resistance to a second line antibiotic, termed 'extensively drug-resistant tuberculosis' (XDR-TB)[17]. Drug resistant strains of tuberculosis show poor treatment outcomes with only 55% of MDR and 34% of XDR cases managed successfully, relative to 82% across all tuberculosis cases[17,21]. Importantly, XDR and MDR TB remains transmissible [22].

A major reason for the persistence of tuberculosis is the limited efficacy of the BCG vaccine and lack of an alternative vaccination[17]. Although BCG vaccination protects against extra-pulmonary tuberculosis in children, it's efficacy is limited against pulmonary tuberculosis in adults[23], which accounts for the majority of global tuberculosis burden and transmission[17]

In summary, tuberculosis has proven a recalcitrant foe of humanity causing disease throughout human history. Although modern clinical interventions have meant that tuberculosis is no longer the great white plague it once was, it remains a major cause of morbidity and mortality.

1.2 Tuberculosis pathogenesis

Tuberculosis typically occurs following the inhalation of aerosolised *M. tuberculosis* coughed by an individual with active diesease[1]. Unlike many other pathogens *M. tuberculosis* optimally transmits via small droplets containing 1-3 bacteria[24,25]. Larger droplets show less infectivity due to deposition in the upper respiratory tract wherein mycobacteria are susceptible to destruction by the vast cohort of microbiota primed macrophages activated via toll-like receptor (TLR) ligation[25]. TLR stimulation of macrophages is thought to potentiate mycobacterial killing through the induction antimicrobial effector pathways including the inducible nitric oxide synthase (iNOS) pathway and production of the antimicrobial peptide cathelicidin following vitamin D receptor signalling[26,27].

The carriage of mycobacteria within small droplets allows the defences of the upper respiratory tract to be circumvented and permits deposition of mycobacteria in the relatively commensal free pulmonary alveoli[25,28]. Within the alveoli, mycobacteria

do not have to contend with microbiota primed macrophages and circumvent de novo TLR ligation through masking of exposed pathogen associated molecular patterns (PAMPs) with surface phthiocerol dimycocerosate lipid[25,29]. This early modulation of innate immunity mediated by mycobacteria is not restricted to macrophages, as virulent mycobacteria are also able to stymie neutrophil recruitment early in infection by inducing the production of anti-inflammatory lipoxins in infected macrophages [S.Candel, unpublished results].

In spite of their picaresque infiltration, invading mycobacteria still encounter microbicidal tissue resident alveolar macrophages which readily engulf mycobacteria following infection[30]. To avoid destruction within alveolar macrophages mycobacteria orchestrate their escape through recruitment of growth permissive monocytes to which they are able to transfer in a process driven by mycobacterial surface phenolic glycolipid and host STING induced CCL2 production[29,30]. Within macrophages virulent mycobacteria adopt a variety of strategies to survive and replicate. Following phagocytosis, mycobacteria are able to both avoid phagosome-lysosome fusion through the secretion of serine/threonine protein kinase G as well as survive within acidified compartments through the expression of the acid tolerance factor MarP[31,32].

Taken together these measures allow *M. tuberculosis* to masterfully evade or modulate initial host defences from the early stages of infection, this culminates in the transport of viable mycobacteria within growth permissive monocytes from the alveoli across the epithelial barrier into the deeper lung parenchyma[33]. Within the parenchyma additional macrophages are recruited to the site of infection (further discussed in Chapter 1.5) followed by other leucocytes which aggregate to form an

organised structure known as a granuloma, the pathognomonic structure of tuberculosis infection[34,35].

Within the first three weeks following infection mycobacterial growth is rapid before slowing with the onset of adaptive immunity, potentially resulting in eradication of infection with subsequent calcification of the lesion[33]. As *M. tuberculosis* is primarily intracellular during its life cycle, adaptive immune control of tuberculosis relies on cell mediated immunity[35]. Interleukin-12 (IL-12) produced by macrophages and dendritic cells following phagocytosis of mycobacteria drive development of Th1 CD4+ T cells which in turn produce IFN-γ[35]. IFN-γ synergises with tumour necrosis factor (TNF) produced by macrophages, dendritic cells and T cells to enhance macrophage microbicidal capacity through activation of IFN-γ inducible GTPases, vitamin D receptor signalling and iNOS[35].

Adaptive immunity is not always able to eradicate infection and virulent mycobacteria adopt several approaches to minimise the impact of adaptive immunity. Firstly, tuberculosis shows delayed initiation of adaptive immunity relative to other bacterial infections allowing for a prolonged period of rapid bacterial growth, this is attributed to delayed arrival of antigen-presenting dendritic cells in local lymph nodes[36,37] .Delayed dendritic cell arrival in lymph nodes may be a consequence of reduced chemotaxis and altered expression of adhesion molecules following mycobacterial infection[38]. In addition to stalling adaptive immunity, *M. tuberculosis* is able to reduce the efficacy of adaptive immunity by inhibiting macrophage responsiveness to IFN-γ. This process is mediated through several independent mechanisms involving mycobacterial lipoproteins, peptidoglycans and TLR2 ligation, resulting in reduced expression of IFN-γ target genes[39,40].

In instances where immune control has failed to eradicate infection, transmission to a new host can occur when *M. tuberculosis* accesses airways[25]. While virulent mycobacteria spend much of their life within macrophages, in order to become extracellular, virulent mycobacteria trigger necrosis of infected macrophages leading to granuloma failure[25]. Necrotic regions then erode into the airways permitting aerosol transmission to a new host[25,41].

1.3 Tuberculosis Risk Factors

While tuberculosis is a prevalent illness, the majority of individuals exposed to *M. tuberculosis* do not go on to develop active infection[42,43]. The study of tuberculosis risk factors has been ongoing since the 19th century and has led to the identification of a plethora of risk factors. There is an uneven global distribution of tuberculosis with 30 low- and middle-income countries accounting for 87% of global cases of tuberculosis[44]. It is estimated that expansion of social protection and eradication of extreme poverty would reduce global tuberculosis by 84.3%[45]. The high rates of tuberculosis in developing countries is attributed to several risk factors, primarily: unsanitary living conditions, malnutrition and HIV infection compounded by limited access to healthcare[44,46,47]

HIV infection is the strongest known risk factor for tuberculosis infection and is associated with a 20-fold increased risk[1,44]. Tuberculosis infection in HIV patients often runs a severe course and represents a major cause of hospitalisation and mortality. Other forms of acquired immunodeficiency are also associated with increased risk of tuberculosis including iatrogenic factors. In particular, anti-TNF

therapy such as infliximab and adalimumab is associated with an 2-fold risk of tuberculosis[48].

In addition to environmental and acquired risk factors, there is an increasing understanding of the role of host intrinsic factors in tuberculosis acquisition and outcome. An early indication of this came following the Lübeck disaster in 1930, in which 251 neonates were mistakenly administered virulent *Mycobacterium tuberculosis* via contaminated BCG vaccinations[49]. While mortality following administration was high, there was considerable variation in clinical outcomes across individuals receiving a similar infectious dose, suggesting host intrinsic variation can influence infection outcome[49]. The importance of host intrinsic factors in tuberculosis has been further supported by twin studies which show that 66.*7%* of monozygotic twin siblings develop tuberculosis following infection of an index sibling, as opposed to 23% for dizygotic twins[50,51].

Primary immunodeficiencies are a diverse group of heritable conditions caused by disruptive mutations in genes required for immunity. While there are a large number of primary immunodeficiencies, each is individually rare and are generally associated with a spectrum of susceptibility to pathogens which can include mycobacteria. Severe combined immunodeficiency syndrome (SCID) is an umbrella term for a group of primary immunodeficiencies characterized by a profound deficiency of adaptive immunity[52,53]. SCID can be caused by mutations in a variety of genes, but is mostly commonly associated with mutations in interleukin 2 receptor subunit gamma[53]. SCID patients are predisposed to severe recurrent infection with a broad range of pathogens[53] and can develop a potentially fatal systemic infection with the normally avirulent BCG strain of *M. Bovis* following vaccination, known as 'BCGosis'[54]. Chronic granulomatous disease is a disorder of phagocytic function which is caused by mutations in genes required for nicotinamide

dinucleotide phosphate oxidase enzyme complex (NADPH)[55] function. NADPH is required for the generation of microbicidal reactive oxygen species and disruption of this complex results in an inability of phagocytes to restrict ingested pathogens[55]. Patients with chronic granulomatous disease suffer from recurrent fungal and bacterial infections, including mycobacteria and may also present BCGosis[55–57].

While primary immunodeficiencies such as SCID and chronic granulomatous disease lead increased risk of mycobacterial infection, they are also associated with susceptibility to many other pathogens. In contrast, individuals with apparently normal immunity may present with BCGosis or severe infection due to normally avirulent environmental mycobacteria[58]. This syndrome of narrow susceptibility to mycobacteria is known as mendelian susceptibility to mycobacterial disease (MSMD)[58]. MSMD is a rare condition with only 501 known cases which typically cluster in consanguineous families[59]. Although in many cases of MSMD the genetic cause is unknown, genetic linkage analysis has identified causative mutations in 11 different genes all of which are associated with the IL-12-IFN-γ immune circuit[59,60].

The majority of insights regarding host genetic contribution to tuberculosis acquisition and outcome have been derived from genetic studies in model organisms and patients with primary immunodeficiencies. More recently, the availability of genotyping arrays has facilitated genome wide association studies (GWAS) focusing on identification of genetic determinants of tuberculosis acquisition. One such GWAS identified an association between variants in the gene ArfGAP with SH3 domain, ankyrin repeat and PH domain 1 (ASAP1) and occurrence of pulmonary tuberculosis[61]. Subsequent molecular characterization demonstrated that ASAP1 was downregulated in dendritic cells following

infection with *M. tuberculosis* and depletion of ASAP1 was associated with reduced dendritic cell migration in vitro[61].

In total, 18 GWAS studies have isolated 101 variants associated with tuberculosis however the clinical and molecular relevance of the vast majority of these variants has yet to be determined[62,63]. Additionally, many variants identified in tuberculosis GWAS studies have a low effect size and show a lack of replication across studies[43]. For example ASAP1 variants were initially found to be associated with tuberculosis acquisition in a Russian cohort, but were not found to be predictive in other populations[61,64,65]. Additionally, GWAS studies have generally failed to identify variants in genes and pathways previously known to confer risk to tuberculosis[43]. However, analysis combining results from several GWAS cohorts was able to identify variants in genes associated with immunity against tuberculosis, including in interferon-gamma receptor 2 and macrophage receptor with collagenous structure (MARCO) suggesting that published studies may be underpowered[66]. Alternatively, the lack of reproducibility and low effect size of identified variants may indicate that common variants have limited impact on tuberculosis acquisition. There is an increasing appreciation that large numbers of individually uncommon genetic variants can underpin susceptibility to complex phenotypes, which would be unlikely to be captured by a GWAS study[67]. It is possible this is also the case for tuberculosis acquisition, with the variants causing MSMD representing extreme examples within a broader spectrum of genetic susceptibility defined by a constellation of rare alleles.

1.4 Models of tuberculosis infection

While the study of primary immunodeficiencies has provided insights into host genetic determinants of tuberculosis pathology, the study of complex diseases in human populations is inherently difficult. To address this several laboratory models of tuberculosis infection have been developed. The simplest biological models have used cultured macrophages infected with *M. tuberculosis* to identify novel therapeutic targets[68,69]. Clinical application of such in vitro studies can be limited as isolated infected macrophages do not capture the complex interplay across various leucocyte populations and mycobacteria within tuberculous granulomata[70]. In order to gain insight into the pathophysiology of tuberculosis as well as to validate findings identified by other approaches, animal models which mirror human tuberculosis infection have been extensively utilized[70,71].

Many animal studies use infected guinea pigs with *M. tuberculosis* which results in rapidly fatal infection with the development of necrotic granulomata[72]. Guinea pig studies have provided insights into the immune impact of tuberculosis infection[72] and have also been used to study infection transmission[73]. Additionally, a guinea pig infection study performed in 1928 comparing susceptibility of different inbred families provided an early indication of the importance of host intrinsic factors in mycobacterial infection outcome[74]. Rabbits have also historically been used to study tuberculosis and like guinea pigs, show a high level of susceptibility to infection but also develop cavitating lung lesions mirroring human infection[71]. Non-hominid catarrhines are also used to study tuberculosis due to their genetic and physiological similarity to humans[75]. Studies primarily use *Macaca fascicularis* or *Macaca mulatta* both of which mirror human tuberculosis clinical manifestations and natural history[75,76]. Catarrhine models share similar responses to drugs and immunological agents to humans and have been utilized in vaccination development and drug testing[71,75].

While guinea pig, rabbit and catarrhine models have proven a useful models of tuberculosis infection, their use has been restricted by a dearth of immunological and genetic tools in addition to handling difficulties[77,78]. The ease of handling and the wide repertoire of genetic and immunological tools has led to the mouse becoming the most widely used in vivo model of tuberculosis infection[79].

The murine immune response to tuberculosis has been carefully documented and has provided several fundamental insights into tuberculosis pathogenesis. The usage of genetic knockout mice and neutralizing antibodies has demonstrated the importance of the inflammatory cytokines TNF, IL-12 and IFN-γ in immunity against tuberculosis, deficiency of which causes increased infection susceptibility[76,80–83]. The increased susceptibility to tuberculosis conferred by CD4 or MHC Class II deficiency in mice highlighted the importance of CD4+ T cells in mycobacterial immunity provided a cellular basis for the increased risk and poor prognosis of HIV patients with tuberculosis[76,84]. As well as the insights gleaned from candidate-based studies, forward genetic studies on inbred mice have led to the identification and characterization of the host susceptibility factors Irf8 and Nramp1, both of which have been shown to be clinically relevant (reviewed in Chapter 2.8). Lastly, infection of mice with *M. tuberculosis* via low dose aerosols using exposure chambers is reproducible and relatively straightforward facilitating the widespread adoption of mice in the development of antibiotic therapy and vaccinations[71,76].

While studies in mice have provided fundamental insights into tuberculosis pathogenesis and management, the murine model has several limitations. Mice are not natural hosts of *M. tuberculosis* and shows significant differences in pathology relative to human infection[79]. The majority of commonly used laboratory mouse strains are resistant to tuberculosis and can tolerate relatively large pulmonary bacterial burdens without signs

of illness[76,79]. Furthermore, although *M. tuberculosis* infection of mice results in the formation of granulomata there are significant differences in granuloma architecture and progression relative to humans and other mammalian models[71,76,79]. Granulomata in humans are highly organized structures and active infection results in granulomata with varying degrees of necrosis, fibrosis and calcification[33,76]. Infection in the majority of laboratory mouse strains results in the development of relatively homogenous, loosely organized, non-necrotic granulomata[71,76,79]. The inability of the majority of mouse strains to mirror this aspect of tuberculosis pathogenesis has partially been addressed through the usage of C3HeB/FeJ mice have been found to more closely mirror human disease progression with the formation of necrotic granulomas [70,85,86]

1.5 The zebrafish- *Mycobacterium marinum* model of tuberculosis

Mycobacterium marinum is a virulent mycobacterium which is closely related to the *M. tuberculosis* complex[87]. *M. marinum* infection typically occurs in aquatic animals but it can also infect humans in which it produces a disease known as 'fish tank granuloma', a peripheral granulomatous lesion that histologically resembles dermal tuberculosis[88]. *M. marinum* is a natural pathogen of the zebrafish, in which it causes systemic progressive disease with the formation of organised necrotic granulomas, mirroring human tuberculosis[89,90].

Zebrafish larvae are optically transparent for the first three weeks of life and possess functional macrophages and neutrophils but have yet to develop adaptive immunity[91–93]. Whilst adaptive immunity is important in the control of both *M. tuberculosis* in humans and *M. marinum* in adult zebrafish[90], the initial immune response and granuloma formation are governed by innate immune mechanisms which can be studied in the zebrafish larvae[91].

Zebrafish are amenable to transgenesis and have a selection of reporter lines available, including macrophage and neutrophil fluorescent reporter lines[94,95]. Usage of leucocyte reporter lines infected with fluorescently labelled *M. marinum* allows for real-time, non-invasive imaging of infection development and immunity[96]. Importantly, both the zebrafish and *M. marinum* are genetically tractable which allows for manipulation of both host and bacterial determinants of infection outcome[97]. The small size and ease of handling of zebrafish larvae means husbandry can be conducted on infected larvae arrayed in multi-well plates permitting serial high throughput quantitative and qualitative assessment of infection progression[96]. Using this approach, the zebrafish-*M. marinum* infection model can be utilised as a drug-screening platform[98,99] or in forward genetic studies, which has led to the identification of novel host determinants of infection outcome as described in Chapter 2.9 [100].

The zebrafish-*M. marinum* infection model has provided fundamental insights into the early interactions between host and mycobacterium. Fate tracking studies in the zebrafish have demonstrated the means through which mycobacteria manipulate host defences early in infection to establish a growth niche within growth permissive monocytes (as discussed in Chapter 1.2) [29,30]. The zebrafish has also provided insights into the role of the granuloma during the course of infection. Historically the granuloma was considered to be a solely host protective structure, serving a prison to incarcerate invading mycobacteria however studies in the zebrafish have challenged this view [33,101]. Infection of zebrafish with mycobacteria lacking the region of difference 1 (RD1) virulence locus results in attenuated infection with impaired granuloma formation and reduced bacterial burden, despite normal growth of

mycobacteria within individual infected macrophages[102]. The RD1 locus encompasses components of the type VII secretion system ESX-1, which mediates secretion of a variety of mycobacterial effector proteins[103]. Further investigation found that ESX-1 dependent secretion of the mycobacterial protein ESAT-6 induces expression of the inflammatory matrix metalloprotease MMP9 in adjacent epithelial cells leading to recruitment of additional uninfected macrophages driving granuloma expansion[104].

Detailed studies tracking macrophages in infected zebrafish found that the ESX-1 system also promotes apoptosis of infected macrophages[105]. Kinetic analysis demonstrated that multiple newly recruited, uninfected macrophages phagocytose the contents from a single apoptotic macrophage expanding the mycobacterial intracellular growth niche[105] compounded by egress of infected macrophages leading to the establishment of multiple foci of infection[106]. Taken together the zebrafish has illuminated a model of the granuloma as a dynamic exploited structure, wherein cycles of macrophage apoptosis and recruitment instigated by mycobacterial virulence determinants, drive granuloma formation and facilitate mycobacterial expansion.

Despite the unique advantages offered by the zebrafish-*M. marinum* model it possesses several limitations. The mechanism of transmission of *M. marinum* between fish is not well understood but may occur following consumption of dead infected fish or skin contact with an infected individual[107]. This is considerably different to the aerosol transmission of *M. tuberculosis* between the lungs of humans and limits the study of disease transmission in zebrafish.

While the transparency of zebrafish larvae uniquely allows observation of the early stages of tuberculosis pathogenesis in vivo, adaptive immunity takes several weeks to develop by which time zebrafish are opaque[97]. Additionally, while low levels of IFN-γ can be detected as early as 4dpf (presumably produced by innate immune cells such as natural killer cells), depletion does not appear to influence infection susceptibility in 7dpf larvae, suggesting that the IL-12/IFN-γ circuit is not operant at this developmental staget[31]. Consequently, while a range of defects in the IL-12/IFN-γ circuit have been found to confer increased susceptibility to tuberculosis in humans, this pathway would be difficult to further characterize in zebrafish larvae. While adult fish could be potentially be used to study these mechanisms, their lack of transparency abrogates a major strength of the model and largely limits the zebrafish to the study of innate immunity. However, although adaptive immunity plays an important role in control of tuberculosis its effects are largely exerted via activation of macrophages which remain a key effector cell throughout infection and are operant early in zebrafish embryonic development[33,35].

Although a significant number of transgenic lines have been developed to label specific leucocyte subsets including macrophages and neutrophils, there is a lack of effective anti-zebrafish antibodies which complicates the identification and characterisation of additional leucocyte subpopulations[108]. This has started to be addressed through transcriptional profiling-based approaches, which have been used to identify a population of innate lymphoid cells in the zebrafish[109]

While there is an established zebrafish mutant library containing null alleles for the majority of coding genes and recently developed techniques for rapidly generating and screening knockout animals, zebrafish lack established techniques to

generate conditional mutants[110,111]. Although it is still possible to study some embryonic lethal alleles in zebrafish larvae due to the presence of maternally derived RNA in animals with global knockouts, this is gene dependent and time limited. Furthermore, performing loss of function studies solely in animals with a global knockout of a given gene raises the question as to whether observed phenotypes are autonomous to a given cell population of interest. There are however alternative approaches and recently developed techniques available in zebrafish which can be used to address these issues. One such technique that has become established in zebrafish is the generation of parabiotic zebrafish through the fusion of genetically labelled blastulae resulting in partially fused embryos with shared circulation[112]. This technique can be used to assess the phenotype of circulating leucocytes with a given genetic manipulation in the context of a wildtype animal and vice versa but is technically demanding and perturbs normal embryogenesis[112,113].

Alternatively, the amenity of zebrafish to transgenesis combined with the CRISPR/cas9 system can be leveraged to generate animals with tissue specific knockouts although these approaches have not yet been widely utilised. For instance, CRISPR/cas9 mediated homology directed repair can be used to insert loxP sites flanking an exon within a target gene, in conjunction with transgenesis to engineer zebrafish expressing the Cre recombinase in a tissue specific manner[114]. Cre excises loxp flanked DNA in cells in which it is expressed, disrupting gene function and mirroring an approach widely used in mouse genetic studies[115]. Additionally, this approach has also be used with pharmacologically inducible Cre permitting temporally regulated gene disruption[114]. However, this approach currently

suffers from low efficiency, and is time consuming as it requires genetic manipulations across multiple generations[114].

An alternate approach involves generating transgenic zebrafish expressing cas9 on a tissue specific promoter, in addition to a guide RNA specific for the gene to be disrupted[116]. This results in cas9 mediated DNA cleavage at a specified locus within a cell population of interested followed by error-prone repair, typically resulting in insertions or deletions[116]. While this approach can be used to generate tissue specific knockouts, genetic mosaicism is inevitable and as not all DNA cleavage events will yield null alleles, may result in a milder phenotype relative to that in a straightforward knockout animal[116].

Chapter 2

Introduction to Forward Genetic Studies

2.1 Overview

Forward genetic studies performed in patients with primary immunodeficiencies and animal models of tuberculosis have been instrumental in understanding tuberculosis pathophysiology[43,100,117]. These efforts have been continued in this study, with the initiation of a forward genetic screen conducted in zebrafish larvae to identify host determinants of mycobacterial infection outcome. Here, the forward genetic approach is discussed focusing on techniques applicable to the zebrafish, followed by a review of insights gleaned from forward genetic studies with an emphasis on those regarding tuberculosis.

2.2 Forward vs Reverse Genetics

'Forward' and 'reverse' genetics are the two contrasting approaches used for characterizing gene function. Reverse genetics involves the targeted disruption of a gene of interest, followed by characterization of the resulting phenotype. In contrast, forward genetic studies seek to determine the genetic basis of a known phenotype relevant to a process of interest. Forward genetics is an unbiased approach, unburdened by pre-existing assumptions of a given process. Forward genetic studies can demonstrate the importance of novel genes and are particularly applicable to the study of poorly characterized processes. However, this lack of bias can be detrimental and result in genes already known to be important in a particular process being reidentified following the laborious processes of genetic mapping. In contrast to forward genetics, reverse genetics is a hypothesis driven approach which utilizes pre-existing knowledge to investigate a biological process. Reverse genetic approaches are suited to the molecular dissection of a processes with known genetic determinants, in addition to investigation of genes and their homologs known to be relevant in related processes. However, as reverse genetic approaches are fundamentally biased by pre-existing knowledge and assumptions, they are less likely to

facilitate completely novel discoveries relative to forward genetics. While conceptually opposing, forward and reverse genetic approaches are complementary. The identification of a novel gene or pathway in a forward genetic study facilitates reverse genetic studies which in turn provide mechanistic detail to further elucidate a biological process.

2.3 The Forward Genetic Approach

Although forward genetic approaches can be used to study spontaneous phenotypes in naturally occurring populations, in laboratory studies genetic diversity is typically induced through mutagenesis. Forward genetic studies in intentionally mutagenized populations are known as mutagenesis screens. In order to generate heritable genetic lesions, several approaches can be adopted. Historically, high energy radiation such as γ-radiation has been used, but this often leads to gross chromosomal abnormalities which can complicate genetic mapping[118]. Chemical mutagenesis studies typically use alkylating agents such as N-ethyl-N-nitrosourea (ENU) and Ethyl methanesulfonate (EMS) to induce point mutations throughout the genome[118,119]. Mutagenized populations are then screened to isolate induced phenotypes, which can then be linked to an induced mutation within a single gene following genetic mapping. Chemical mutagenesis is a reliable, straightforward means of generating high mutagenic loads and has been applied to a variety of model organisms and is the most widely used approach in zebrafish studies[118]. Insertional mutagenesis is another mutagenesis approach which involves the integration of DNA from exogenous transposons or viruses into the genome[119]. This can potentially disrupt gene function by insertion of the exogenous sequence into a gene or its regulatory sequences. In the zebrafish insertional mutagenesis is achieved through the injection of pseudotyped murine retroviruses into embryos[120–122]. However this approach is considerably less efficient than chemical

mutagenesis, thus may require additional screening to identify phenotypic individuals[121,122]. The major advantage of insertional mutagenesis is that disrupted genes can be rapidly identified simply through sequencing of DNA flanking retroviral insertion sites[118,120,122].

2.4 Mutant Mapping

Regardless of the process being studied, forward genetic studies typically follow the same stages. Firstly, a phenotype indicative of variation in the biological process being studied is identified. Subsequently, screening of a genetically diverse population is carried out with isolation of phenotypic individuals. To identify a causative mutation, genetic mapping is performed to define the genomic region harboring the mutation, followed by targeted investigation of genes within the region.

Mapping causative mutations is often the most challenging aspect of forward genetic studies. Typically, the first stage of mapping involves the identification of a genomic region harboring the causative mutation known as the 'mapping interval'. There are several approaches used to define a mapping interval, all of which rely on the principle of genetic linkage; phenotypic animals will show infrequent recombination between the causative mutation and adjacent genetic markers, whereas these same markers will segregate randomly in related non-phenotypic organisms[123].

Bulked segregant analysis (BSA) is an established mapping approach that involves genotyping pooled DNA from phenotype sorted organisms for a panel of known polymorphic markers[124]. This provides a qualitative indication of the degree of linkage between a given genetic marker and mutation[124]. In zebrafish, BSA is generally performed by genotyping for a defined panel of sequence length polymorphisms or microsatellite repeat regions[125,126]. BSA is an effective approach but is labor intensive as each marker

must be tested individually and resolution is limited by the availability of markers in the genomic region harboring the causative mutation.

The availability of genome assemblies with annotated common single-nucleotide polymorphisms (SNPs) has led to the development of SNP based mapping. This involves genotyping a phenotypic mutant population to assess linkage with a panel of defined SNPs[127]. As there are a high density of SNPs throughout the genome, this approach can offer high resolution mapping and can be expedited through the use of SNP genotyping microarrays[128,129].

Usage of next generation sequencing (typically exome sequencing, whole genome sequencing, or RNA sequencing) in forward genetic studies allows for concurrent identification and linkage analysis of genetic markers in phenotypic organisms to generate a mapping interval, this is known as 'mapping by sequencing' (MBS)[123,130]. There are several different approaches for MBS which differ by the type of next generation sequencing used as well as the analysis principle used to define the initial mapping interval. Many approaches define a mapping interval by comparison of allele frequency at polymorphic loci between phenotypic and non-phenotypic organisms[123]. Alternatively, when mapping recessive traits, a mapping interval may be defined by identifying genomic regions with extended homozygosity in phenotypic organisms[123,131]. As next generation sequencing data can be used to generate a de novo genome assembly, unlike other approaches MBS can be applied to organisms without prior knowledge of genetic background[123,132]. MBS represents a rapid and effective mapping approach and with the decreasing cost and increasing availability of next generation sequencing has seen increasing adoption in forward genetic studies[131].

2.5 Mutant Identification

The eventual aim of forward genetic studies is to identify the disrupted gene responsible for a given phenotype. In cases where insertional mutagenesis or MBS has been adopted, genes with disruptive mutations can be directly identified and investigated. Where there is a dearth of compelling candidates following MBS or when other mapping approaches have been used, all genes within a mapping interval can be considered candidates and prioritized for investigation according to known biological function and degree of genetic linkage to a phenotype.

Investigation of a candidate gene involves confirmation of genetic linkage by genotyping individual phenotypic and non-phenotypic organisms, this is typically followed by functional investigation such as by attempting to rescue the phenotype through exogenous expression of a candidate gene. A genetic non-complementation test represents a robust means of testing a candidate gene when recessive traits are being studied. This involves crossing a heterozygote isolated from a forward genetic study, to an unrelated animal heterozygous for an independently generated disruptive allele in a candidate gene, followed by screening of the progeny. In instances where the progeny display allelic non-complementation with manifestation of the phenotype being studied, the target gene has been identified.

2.6 Insights from Forward Genetics

Modern forward genetic approaches are derived from classical genetic studies first performed by in 1865 by Mendel, who inferred fundamental principles of genetic inheritance by studying heritable phenotypes in pea plants[133]. Following Mendel's pioneering work,

forward genetic studies have provided fundamental insights into many aspects of biology including the nature of genes, embryogenesis and immunity.

The realization that exposure to high energy radiation induces mutations[134] facilitated a landmark mutagenesis study by Beadle and Tatum in 1941[135]. By studying growth attenuated metabolic mutants of *Neurospora*, the authors were able to identify the association between genes, enzymes and biochemical reactions[135]. A subsequent genetic study performed by Crick in 1961 analyzing suppressor mutants of a growth attenuated bacteriophage mutant lead to the discovery of the triplet genetic code[136]. With developments in molecular biology, it became possible to establish the genetic basis for complex phenotypic traits such as behavior. Early in vivo studies performed by Benzer in the 1960s using EMS mutagenized *Drosophila melanogaster* populations demonstrated induced mutations could lead heritable differences in phototaxis[137]. Similar principles were applied by Brenner in a mutagenesis study in *C. elegans* which lead to the discovery of around 100 genes that were associated with abnormal behavior or morphology[138].

Forward genetic studies have been instrumental in understanding genes important in embryonic development. A large-scale mutagenesis study conducted in *Drosophila* larvae by Nüsslein-Volhard and Wieschaus described 15 loci essential for normal embryogenesis[139]. In order to facilitate developmental forward genetic studies in vertebrates, the zebrafish was developed as a model organism owing to its ease of handling, fecundity, optical transparency and external development[118,140]. In 1996, two major forward genetic studies collectively known as ‘the big screen’ to determine genetic determinants of development in zebrafish lead to the identification of around 1500 mutations in over 400 novel genes required for normal embryogenesis[141].

Forward genetic studies have also provided insights into immunity. Genetic mapping of mice with showed a lack of response following exposure to bacterial lipopolysaccharide lead to the positional cloning of toll-like receptor 4 (TLR4), the first mammalian TLR to be identified[142,143]. Subsequent forward genetic studies in mutagenized mice have led to the identification of additional immune factors involved in TLR signaling[144]. The discovery of polymorphic regions in the human genome enabled mapping of genes associated with human mendelian disorders[145,146]. The earliest example of this was the mapping of the Huntingtin gene as the genetic basis of Huntington's disease in 1983. This was closely followed by the identification of the genes responsible for cystic fibrosis, hemophilia and Duchenne muscular dystrophy[145,147].

Positional cloning of genes associated with the aforementioned conditions often took many years and involved linkage analysis of a large number of individuals. The recent usage of next generation sequencing and mapping by sequencing approaches in medical genetics has enabled the rapid identification of the genetic basis of disease in patients presenting with unknown mendelian disorders[148]. This has facilitated the diagnosis and molecular characterization of several rare disorders including MSMD[60,148].

2.7 Forward Genetics in Tuberculosis - Human studies

The application of both forward and reverse genetic methods in patients with MSMD has led to the identification of causative mutations in 11 different genes: IRF8, STAT1, IL12B, IL12RB1, NEMO, TYK2, CYBB, IFNGR1, ISG15, IFNGR2 and SPPL2A - all of which are associated with the IL-12/ IFN-γ immune circuit[59]. As discussed in Chapter 1.2 in response to mycobacterial infection, IL-12 produced by macrophages induces production and secretion of IFN-γ by T lymphocytes and natural killer cells[35]. IFN-γ in turn activates

macrophages, increasing their microbicidal capacity[35]. Disruption of this pathway in MSMD patients leads to reduced intracellular clearance of mycobacteria by macrophages[149], and in mouse models is associated with rapidly fatal infection with extensive granuloma necrosis[150].

2.8 Forward Genetics in Tuberculosis – Mouse Studies

The gene natural resistance-associated macrophage protein 1 (Nramp1) was identified in mice following forward genetic studies comparing susceptibility of inbred strains to a range of intracellular bacteria, including *M. tuberculosis*[151,152]. Nramp1 is a phagosomal efflux pump primarily expressed in macrophages where it serves to deprive phagosomal bacteria of essential Fe^{2+} and Mn^{2+}[153]. Subsequent clinical studies demonstrated that mutations in human NRAMP1 were associated with susceptibility to several mycobacterial diseases including tuberculosis[154], leprosy[155] and Buruli ulcer, a disease caused by *Mycobacterium ulcerans*[156].

Genetic mapping of the BCG susceptible BXH-2 mouse strain demonstrated a causative mutation in the gene interferon regulatory factor 8 (irf8)[157]. Irf8 mutation results in deranged hematopoiesis, with increased numbers of granulocytes and poorly differentiated hematopoietic progenitor cells resulting in a myeloid leukemia-like state[157]. This is accompanied by a profound macrophage deficiency and a defective IL-12/ IFN-γ response, resulting in increased susceptibility to mycobacterial infection[158,159]. The isolation and characterization of murine irf8 mutants facilitated the identification of deleterious mutations in human IRF8 as a cause of MSMD[160].

2.9 Forward Genetics in Tuberculosis – Zebrafish Studies

The Ramakrishnan laboratory has previously carried out a mutagenesis screen in zebrafish larvae infected with *M. marinum*, to identify host determinants of mycobacterial infection outcome. This has provided several insights into the pathophysiology of mycobacterial infection.

2.9.1 Lysosomal storage disorders increase susceptibility to tuberculosis

Mapping of *fh111*, a hypersusceptible zebrafish mutant isolated from the Ramakrishnan screen demonstrated a causative nonsense mutation in the gene *small nuclear RNA complex polypeptide 1b* (*snapc1b*)[117]. *Snapc1b* functions as a transcriptional regulator and mutants have reduced expression of lysosomal cysteine cathepsins, required for normal degradation of lysosomal material[117]. Under homeostatic conditions *snapc1b* mutant macrophages develop lysosomal accumulation of undigested cellular debris[117]. Following infection, macrophages with lysosomal accumulation showed impaired migration to newly infecting bacteria and were less able to participate in granuloma formation[117]. This results in secondary necrosis of unengulfed infected apoptotic macrophages leading to early granuloma failure[117]. These findings were then applied to human alveolar macrophages from smokers, which display acquired lysosomal accumulation due to indigestible smoke particles[117]. Smoker's macrophages showed reduced migration to *M. tuberculosis* relative to those from non-smokers and potentially represents a cellular basis for the increased risk of tuberculosis infection seen in smokers[117].

2.9.2 Both excessive and deficient inflammation lead to tuberculosis susceptibility

Another mutant to be mapped from the Ramakrishnan screen, had increased susceptibility to *M. marinum* due to a regulatory mutation in the gene *leukotriene A4 hydrolase* (*lta4h*)[100]. Lta4h is an enzyme which catalyses the synthesis of the proinflammatory eicosanoid leukotriene B4 (ltb4). Disruption of *lta4h* leads to increased susceptibility to infection due to shunting of eicosanoid substrates to biosynthetic pathways responsible for the production of anti-inflammatory lipoxins[100].

Subsequent investigation identified rs17525495, a biallelic SNP in the promoter of human *LTA4H* associated with polarised expression[161]. rs17525495 allelic status was found to influence treatment outcome in patients with tuberculosis meningitis (a severe form of TB managed with anti-inflammatory glucocorticoids). Homozygosity for either rs17525495 allele was associated with increased infection mortality relative to heterozygotes, indicating both over- and under- expression of LTA4H is pathological[161]. Further investigation demonstrated glucocorticoid treatment was beneficial in tuberculosis meningitis patients homozygous for the rs17525495 allele associated with high LTA4H expression but harmful in individuals homozygous for the allele associated with low LTA4H expression[161].

To characterise the molecular basis of susceptibility in LTA4H homozygotes additional investigation was carried out in the zebrafish. This demonstrated that susceptibility to mycobacterial in both *lta4h* high and low states converges on macrophage necrosis due to TNF dysregulation[161,162]. Increased lipoxin production in *lta4h* deficient larvae resulted in an anti-inflammatory state with reduced expression of TNF permitting increased mycobacterial growth resulting in necrosis of infected

macrophages[100,161]. In contrast, larvae overexpressing *lta4h* have increased levels of *tnf* with reduced mycobacterial growth shortly after infection, followed by necrosis of infected macrophages[161,162]. Detailed mechanistic studies determined that macrophage necrosis in high TNF states occurs due an inter-organelle pathway triggered by increased production of reactive oxygen species and culminating in Ca^{2+} transfer to the mitochondria from the endoplasmic reticulum (ER) resulting in opening of mitochondrial transition pores[163]. This pathway of programmed necrosis could be prevented by disrupting cellular calcium intake and transfer to the mitochondrion, potentially representing a novel therapeutic approach[163].

As well as demonstrating the deleterious role of both hypo- and hyperinflammation in tuberculosis pathology, these studies demonstrated how genotype tailored therapy can optimise tuberculosis treatment outcome. This also highlights the strength of the zebrafish-*M. marinum* genetic approach: variations in a gene initially isolated in a zebrafish forward genetic study were found to have clinical relevance in a patient cohort, which could then be further characterised by mechanistic dissection in the zebrafish providing additional therapeutic targets.

Chapter 3

Forward genetic screen to identify host determinants of immunity against mycobacteria

3.1 Summary

The mutants discussed in the last chapter were identified from a F2 early pressure screen on ENU mutagenized zebrafish performed in the laboratory of Dr. Cecilia Moens. After the Ramakrishnan laboratory moved to Cambridge, I was part of a team that initiated a forward genetic study here. In this study F3 mutagenized zebrafish larvae were infected with *Mycobacterium marinum* (*M. marinum*) to identify host determinants of mycobacterial infection outcome. 279 unrelated mutant families have been screened, with the identification of 31 recessive traits conferring susceptibility to *M. marinum* infection. I have participated in the mapping of 5 mutants via exome sequencing bulked DNA from phenotype sorted larvae followed by SNP based linkage analysis.

3.2 Study design and isolation of phenotypic mutants

We performed a forward genetic study on mutagenized zebrafish derived from the Zebrafish Mutation Project (ZMP) library[110]. To generate this library, adult fish were mutagenized by exposure to ENU before being outcrossed to wildtype animals to produce F1 families heterozygous for induced mutations[110] (Figure 1A). Cryopreserved milt of random F1s from the ZMP library was used to fertilise eggs from wildtype females to produce F2 families (Figure 1B). Random sibling incrosses of F2 fish was carried out, followed by intravascular infection of F3 larvae with *M. marinum* at 2 days post fertilisation (dpf) (Figure 1C). Infection status of larvae was then assessed by fluorescence microscopy at 5 days post-infection (dpi).

In wildtype larvae at 5dpi, *M. marinum* infection manifests as compact, discrete bacterial aggregates due to intracellular infection of individual macrophages,

along with larger clusters of bacteria within nascent granulomata[91,100] (Figure 2A, 2C). In this study mutant families were identified in which larvae displayed a distinctive infection morphology with the presence of serpentine aggregates of mycobacteria termed ‘cords’ (Figure 2B, 2D). Prior studies have demonstrated mycobacterial cording occurs when mycobacteria released into the extra-cellular environment from necrotic macrophages replicate profusely[100,164] Mycobacterial cording in zebrafish larvae is visually distinct from intracellular bacterial growth in wildtype larvae (Figure 2) and has been used in this study as a phenotypic proxy for susceptibility to infection.

When a F3 clutch containing larvae with mycobacterial cording at approximately mendelian ratios was identified, its male F2 parent was outcrossed to wildtype animals to generate F3 families (Figure 1D). Random incrosses of at least 4 F3 sibling was then performed, followed by infection and screening of F4 larvae in order to re-identify the previously observed phenotype. This process of outcross and re-identification was performed to confirm that observed phenotypes were due to a single heritable trait as opposed to polygenic or environmental factors.

In total 279 mutagenized zebrafish families have been screened for the presence of bacterial cording. Within this cohort 31 phenotypic mutants were identified, 17 of which have been confirmed in a subsequent generation, with 12 families pending re-screening. In all isolated mutants with confirmed phenotypes, clutches from approximately one quarter of random sibling pairs contained phenotypic larvae, indicating that all share a recessive mode of inheritance.

Figure 1

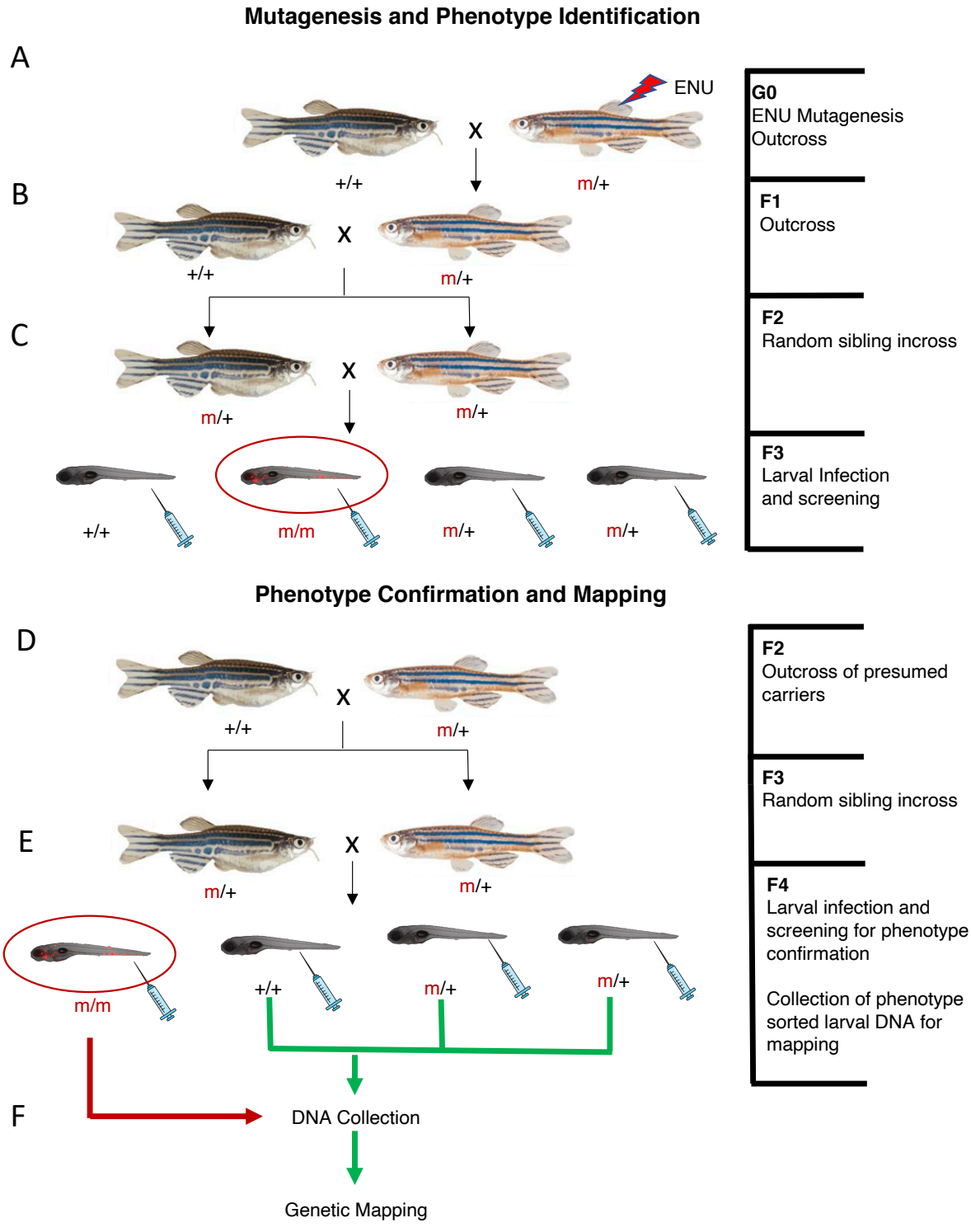
Mutagenesis and Phenotype Identification
A
ENU
X
+/+
m/+
B
X
+/+
m/+
C
X
m/+
m/+
+/+
m/m
m/+
m/+
G0
ENU Mutagenesis
Outcross
F1
Outcross
F2
Random sibling incross
F3
Larval Infection
and screening
Phenotype Confirmation and Mapping
D
X
+/+
m/+
E
X
m/+
m/+
m/m
+/+
m/+
m/+
F2
Outcross of presumed
carriers
F3
Random sibling incross
F4
Larval infection and
screening for phenotype
confirmation
Collection of phenotype
sorted larval DNA for
mapping
F
DNA Collection
Genetic Mapping

Figure 1

Crossing scheme of mutagenesis screen to identify mutant zebrafish with increased susceptibility to mycobacterial infection.

(**A**) G0 ENU mutagenized zebrafish were outcrossed to generate F1 families heterozygous for induced mutations.

(**B**) F1 families were then outcrossed to generate F2 families.

(**C**) Random F2 sibling pairs were incrossed to generate F3 larvae.
2dpf F3 larvae were then infected with 150-250 CFU *M. marinum* and screened at 5dpf to identify clutches containing phenotypic larvae.

(**D**) F2 parents of phenotypic clutches were outcrossed to generate F3 families.

(**E**) F3 sibling pairs were then incrossed to generate F4 larvae which were infected and screened to confirm presence of the previously identified phenotype.

(**F**) DNA from phenotype sorted F4 larvae was bulked and exome mapped to generate a mapping interval which was further resolved by SNP-based linkage analysis.

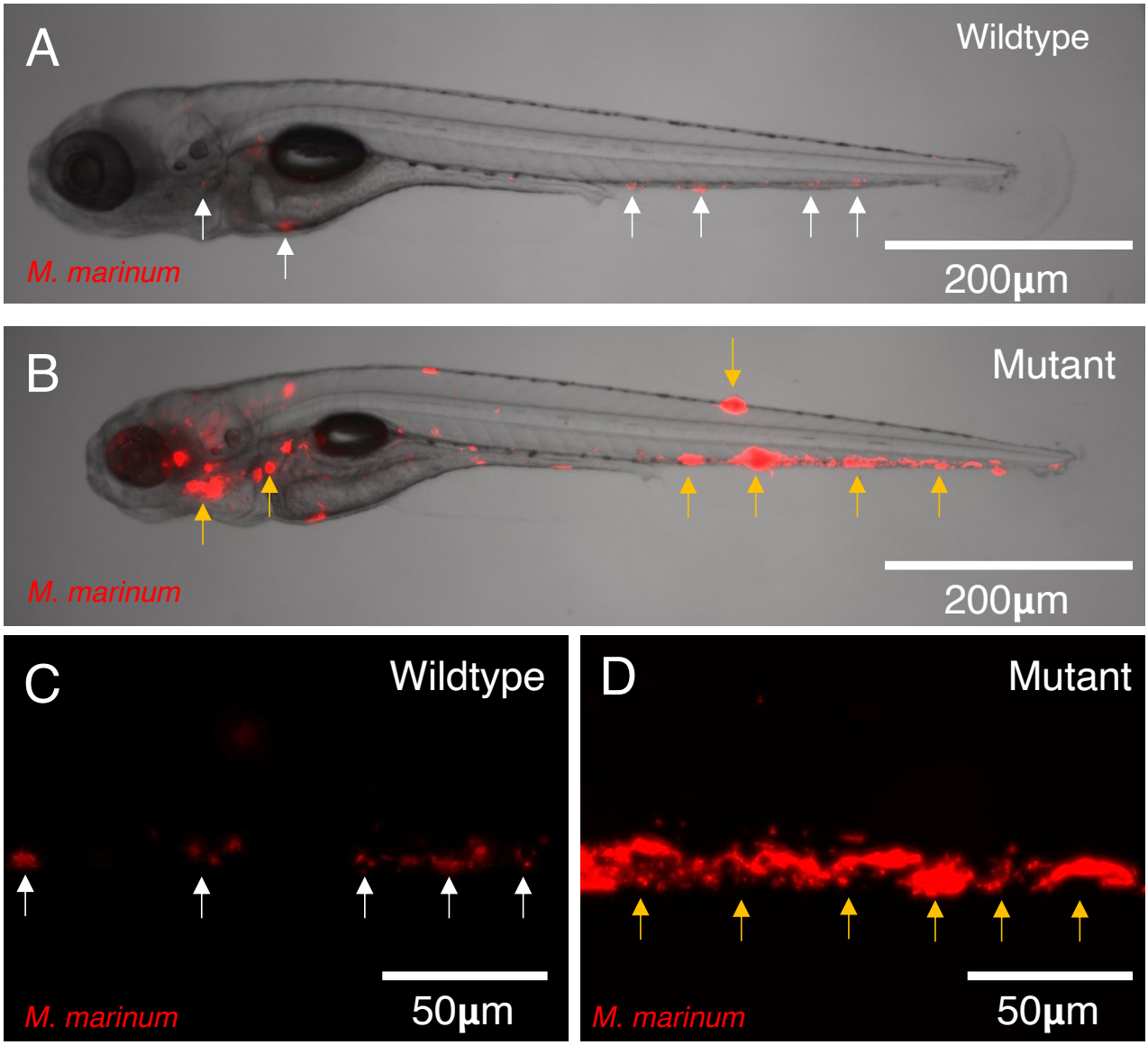

Figure 2

M. marinum cording in hypersusceptible mutant larvae is morphologically distinct from infection in wildtype (WT) larvae.

(**A-D**) Micrographs of 7dpf sibling WT and hypersusceptible mutant larvae at 5dpi infected with ~160 CFU of red fluorescent *M. marinum.* White arrows: individual infected macrophages and nascent granulomata; Yellow arrows: mycobacterial cording.

(**A,B**) 4x brightfield micrographs of WT (**A**) and mutant sibling (**B**) larvae with fluorescent overlay showing *M. marinum.*

(**C**,**D**) 20x fluorescent micrographs of the caudal haemopoietic tissue in WT (**C**) and mutant (**D**) sibling larvae infected with *M. marinum.*

3.3 Mutant Mapping

Following phenotype confirmation, isolated mutants are currently at different stages of genetic mapping (Table 1). Exome sequencing has been performed on bulked phenotype sorted larvae from 5 mutant families (Figure 1E; Table 1). Sequences were then analysed by a computational pipeline define a mapping interval through comparison of allelic frequency at polymorphic loci across the genome in pools of phenotype- sorted larvae (see methods) (Figure 3). Exome sequencing data was used to develop genotyping assays for SNPs within the mapping interval of each mutant family (see methods). Genotyping was then performed on individual phenotypic larvae to assess the level of linkage between a given SNP and the causative mutation. As all isolated mutants show autosomal recessive inheritance, mapping intervals were further resolved by determining conserved regions of homozygosity across recombinant phenotypic larvae (Figure 3B, 3D, 3F, 3H).

For the remainder of my project, I focused mainly on the *Guaguancó* mutant. SNP-based linkage analysis (see methods) of recombinant *Guaguancó* mutant larvae demonstrated the causative mutation was linked to a ~1 MB region in Chromosome 8 containing 21 genes (Figure 3A, B). To prioritise genes within this interval for further investigation, RNA-seq analysis was performed on individual uninfected *Guaguancó* and wildtype sibling larvae at 3, 5 and 7 dpf (see methods). This demonstrated that *Guaguancó* mutant larvae had reduced expression of 5 genes within the mapping interval and only 3 genes: *uxt*, *pim2* and zgc:88609 were downregulated across all time points (Figure 4A). Analysis of sequencing data demonstrated that *Guaguancó* mutants were homozygous for a nonsense allele in

the first exon of the gene *ubiquitously expressed transcript* (*uxt*) (Figure 4B, C), but had no mutations predicted to be disruptive in other genes differentially regulated in *Guaguancó* mutants).

Zebrafish *uxt* is an ortholog of human UXT, a poorly characterised protein consisting of 169 amino acids and a member of the prefoldin protein family[165]. Uxt appears to be well conserved across vertebrates with zebrafish Uxt sharing 64% and 63% amino acid identity human and murine orthologs respectively (Appendix 1)[165]. Additionally, structural prediction algorithms indicate zebrafish, human and murine Uxt orthologs share the basic structure consisting of an antiparallel coiled coil separated by two beta hairpins (Appendix 1). UXT which has been implicated in a range biological process including transcriptional regulation of androgen and oestrogen receptor signalling, enhancement of NF-κB signalling in response to viral infection and inhibition of extrinsic apoptosis[166–169]. The known biological roles of UXT are further reviewed in Chapter 5.1.

To confirm that the *Guaguancó* phenotype was due to disruption of *uxt,* a zebrafish family with a second nonsense allele of *uxt*, *sa8704* was obtained from the ZMP library (Figure 4A). Homozygous progeny of $uxt^{sa8704/+}$ incrosses were found to present with mycobacterial cording at 5dpi, phenocopying $uxt^{Guaguancó/Guaguancó}$ larvae (Figure 4B). A genetic complementation test was then performed by infecting and screening larvae from a $uxt^{sa8704/+}$ x $uxt^{Guaguancó/+}$ outcross. Compound heterozygous larvae did not show genetic complementation and infection resulted in mycobacterial cording at 5dpi; wildtype and larvae heterozygous for a single allele presented with normal infection (Figure 4E).

Days post infection (dpi) until mycobacterial cording visible	3dpi		4dpi		5dpi		6dpi
Positional Cloning Completed			*Guaguancó (uxt)*				
Mapping Interval Defined	*Timba*			*Kalamatianos*	*Montuno Yambú*		
Phenotype confirmed		*Carpaea*	*Syrtos Morris Sirtaki*	*Hasapiko*	*Pachanga Antichristos*	*Kartzilamas*	*Guajira Zeibekiko*

Table 1

Mapping progress of isolated mutants with confirmed phenotypes.

Mutants where the phenotype has been confirmed in a subsequent generation, but no mapping has taken place are shown in red. Mutants where exome mapping has been used to define a mapping interval which are currently being further resolved by SNP-based linkage analysis are shown in orange. Lastly, the *Guaguancó* mutant for which positional cloning has been completed is shown in green.

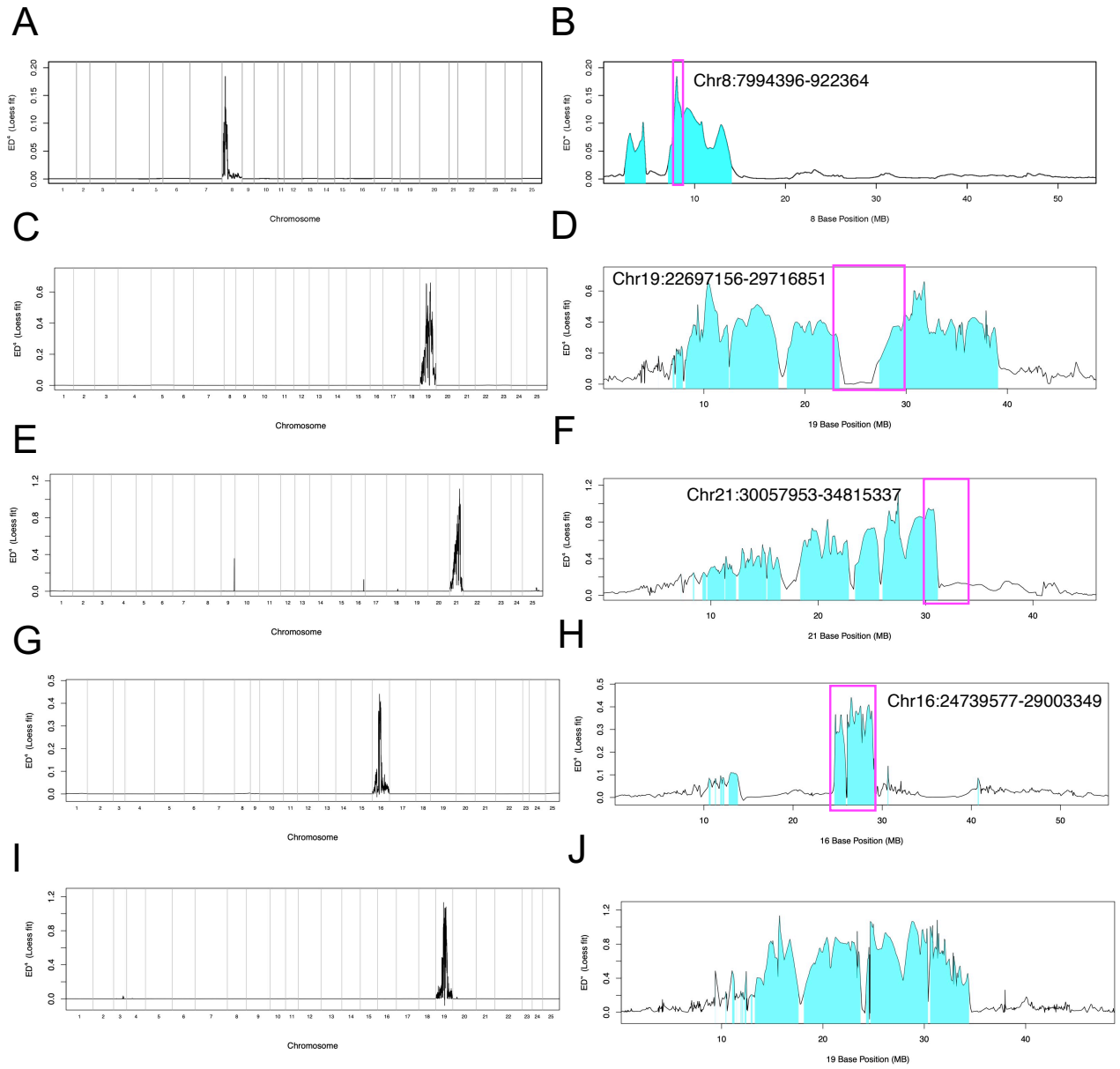

Figure 3

Mapping intervals of *Guaguancó*, *Kalamatianos*, *Montuno*, *Timba* and *Yambu* mutant families

(**A-J)** Loess fit curves of exome mapping analysis, plotting the fourth power of Euclidian distance (ED^4) between allele frequencies in bulked phenotype sorted larvae from *Guaguancó* (**A**,**B**), *Kalamatianos* (**C**, **D**), *Montuno* (**E**, **F**), *Timba* (**G**,**H**) and *Yambu* (**I**,**J**) mutant families. ED increases proportionally with decreasing distance from the causative mutation.

(**A**, **C**, **E**, **G**, **I**) ED^4 scores across the genome for *Guaguancó* (**A**), *Kalamatianos* (**C**), *Montuno* (**E**), *Timba* (**G**) and *Yambu* (**I**) mutants. Grey vertical lines represent chromosome boundaries.

(**B**, **D**, **F**, **H**, **J**) ED^4 scores across individual chromosomes containing linked region peaks (shown in blue) associated with *Guaguancó* (**B**), *Kalamatianos* (**D**), *Montuno* (**F**), *Timba* (**H**) and *Yambu* (**J**) mutants. Position of the mapping interval determined by linkage analysis in individual phenotypic larvae shown in magenta boxes and labelled.

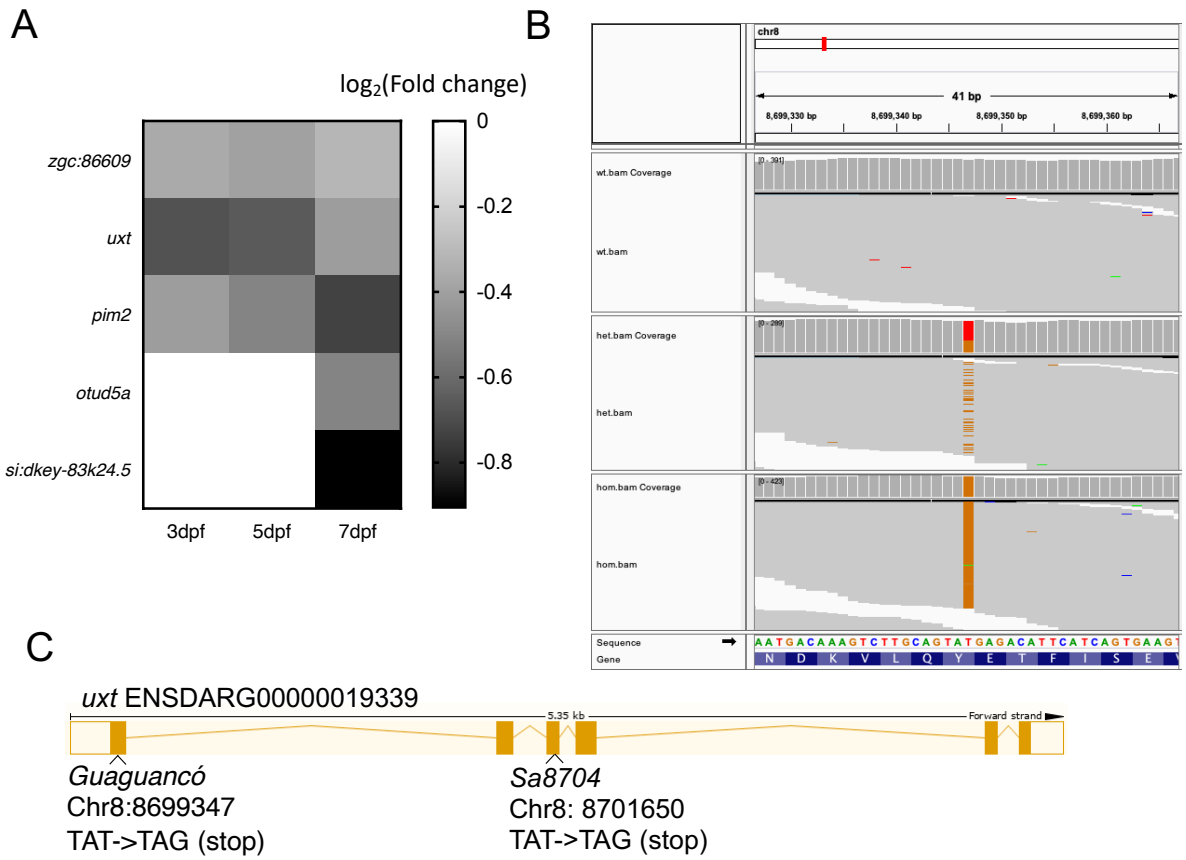
A
log2(Fold change)
0
-0.2
-0.4
-0.6
-0.8
zgc:86609
uxt
pim2
otud5a
si:dkey-83k24.5
3dpf
5dpf
7dpf
B
chr8
41 bp
8,699,330 bp
8,699,340 bp
8,699,350 bp
8,699,360 bp
wt.bam Coverage
wt.bam
het.bam Coverage
het.bam
hom.bam Coverage
hom.bam
Sequence
Gene
C
uxt ENSDARG00000019339
5.35 kb
Forward strand
Guaguancó
Chr8:8699347
TAT->TAG (stop)
Sa8704
Chr8: 8701650
TAT->TAG (stop)
D (I)
n 13 30 15
% of larvae
Cording
Normal Infection
Sa8704
+/+ +/- -/-
(II)
n 27 50 24
Guaguancó
E
n 22 21 20 22
Sa8704
Guaguancó
F
n 58 36
WT
Δuxt

Figure 4

Genetic disruption of *uxt* is responsible for increased susceptibility to *M. marinum* infection in *Guaguancó* mutants.

(**A**) Heat map showing relative expression of *Guaguancó* candidate genes in *Guaguancó*$^{-/-}$ larvae relative to WT sibling controls. Expression measured in individual uninfected larvae by RNA-seq at 3, 5 and 7 dpf with normalised expression counts averaged across 12 biological replicates per group.

(**B**) RNA-seq reads aligned with exon 1 of *uxt* from sibling wildtype (wt) (I), heterozygous (het) (II) and homozygous (hom) (III) *Guaguancó* larvae. Reference sequence shown at the bottom. Bases from individual reads matching the reference sequence in are shown in grey. Bases which do not match the reference sequence are colored (green for adenine, orange for guanine, blue for cytosine red for thymine). White indicates lack of coverage in a given read.

(**C**) Diagram of zebrafish *uxt* gene showing exons (yellow blocks) and introns (lines) labelled with the location of nonsense mutation identified in *Guaguancó*$^{-/-}$ larvae in addition to *S sa8704,* an independently generated *uxt* nonsense allele.

(**D**) Quantification of mycobacterial cording in larvae from incrosses of (I)*uxt*$^{sa8704/+}$ *(II)uxt*$^{Guaguancó/+}$ parents at 5dpi with ~200 CFU of *M. marinum.*

(**E**) Quantification of mycobacterial cording in larvae from *uxt*$^{sa8704/+}$ x *uxt*$^{Guaguancó/+}$ outcross at 5dpi with ~200 CFU of *M. marinum.*

3.4 Discussion – Forward Genetic Study

Our forward genetic screen has isolated 31 mutant zebrafish families with increased susceptibility to *M. marinum* infection. This study is ongoing with isolation of additional mutants and confirmation of previously identified phenotypes. Further identification and collection of mutant larvae from exome mapped mutant families is ongoing to further resolve their respective mapping intervals, in conjunction with functional investigation of biologically compelling candidate genes.

Our screen design has proven efficacious in isolating susceptible mutants in innate susceptibility to TB, as adaptive immune cells are yet to develop at the larval stages. Therefore, mutations in host susceptibility genes that alter the adaptive arm of immunity will not be isolated. On the other hand, many innate immune determinants continue to remain in play during adaptive immunity, often in interplay with adaptive immunity[35]. Mutants identified in the screen have not only been found confer susceptibility in adult zebrafish but also in adult humans[100,161].

Another limitation of the screen is that while some induced mutations should result in resistance to infection, and two such resistant mutants have been identified from candidate gene searches in zebrafish larvae[104] (J. Fan and L. Ramakrishnan, personal communication), we have to date only identified one resistance mutant in the previous forward genetic screen conducted in Seattle[100], and none in the Cambridge screen described here. This is likely due to the fact our screen design is not amenable to the identification of resistant mutants. While hypersusceptibility in mutant larvae can manifest as the readily identifiable mycobacterial cording, there is reliable binary identifiable correlate of resistance. Isolation of resistant mutants could

be achieved by assaying survival of mutant larvae or quantifying infection burden over time but either approach would significantly constrain screening throughput. This highlights that we may well be missing important resistance alleles, as well as the importance of an ideal screening phenotype such as bacterial cording.

Due to the laboriousness of eliciting an infection phenotype, the throughput of this study is relatively modest relative to previous zebrafish developmental studies but compares favourably to other forward genetic studies of immune determinants in vertebrates[100,141,153]. Across mutant families for which mapping intervals have been defined, regions either have no overlap or compound heterozygotes show genetic complementation (data not shown), indicating that none share causative mutations. Mapping intervals also show no overlap with mapped genes from the previous Ramakrishnan lab screen indicating minimal saturation in this approach[100,117]. Although the unbiased nature of this screen may mean that isolated mutants map to genes associated with tuberculosis immunity, understanding of genetic determinants of mycobacterial infection outcome is far from complete, so it is likely that a proportion of isolated mutants will map to novel genes. Indeed, the *Guaguancó* mutant was found to map to a nonsense mutation in *uxt*, a poorly characterised protein with no previously known role in mycobacterial immunity.

Chapter 4

Cellular characterisation of *uxt* mutant phenotype

4.1 Macrophages in *uxt* mutants are more numerous at baseline but morphologically abnormal

Having confirmed that the *Guaguancó* mutant maps to a mutation in *uxt,* we next sought to characterise the cellular basis of susceptibility in *uxt* mutant larvae. Global macrophage deficit has been associated with mycobacterial cording due to insufficient granuloma replenishment, leading to secondary necrosis of infected macrophages and granuloma failure[170].To ascertain whether *uxt* deficient larvae have fewer macrophages, we generated $uxt^{-/-}$ zebrafish expressing the fluorescent macrophage reporter *mpeg1:Brainbow* and counted macrophages in the trunk of uninfected larvae. This demonstrated that *uxt* mutants had a baseline increase in trunk macrophages from 7dpf relative to wildtype and phenotypically normal $uxt^{+/-}$ siblings (Figure 5A). While peripheral macrophages in larvae are largely derived from precursors that develop in the caudal haematopoietic tissue from 32 hours post fertilisation, the tissue resident macrophage population of the brain (microglia) represent a distinct population that develop from precursors that originate in the rostral blood island[93,171,172] .We found that *uxt* mutants had increased numbers of midbrain macrophages in uninfected larvae from 5dpf (Figure 5B), showing that *uxt* disruption is associated with an increase in multiple macrophage populations. Time-lapse imaging of *uxt* mutant macrophages in uninfected animals indicated that *uxt* deficient macrophages may be less migratory with a non-significant trend of reduced speed and displacement. Gene set enrichment analysis of RNA-seq data identified an overrepresentation of downregulated genes associated with leucocyte

chemotaxis and migration in *uxt* mutants (Appendix 2), further suggesting that *uxt* may influence macrophage migration.

Susceptibility to infection with increased macrophage numbers could occur in the context of acute myeloid leukaemia, in which there is an accumulation of poorly differentiated myeloid cells. Confocal imaging showed that relative to wildtype siblings, *uxt* mutant macrophages have a comparable volume (Figure 5C) but a highly ramified morphology with a decrease in sphericity (Figure 5E,D), more closely resembling mature differentiated macrophages than undifferentiated leukemic cells[173,174]. Furthermore, *uxt* appears to have essential functions beyond immunity in zebrafish, as uninfected homozygous *uxt* mutants do not survive beyond 30dpf but appear normal at 7dpf (data not shown).

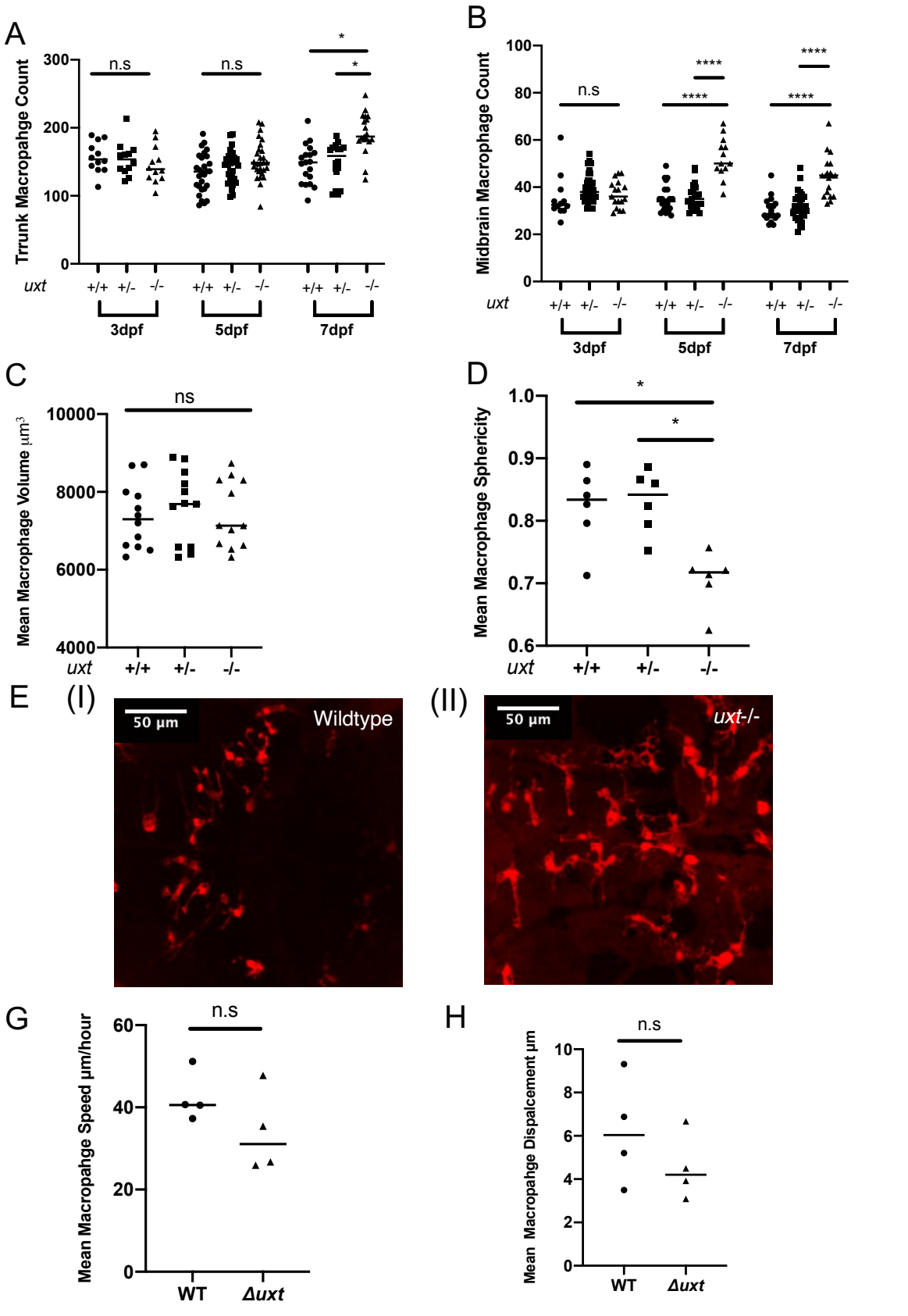
A
Trrunk Macropahge Count
300
200
100
0
n.s
n.s
*
*
uxt
+/+ +/- -/-
+/+ +/- -/-
+/+ +/- -/-
3dpf
5dpf
7dpf
B
Midbrain Macrophage Count
100
80
60
40
20
0
n.s
****
****
****
****
uxt
+/+ +/- -/-
+/+ +/- -/-
+/+ +/- -/-
3dpf
5dpf
7dpf
C
Mean Macrophage Volume µm3
10000
8000
6000
4000
ns
uxt
+/+ +/- -/-
D
Mean Macrophage Sphericity
1.0
0.9
0.8
0.7
0.6
*
*
uxt
+/+ +/- -/-
E
(I)
50 µm
Wildtype
(II)
50 µm
uxt-/-
G
Mean Macropahge Speed µm/hour
60
40
20
0
n.s
WT
Δuxt
H
Mean Macropahge Dispalcement µm
10
8
6
4
2
0
n.s
WT
Δuxt

Figure 5

At baseline *uxt* mutants have increased numbers of macrophages that possess a ramified morphology.

(**A** and **B**) Quantification of fluorescent macrophages in the trunk (A) and midbrain (B) of uninfected *mpeg1:Brainbow*, *uxt*$^{+/-}$ incross larvae at 3,5 and 7 dpf.

(**C** and **D**) Mean volume (**C**) and sphericity (**D**) of macrophages in the midbrain of uninfected *mpeg1:Brainbow*, *uxt*$^{+/-}$ incross larvae at 5dpf. Volume and sphericity quantification performed on confocal image stacks.

(**E**) Confocal images of red fluorescent midbrain macrophages at 5dpf in wildtype (**I**) and *uxt*$^{-/-}$ (**II**) sibling larvae from *mpeg1:Brainbow*, *uxt*$^{+/-}$ incross

(**G** and **H**) Mean speed (**G)** and displacement (**H**) of macrophages in the caudal haematopoietic tissue of 7dpf wildtype and sibling Δ*uxt* CRISPR-mediated mutant (crispant) larvae (see methods). Quantification performed on macrophage tracking data derived from time-lapse confocal microscopy images.

Statistical significance assessed using Kruskal-Wallis test with Dunn's multiple comparison test (A,B,C,D) and Mann-Whitney test (G, H). n.s not significant, * $p< 0.05$, **** $p<0.0001$

4.2 Granuloma formation in *uxt* mutants is initially normal

As macrophage migration defects resulting in impaired granuloma participation have previously been found to result in mycobacterial cording[117] and uninfected *uxt* mutant macrophages may be somewhat less migratory, we next investigated macrophage migration and granuloma formation in infected *uxt* mutants. Time-lapse imaging showed that uninfected macrophages in infected *uxt* deficient animals have comparable migration speed and displacement relative to those in wildtype siblings (Figure 6A,B). To functionally assess granuloma formation in *uxt* deficient animals, mutant larvae and wildtype siblings were infected with *M. marinum* and granuloma volume quantified at 3dpi. This showed that *uxt* mutant larvae formed organised granulomas of an equivalent volume and bacterial burden relative to wildtype siblings (Figure 6C,D,E). These findings suggest while *uxt* may influence homeostatic macrophage migration, it is dispensable in the context of mycobacterial infection and granuloma formation.

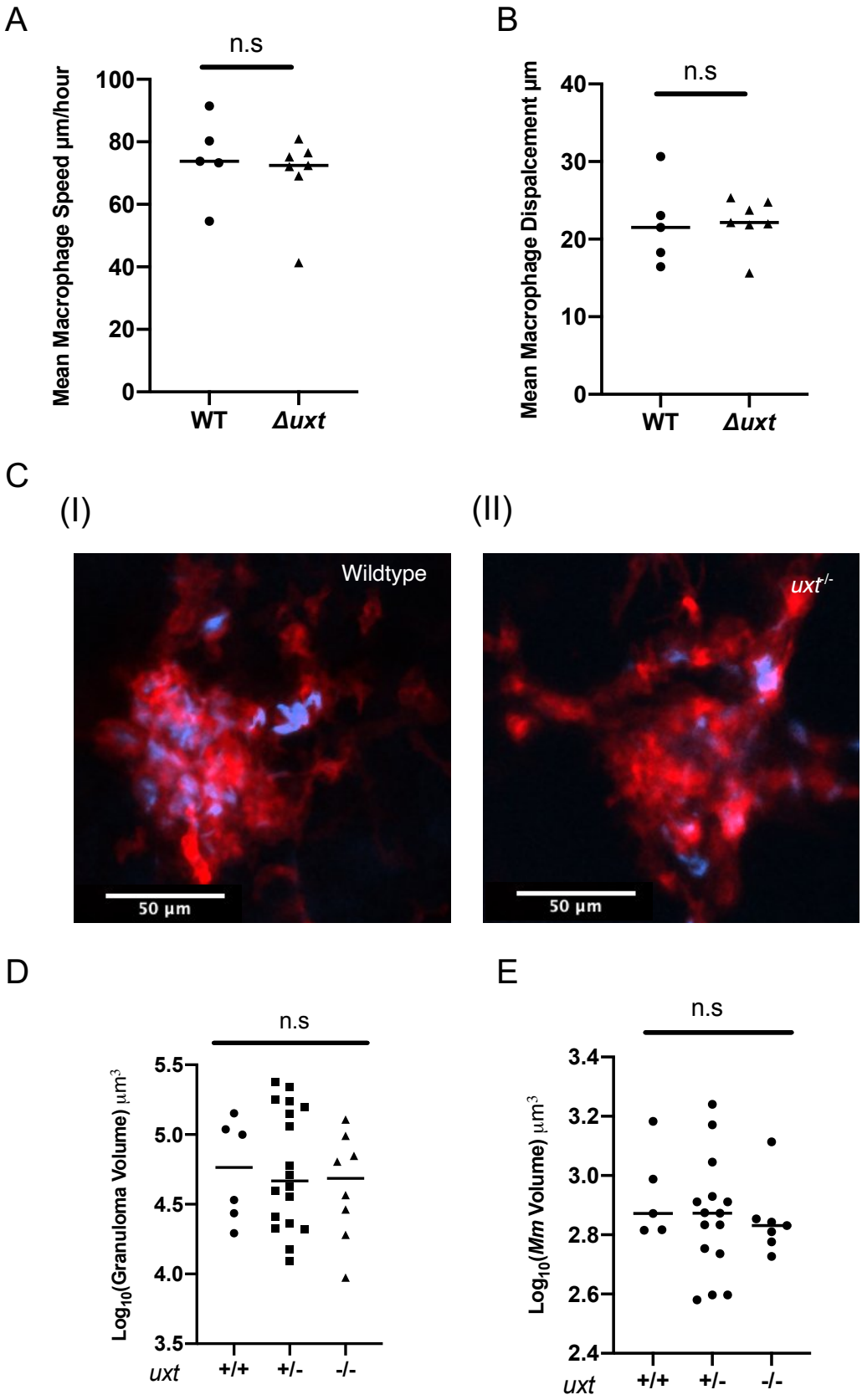
A
n.s
Mean Macrophage Speed µm/hour
100
80
60
40
20
0
WT
Δuxt
B
n.s
Mean Macrophage Dispalcement µm
40
30
20
10
0
WT
Δuxt
C
(I)
(II)
Wildtype
uxt-/-
50 µm
50 µm
D
n.s
Log10(Granuloma Volume) µm3
5.5
5.0
4.5
4.0
3.5
uxt
+/+
+/-
-/-
E
n.s
Log10(Mm Volume) µm3
3.4
3.2
3.0
2.8
2.6
2.4
uxt
+/+
+/-
-/-

Figure 6
uxt mutants show normal macrophage migration and granuloma formation in response to infection

(**A** and **B**) Mean speed (**A)** and displacement (**B**) of uninfected macrophages in the caudal haematopoietic tissue of wildtype and sibling Δ*uxt* crispant larvae at 3dpi with ~200 CFU of *M. marinum* in the hindbrain ventricle. Quantification performed on time-lapse confocal microscopy images, segmented to exclude infected macrophages.

(**C**) Confocal images of red fluorescent macrophages and blue fluorescent *M. marinum* in granulomata of wildtype (**I**) and *uxt*$^{-/-}$ (**II**) larvae at 3dpi with ~100 CFU of *M. marinum* in the hindbrain ventricle.

(**D** and **E**) Volume of granulomata (**D**) and intra-granuloma *M. marinum* (*Mm*) (**E**) in infected *mpeg1:Brainbow*, *uxt*$^{+/-}$ incross larvae at 3dpi with ~200 CFU of *M. marinum* in the hindbrain ventricle. Quantification performed on confocal image stacks.

Statistical significance assessed using Mann-Whitney test (B, C) and unpaired t test (E, F). n.s not significant.

4.3 Macrophages in *uxt* mutants have normal microbicidal capacity yet become depleted during infection

Microbicidal capacity in Uxt deficient larvae was then assayed by quantifying bacterial burdens in individual infected macrophages at 2dpi. At this time point *uxt* mutant and wildtype sibling larvae had similar numbers of infected macrophages (Figure 7A) which possessed comparable bacterial burdens (Figure 7B). Positive control larvae with an induced microbicidal defect through depletion of Tnf receptor-1 (via injection of a modified antisense oligonucleotide), showed an increase in both number and mean bacterial burdens of infected macrophages, independent of *uxt* genotype (Figure 7A,B). These findings indicated that Uxt deficiency is not associated with macrophage microbicidal deficiency. However, by 4dpi macrophages in Uxt deficient animals showed an increased mean macrophage bacterial burden relative to wildtype siblings, which was comparable to that of Tnf receptor-1 deficient larvae (Figure 7C, D). Further analysis revealed that at 4dpi *uxt* mutants possess fewer infected macrophages relative to wildtype and Tnf receptor-1 deficient animals (Figure 7E) but (unlike Tnf receptor-1 deficient animals) do not have an increase in total bacterial burden (Figure 7F). Enumeration of CHT macrophages in infected animals at 1 and 5 dpi confirmed depletion of macrophages in *uxt* mutants during the course of infection (Figure 7G) which was not observed following injection of heat-killed *M. marinum* (Figure 7H). These findings are suggestive of a model whereby uxt mutant macrophages are initially able to restrict infection but become depleted upon infection with viable bacteria.

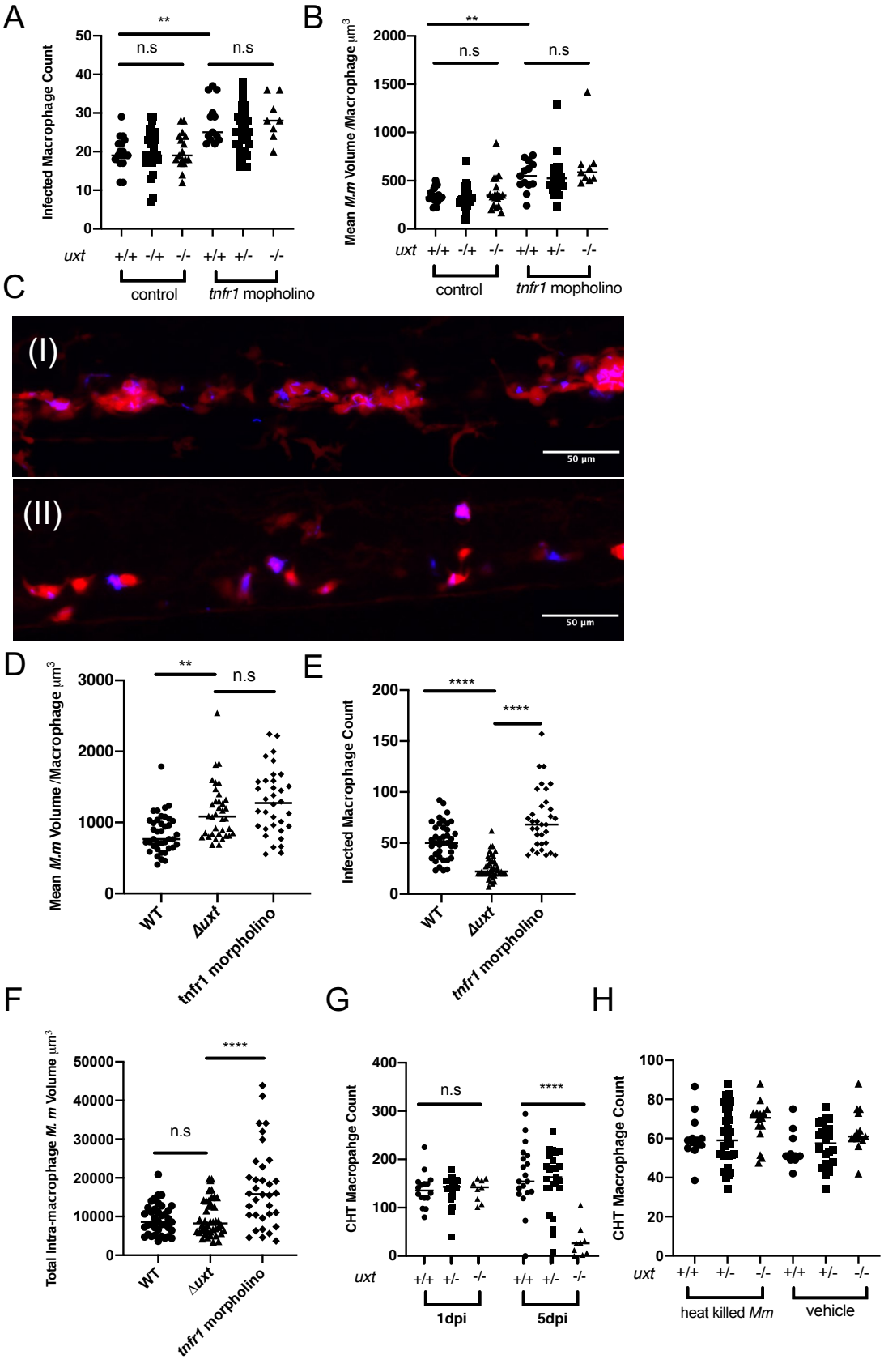
A
Infected Macrophage Count
**
n.s
n.s
uxt
+/+ -/+ -/-
+/+ +/- -/-
control
tnfr1 mopholino
B
Mean M.m Volume /Macrophage µm3
**
n.s
n.s
uxt
+/+ -/+ -/-
+/+ +/- -/-
control
tnfr1 mopholino
C
(I)
50 µm
(II)
50 µm
D
Mean M.m Volume /Macrophage µm3
**
n.s
WT
Δuxt
tnfr1 morpholino
E
Infected Macrophage Count
****
****
WT
Δuxt
tnfr1 morpholino
F
Total Intra-macrophage M. m Volume µm3
****
n.s
WT
Δuxt
tnfr1 morpholino
G
CHT Macropahge Count
n.s
****
uxt
+/+ +/- -/-
+/+ +/- -/-
1dpi
5dpi
H
CHT Macrophage Count
uxt
+/+ +/- -/-
+/+ +/- -/-
heat killed Mm
vehicle

Figure 7
Macrophages in Uxt deficient animals have normal microbicidal capacity but become depleted during infection

(**A**) Enumeration of fluorescent macrophages in the CHT of *mpeg1:Brainbow*, *uxt*$^{+/-}$ incross larvae and siblings injected with tnfr1 morpholino at 2dpi with ~200 CFU of *Δerp M. marinum (M. m).* Macrophage counts performed on confocal microscopy images of CHT.

(**B**) Mean *M.m* volume per infected macrophage in the CHT of *mpeg1:Brainbow*, *uxt*$^{+/-}$ incross larvae and siblings injected with tnfr1 morpholino at 2dpi with ~200 CFU of *Δerp M.m* . Volumetric analysis was performed on confocal microscopy image stacks.

(**C**) Confocal images of red fluorescent macrophages and blue fluorescent *M. marinum* in the caudal haematopoietic tissue of wildtype (**I**) and *Δuxt* crispant (**II**) larvae at 4dpi with ~120 CFU of *Δerp M. marinum.*

(**D**) Mean *M.m* volume per infected macrophage in the CHT of *mpeg1:Brainbow*, *Δuxt* crispant larvae and siblings injected with tnfr1 morpholino at 4dpi with ~120 CFU of *Δerp M.m*. Volumetric analysis was performed on confocal microscopy image stacks.

(**E**) Enumeration of fluorescent macrophages in the CHT of *mpeg1:Brainbow*, *Δuxt* crispant larvae and siblings injected with tnfr1 morpholino at 4dpi with ~120 CFU of *Δerp M.m.* Macrophage counts performed on confocal microscopy images of CHT.

(**F**) Total volume of intra-macrophage *M. m* in the CHT of *mpeg1:Brainbow*, *Δuxt* crispant larvae and siblings injected with tnfr1 morpholino at 4dpi with ~120 CFU of *Δerp M.m..* Volumetric analysis was performed on confocal microscopy image stacks.

(**G**) Enumeration of fluorescent macrophages in the CHT of *mpeg1:Brainbow*, *uxt*$^{+/-}$ incross larvae at 1 and 5dpi with ~200 CFU of *M. marinum.*

(**H**) Enumeration of fluorescent macrophages in the CHT of *mpeg1:Brainbow*, *uxt*$^{+/-}$ incross larvae at 5dpi with ~1000 heat killed *M. marinum.*

Statistical significance assessed by Kruskal Wallace test with Dunn's Multiple Comparison test n.s not significant ** $p<0.005$, **** $p<0.0001$

4.4 Macrophage death in *uxt* mutants cannot be rescued by inhibition of conventional cell death pathways

Our earlier observations that *uxt* deficient macrophages become depleted during infection despite showing normal microbicidal capacity and granuloma formation suggested that *uxt* deficiency may result in aberrant cell death during infection. In previous studies, UXT has been found to have an anti-apoptotic role following exposure of 293T cells to TNF in vitro and has also been shown to regulate the pro-apoptotic factor sterile α and HEAT armadillo motif-containing protein (SARM) [169,175]. We ruled out apoptosis as the cause of macrophage death in *uxt* mutants through treatment with the pan-caspase inhibitor Q-VD-OPh (Figure 8A) and by overexpression of the anti-apoptotic protein Bcl2 (Figure 8B), neither of which rescued *uxt* mutant hypersusceptibility. UXT has previously been shown to be an inhibitor of p53, a tumour suppressor gene known to regulate both apoptosis and cyclophilin D mediated programmed necrosis[176,177]. Neither knockout of p53 via CRISPR/cas9 (see methods) (Figure 8C) nor treatment with the cyclophilin inhibitor alisporivir, (Figure 8D) influenced *uxt* mutant hypersusceptibility. Programmed necrosis of infected macrophages in the context of elevated TNF has previously been described, in which activation of RIPK1 results in increased levels of reactive oxygen species (ROS) and culminates in mitochondrial Ca^{2+} overload, following Ca^{2+} uptake from L-type calcium channels[163]. However, this pathway does not appear to be operant in *uxt* mutants as neither treatment with the receptor-interacting serine/threonine-protein kinase 1 (RIPK1) inhibitor necrostatin-1 (Figure 8E) nor treatment with the ROS scavenger NAC (Figure 8F) alleviated the *uxt* infection phenotype. This was confirmed by treatment with the L-type calcium channel

inhibitors nifedipine and diltiazem (Figure 8G, H), neither of which impacted *uxt* mutant susceptibility, suggesting cell death in uxt mutants is independent of Ca^{2+} overload.

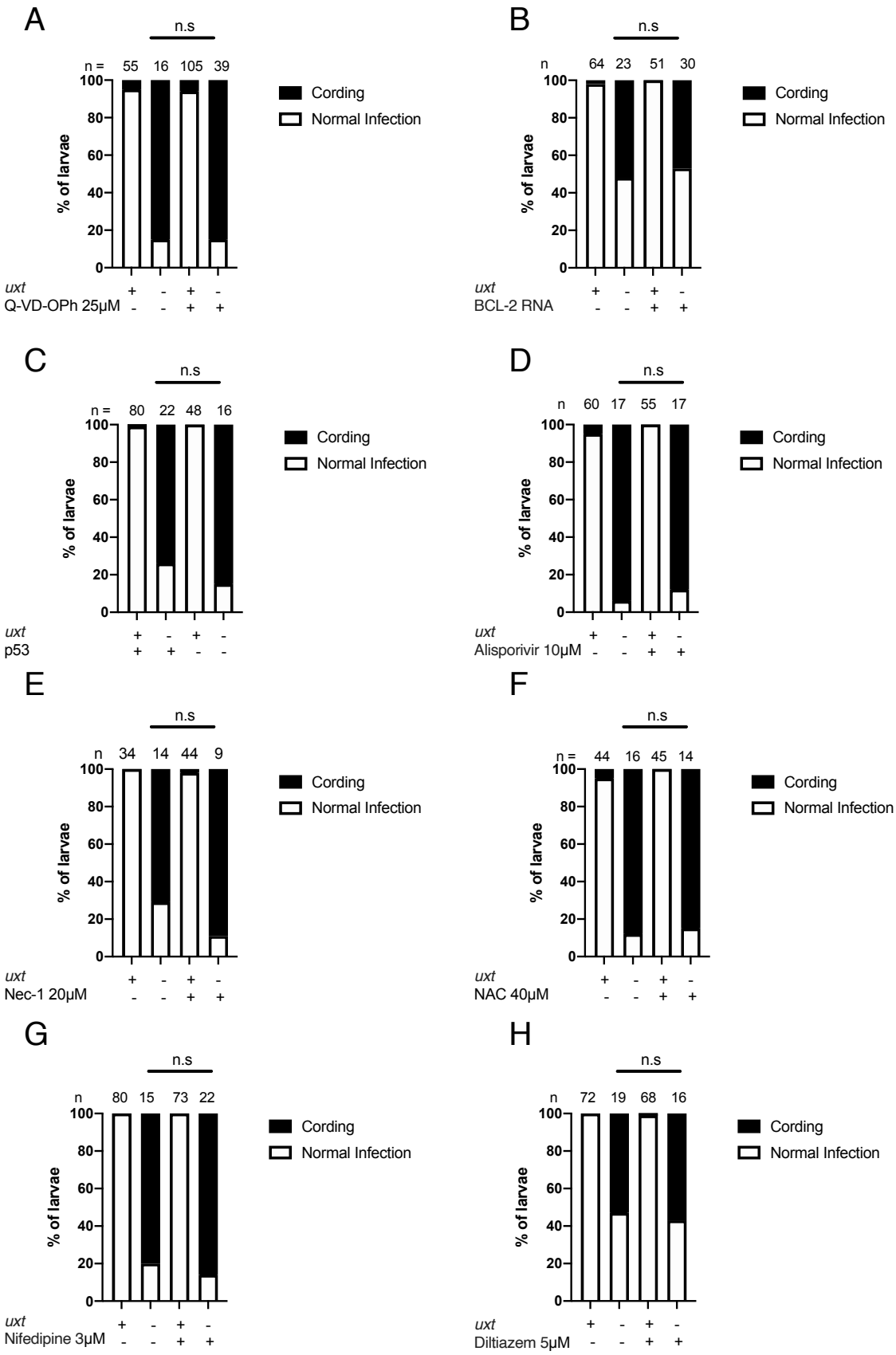
A
n.s
n = 55 16 105 39
% of larvae
100
80
60
40
20
0
Cording
Normal Infection
uxt + - + -
Q-VD-OPh 25μM - - + +
B
n.s
n 64 23 51 30
% of larvae
Cording
Normal Infection
uxt + - + -
BCL-2 RNA - - + +
C
n.s
n = 80 22 48 16
% of larvae
Cording
Normal Infection
uxt + - + -
p53 + + - -
D
n.s
n 60 17 55 17
% of larvae
Cording
Normal Infection
uxt + - + -
Alisporivir 10μM - - + +
E
n.s
n 34 14 44 9
% of larvae
Cording
Normal Infection
uxt + - + -
Nec-1 20μM - - + +
F
n.s
n = 44 16 45 14
% of larvae
Cording
Normal Infection
uxt + - + -
NAC 40μM - - + +
G
n.s
n 80 15 73 22
% of larvae
Cording
Normal Infection
uxt + - + -
Nifedipine 3μM - - + +
H
n.s
n 72 19 68 16
% of larvae
Cording
Normal Infection
uxt + - + -
Diltiazem 5μM - - + +

Figure 8
Macrophages in Uxt deficient animals have normal microbicidal capacity but become depleted during infection

(**A**) Quantification of bacterial cording in *uxt*$^{+/-}$ in cross larvae treated with Q-VD-OPh or DMSO control at 5dpi with ~200 CFU of *M. marinum.*

(**B**) Quantification of bacterial cording in *uxt*$^{+/-}$ in cross larvae injected with *bcl2* RNA or vehicle control at 5dpi with ~100 CFU of *M. marinum.*

(**C**) Quantification of bacterial cording in *Δp53 crispant uxt*$^{+/-}$ in cross larvae and sibling controls at 5dpi with ~150 CFU of *M. marinum.*

(**D**) Quantification of bacterial cording in *uxt*$^{+/-}$ in cross larvae treated with alisporivir or DMSO control at 5dpi with ~220 CFU of *M. marinum.*

(**E**) Quantification of bacterial cording in *uxt*$^{+/-}$ in cross larvae treated with necrostatin-1 (Nec-1) or DMSO control at 5dpi with ~200 CFU of *M. marinum.*

(**F**) Quantification of bacterial cording in *uxt*$^{+/-}$ in cross larvae treated with NAC or DMSO control at 5dpi with ~150 CFU of *M. marinum.*

(**G**) Quantification of bacterial cording in *uxt*$^{+/-}$ in cross larvae treated with nifedipine or DMSO control at 5dpi with ~200 CFU of *M. marinum.*

(**H**) Quantification of bacterial cording in *uxt*$^{+/-}$ in cross larvae treated with diltiazem or DMSO control at 5dpi with ~100 CFU of *M. marinum.*

(**A-H**) Statistical significance assed with Fisher's exact test. n.s not significant.

(**A,D,E,F,G,H**) All pharmacological inhibitors added to fish water at stated concentrations and changed every 24 hours.

4.5 Discussion – Characterisation of *uxt* mutant phenotype

uxt mutants have a complex phenotype, with those at baseline and after infection being contradictory at first glance. At baseline, *uxt* mutants have an increase in macrophage numbers which would be expected to confer resistance to infection, yet show increased suseptiblity[170]. While morphologically abnormal at baseline in addition to showing downregulation of macrophage associated genes as measured by RNA-seq (Appendix 3), *uxt* mutant macrophages appear to function normally during the initial stages of infection, as evidenced by their normal microbicidal capacity and ability to form granulomata.

The cellular basis of susceptibility to mycobacterial infection in Uxt deficient larvae appears to stem from increased macrophage death in the granuloma. However, inhibition of conventional cell death pathways has thus far failed to alleviate infection susceptibility in *uxt* mutant larvae (Figure 9). UXT deficiency has previously been associated with apoptosis in the context of inflammation but susceptibility of *uxt* mutants could not be relieved through pan-caspase inhibition or by overexpression of *bcl2*[166,175,176]. The caspase independence of the *uxt* phenotype also excludes pyroptosis (a modality of cell death in which caspase activation facilitates formation of plasma membrane pores by gasdermin proteins) as a potential means of cell death[178]. Ferroptosis is another form of regulated cell death in which there is a failure of glutathione antioxidant defences resulting in accumulation of toxic lipid peroxidases which has been shown to occur in *M. tuberculosis* infected macrophages in vitro[179]. However, replenishment of glutathione through treatment with NAC in Uxt deficient larvae did not rescue susceptibility. The RIPK1

independence of the *uxt* phenotype is also informative, as RIPK1 activity is associated with several modes of cell death including necroptosis (where RIPK1 activation of RIPK3 leads to oligomerisation of mixed lineage kinase domain-like protein which mediates membrane permeabilization) in addition to the previously described pathway of regulated cell death in *M. marinum*- infected macrophages with excess TNF[163,178]. Opening of mitochondrial permeability transition pores in response to cellular stressors such as Ca^{2+} overload and oxidative stress can result in cell death following dissipation of mitochondrial membrane potential and breakdown of mitochondrial membranes[178]. I have also shown that neither treatment with a ROS scavenger, nor inhibition of L-type calcium channels nor cyclophilin inhibition rescues *uxt* mutant susceptibility suggesting that cell death in *uxt* mutants is not dependent on opening of mitochondrial permeability transition pores.

While the mechanism of cell death in *uxt* mutants remains elusive, there are still modalities of regulated cell death that have not been assessed. Parthanatos is a caspase independent form of regulated cell death caused poly (ADP-ribose) polymerase 1 (PARP-1) overactivation[178]. PARP-1 becomes activated following DNA damage and facilitates recruitment of DNA repair machinery through modification of proteins adjacent to the site of damage with ADP-ribose derived from cleavage of NAD^{+}[180]. In instances with excessive DNA damage, overactivation of PARP-1 leads cell death due to the metabolic collapse following depletion of NAD^{+} and DNA fragmentation due to accumulation of ADP-ribose polymers promoting translocation of mitochondrial associated 1 (AIF) to the nucleus[178,180]. Parthanatos has been found to be operant in macrophages following oxidative stress induced by LPS exposure[181]. To test if parthanatos is occurring in *uxt* mutant macrophages, *uxt*$^{+/-}$

Δ*parp-1* crispant larvae will be generated and screened. Alternatively, the possibility that *uxt* mutant macrophages undergo lysosome dependent cell death has not been excluded. Lysosome dependent cell death occurs following permeabilization of lysosomal membranes resulting in the release of proteolytic cathepsins into the cytosol[178]. While lysosomal permeabilization can occur due to apoptotic signalling it can also proceed due to pore formation mediated by Bcl2- associated X protein (BAX)[178,182]. If cell death in *uxt* mutants is due to lysosomal destabilisation, depletion of lysosomal cathepsins or inhibition of *bax* may rescue susceptibility to infection.

Although all of the pharmacological inhibitors of cell death used in this study have previously been used in zebrafish (Table 2), their efficacy is unclear due to lack of sufficient validation and controls. For instance, while the pancaspase inhibitor Q-VD-OPh has been shown to be effective in inhibiting apoptosis of infected granuloma macrophages in zebrafish over 24 hours, it's efficacy over longer periods is unclear[183]. It also remains a possibility that any beneficial effect from caspase inhibition in *uxt* mutants may be masked by the occurrence secondary necrosis of infected macrophages.. Additionally, while BCL2 overexpression has been shown to reduce apoptosis both in vivo and in vitro, in this study unlabelled RNA was injected into embryos with no means of confirming ongoing expression at the time of screening[184]. In future this could be addressed through the generation of a transgenic zebrafish line expressing labelled BCL2. Investigating excessive apoptosis as a potential mechanism of susceptibility is further complicated by the difficulty in devising a suitable positive control for such studies in zebrafish, This would ideally require a control line demonstrated to have increased susceptibility to infection as a result of excess apoptosis, of which there are no known examples.

While a positive control for the apoptosis studies is difficult, the other inhibitors used in this study have previously been shown to alleviate macrophage death as a consequence of elevated TNF in infected larvae (Table 2)[163]. Infected larvae injected with TNF could therefore serve positive controls to verify efficacy of the majority of pharmacological inhibitors used in this study. Another complimentary approach to investigate cell death in *uxt* mutants would be adopting a genetic approach to disrupt factors required for a given modality of regulated cell death in *uxt* mutants. For example apoptosis could be inhibited through genetic disruption of caspase-9, an initiator caspase required for intrinsic apoptosis[185].

Regardless of the precise means of cell death, this study has shown that *uxt* is important in the context of mycobacterial immunity. Additionally, *uxt* appears protective against infection with *Salmonella enterica* var.Typhimurium, with increased mortality observed in *uxt* mutants relative to wildtype siblings (Figure 10).

A question which remains outstanding is whether the phenotype observed in *uxt* deficient macrophages is cell autonomous or secondary to *uxt* deficiency in other cell types, this is particularly pertinent as *uxt* is broadly expressed and required for adult viability. There are several approaches which could be used to address this such as the generation of macrophage specific *uxt* knockouts. This could be done through utilisation of the CRISPR/cas9 system to induce cre-lox recombination targeting of *uxt* in macrophages or through transgenesis engineer fish selectively expressing cas9 in macrophages in addition to guide RNA specific for *uxt* (described in Chapter 1.4). A complimentary approach would be to attempt rescue infection susceptibility of the *uxt* mutant larvae isolated in this study through transgenesis using a construct containing *uxt* on a macrophage specific promoter.

It should be noted however that this study has demonstrated that Uxt deficiency results in death of macrophages upon infection and with the exception of extrinsic apoptosis (which does not appear to be operant in this context) cell death is a generally a cell autonomous process[178]. This is suggestive of a macrophage autonomous role for *uxt* in infection, though this does not exclude a broader contribution of *uxt* expression in other cell types.

Inhibitor	Action	Published use in Zebrafish	Reference(s)
Q-VD-OPh	Pan-caspase Inhibitor	Reduction of TUNEL staining in granuloma *M. marinum* infected macrophages. Reduction of acridine orange and TUNEL staining in *fad24* mutant larvae with aberrant myocyte apoptosis	Yang et al. 2012[183] Walters et al. 2008[186]
Alisporivir	Cyclophilin Inhibitor	Rescue of mitochondrial permeability transition pore dependent programmed necrosis of macrophages infected with *M. marinum* in zebrafish with elevated TNF.	Roca et al. 2013[162] Roca et al. 2019[163]
Necrostatin-1	RIPK1 Inhibitor	Rescue of *ripk1* dependent programmed necrosis of macrophages infected with *M. marinum* in zebrafish with elevated TNF. Rescue of photoreceptor necroptosis in *pde6c* deficient zebrafish	Roca et al. 2013[162] Roca et al. 2019[163] Viringipurampeer et al. 2013[187]

Inhibitor	Action	Published use in Zebrafish	Reference(s)
N-Acertyl Cysteine	ROS scavenger	Rescue of mitochondrial ROS dependent programmed necrosis of macrophages infected with *M. marinum* in zebrafish with elevated TNF. Reversal of oxidative damaged induced by unpredictable chronic stress in adult zebrafish	Roca et al. 2013[162] Moceilin et al. 2019[188]
Nifedipine	L-type calcium channel inhibition	Prevention of mitochondrial Ca^{2+} overload and subsequent programmed necrosis of macrophages infected with *M. marinum* in zebrafish with elevated TNF.	Roca et al. 2019[163]
Diltiazem	L-type calcium channel inhibition	Prevention of mitochondrial Ca^{2+} overload and subsequent programmed necrosis of macrophages infected with *M. marinum* in zebrafish with elevated TNF.	Roca et al. 2019[163]

Table 2

Pharmacological inhibitors of cell death used in this study and their prior application in zebrafish

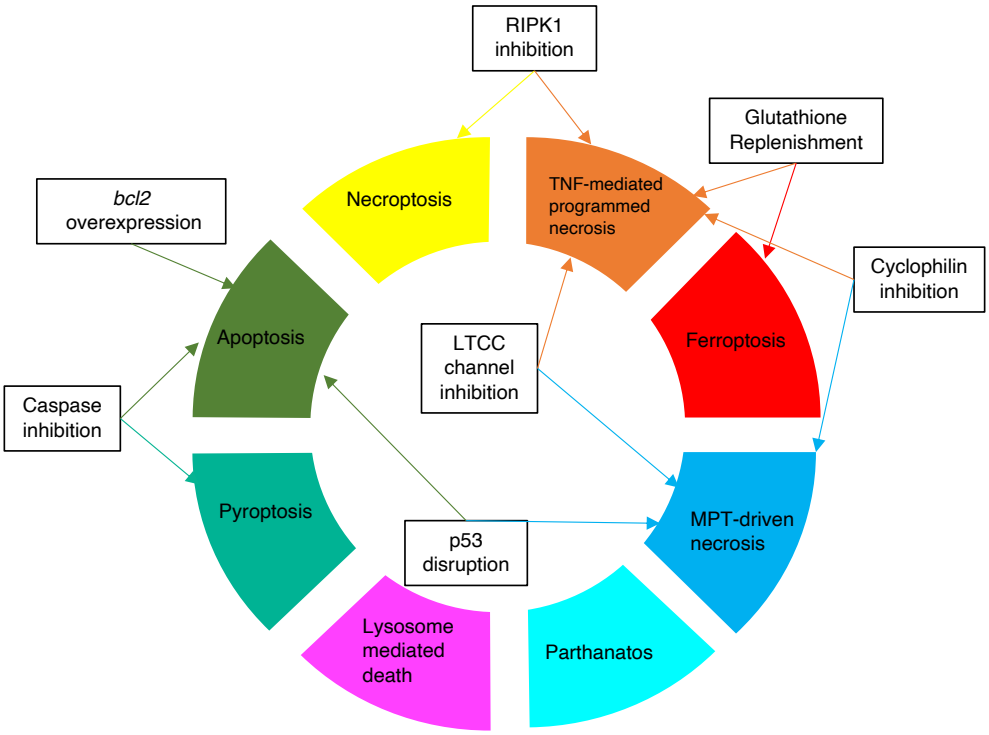

Figure 9
Pathways of regulated cell death (labelled segments) with interventions used in this study attempting to ameliorate cell death in *uxt* mutants (boxes). Arrows represent the modes of cell death disrupted by a given intervention. None of the listed interventions were able to reverse *uxt* mutant susceptibility to infection.

N.B
MPT: mitochondrial permeability transition pore

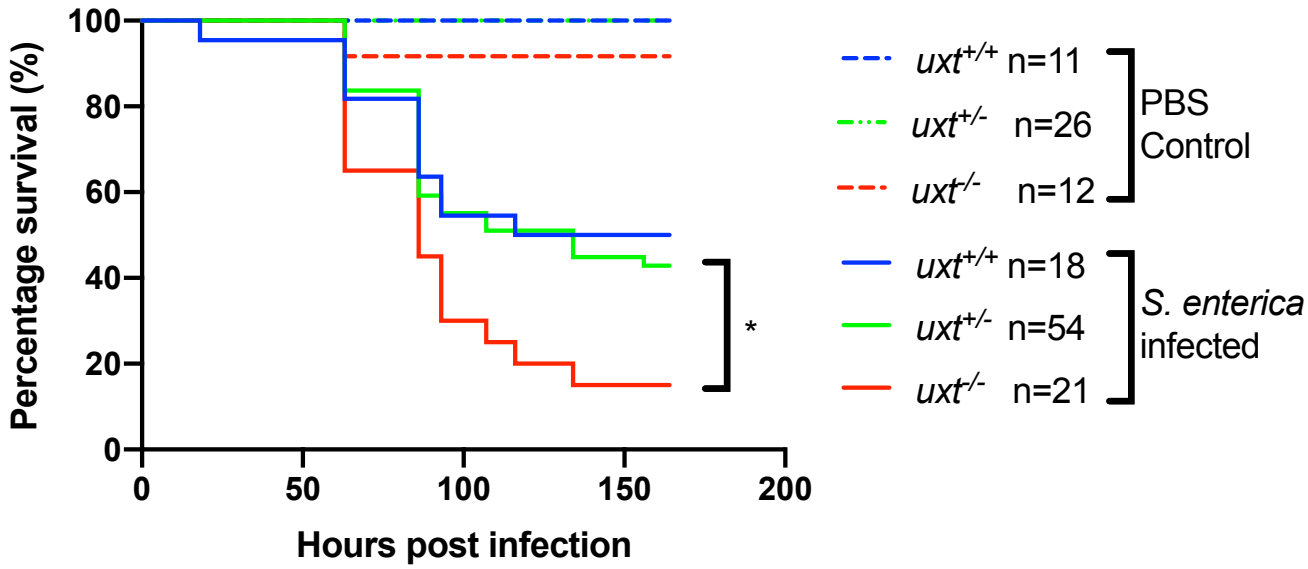

Figure 10
uxt mutant larvae show reduced survival following infection with *Salmonella enterica var.* Typhimurium

Survival of *uxt*$^{+/-}$ incross larvae injected at 2dpf with either ~180 CFU *Salmonella enterica var.* Typhimurium or PBS via the caudal artery. Data for uxt$^{+/+}$ and uxt$^{+/-}$ combined as 'WT' group.

Statistical significance assed with Mantel-Cox test. p = 0.0206

Chapter 5

Prefoldins and mycobacterial infection

5.1 Introduction to Prefoldins

UXT is a member of the prefoldin family of proteins and was initially isolated in 1999 following exon trapping on P1-based artificial chromosomes mapping to the human genomic region Xp11[189]. This study demonstrated that UXT is a 157 amino acid protein which shows 90% amino acid identity between mice and human orthologs but lacked homology with other mapped genes[189]. Subsequent analysis indicated that *UXT* was broadly expressed across adult tissues (consequently being dubbed 'ubiquitously expressed transcript'), as well as in a variety of tumour types[189].

Shortly before the isolation of UXT, prefoldin- a hexameric chaperone complex composed of prefoldin family monomers (excluding UXT) was discovered[190]. The prefoldin complex was identified independently in both mammalian cells as a species binding unfolded actin in reticulocyte lysate and in a forward genetic study in yeast aiming to identify genes required for viability in γ-tubulin mutants[191,192]. Functional analysis of the mammalian prefoldin complex demonstrated it selectively binds and transfers unfolded actin and tubulin to the cytosolic chaperonin c-cpn resulting in productive folding[192]. Subsequent purification demonstrated prefoldin is a 200 kDa complex consisting of 6 polypeptides termed prefoldin (PFDN) 1-6[192]. Deletion of prefoldin complex monomers in *Saccharomyces cerevisiae* led to a range phenotypes including reduced proliferation and increased sensitivity to cold and osmotic stress as a consequence of abnormal cytoskeletal formation[191,192]. The importance of the prefoldin complex in cytoskeletal assembly appears to be conserved across eukaryotes, as the aforementioned phenotypes in prefoldin knockout yeast could be rescued through exogenous expression of human and plant orthologs of prefoldin monomers[191–193]. The prefoldin complex also

appears to have additional roles and has shown to limit protein aggregation during endoplasmic reticulum stress and proteasome inhibition[194].

The prefoldin complex is evolutionary ancient and thought to originate in archaea in which prefoldin monomers show a high-level sequence and secondary structural conservation relative to eukaryotic orthologs[195,196]. While prefoldin in eukaryotes shows narrow substrate specificity, archaeal prefoldin recognises a wide range of unfolded polypeptides and functions as a broadly acting co-chaperone of ATP-dependent chaperonins[196–198].

The structure of the prefoldin complex has been solved in the archaebacteria *Methanobacterium thermoautotrophicum* by X-ray crystallography[195]. This demonstrated prefoldin monomers have highly organised structures and can be divided into two groups termed α (corresponding to eukaryotic PFDN3 and 5) and β class (PFDN1,2,4 and 6) prefoldins based on secondary structural elements[195]. All prefoldin monomers share a basic structure of a coiled coil which is connected by either one or two β hairpins in β and α class prefoldins respectively[195]. The prefoldin hexamer consists of two α and four β prefoldin subunits and is assembled via interactions between β hairpins of the constituent monomers[195]. The structural core of the complex is formed by a dimer of α class prefoldins to which the four β class prefoldins bind[195]. The assembled prefoldin complex resembles a flower with a pistil composed of double β barrel formed by β hairpins of the prefoldin monomers whose coiled coils resemble petals (Appendix 5)[195]. This basic structure appears to be shared by eukaryotic prefoldin as shown by electron microscopy[199].

While the structure and primary role of the prefoldin complex is somewhat well characterised the contribution and function of the individual prefoldin monomers

remains largely unknown. Mice will a null mutation in *Pfdn1* develop to term but do not survive beyond 5 weeks and manifest a variety of phenotypes, including ciliary dyskinesia and neuronal degeneration indicative of cytoskeletal defects in addition to hydrocephaly and impaired development and function of lymphocytes[200]. Mice with a missense mutation in *Pfdn5* also showed neuronal degeneration and hydrocephaly, but defects appeared to be largely restricted to the nervous system, with the exception of male sterility [201]. Differences in the phenotypes in *Pfdn1* and *Pfdn5* mice may be due to differences in the nature of the mutations used in these studies but may also be due to as yet uncharacterised roles of individual prefoldin monomers. The in vivo relevance and the function of other prefoldin complex monomers remains largely unknown.

Unlike PFDN 1-6, UXT is not part of the prefoldin complex and appears to have evolved from prefoldin complex monomers during the Cambrian period in Olfactores as evidenced by the presence of *UXT* orthologs exclusively in tunicates and vertebrates[165]. Prefoldin family proteins such as UXT which do not form part of the prefoldin chaperone complex are known as non-canonical prefoldins. UXT in conjunction with both canonical and other non-canonical prefoldins forms a multimeric protein complex variously called the UXT/URI1 complex or the non-canonical prefoldin like complex (PFDL)[190,198]. The PFDL was first discovered in 2003 when UXT was isolated following yeast-two hybrid experiments aiming to identify novel binding partners of E3 ubiquitin-protein ligase S-phase kinase-associated protein 2 (SKP2), a protein involved in cell cycle regulation[202]. Subsequent immunoprecipitation and mass spectrometry demonstrated that UXT formed part of a multimeric protein complex also containing the prefoldin monomers

PFDN6, PFDN2 in addition to the non-canonical prefoldins URI1 (unconventional prefoldin RPB5 interactor) and PDRG1 (p53 and DNA damage regulated 1) [202]. Although the structure of this complex has not been solved it is thought to share a similar basic structure to the prefoldin complex as it consists of 2 alpha class prefoldins, UXT and URI1 in addition to the beta-class prefoldins PFDN6, PFND2 and PDRG1 (Appendix 5)[190,198].

The cellular role of the PFDL is relatively unclear but appears have activity as a chaperone, though shows different substrate specificity to the prefoldin complex. The best characterised substrate of the PFDL is RNA polymerase II, which is mediated through a specific interaction between URI1 and RNA polymerase II subunit E (POL2RE)[203,204]. The PFDL acts as a co-chaperone in conjunction with HSP90 to promote assembly of RNA polymerase complex II in the cytosol but also negatively regulates RNA polymerase transcriptional activity in the nucleus [198,203–205]. The PFDL also regulates transcription through an interaction of URI1 with the general transcription factor IIF (TFIIF). URI1 overexpression in COS1 cells reduced Gal-VP16 activated transcription and was dependent on URI1 binding to TFIIF[206] . The chaperone activity of the PFDL also contributes in the assembly of the phosphatidylinositol-3-kinase-related protein kinases, including mammalian target of rapamycin (mtor)[207].

UXT has been associated with a range of cellular processes and appears to specifically influence transcription independently of the PFDL role in RNA polymerase assembly. UXT has been shown to directly bind to androgen receptor and acts in tandem with URI1 to regulate androgen receptor signalling in prostate cancer cells[208,209]. UXT also interacts and modulates oestrogen receptor activity in

breast cancer cells with UXT knockdown associated with increased oestrogen receptor transcriptional activity in vitro. UXT also inhibits the transcription factor EVI1, with UXT binding associated with reduced EVI1 mediated cell transformation in vitro [167,210].

UXT influences inflammatory signalling as a component of the NF-kappa-B enhanceosome and appears to exert this role through forming a complex with p65 upon TNF-α stimulation[166]. UXT knockdown is associated with abrogated expression of antiviral factors and increased susceptibility to vesicular stomatitis virus in cultured cells as a consequence of reduced NF-κB signalling[168]. As previously mentioned, UXT has been implicated in cell survival both by regulating SARM mediated apoptosis and protecting against TNF mediated apoptosis and exerts these roles through direct interaction with mediators of cell death[169,175]. UXT regulates TNF mediated apoptosis by binding to TNF receptor-associated factor 2 (TRAF2) and preventing recruitment of Fas-associated protein with death domain (FADD) to TNF receptor complex I, inhibiting formation of the pro-apoptotic TNF receptor complex II and subsequent caspase activation and apoptosis[169]. While there is little characterisation of UXT vivo, constitutive deletion in mice resulted in embryonic lethality (as was found to be the case in zebrafish in this study), and a conditional knockout in the male germline resulted in male sterility, a mirroring *Pfdn5* knockout mice[201,211]. Morpholino knockout of zebrafish *uxt* has been associated with aberrant angiogenesis and gross morphological defects from 24 hours post fertilisation which was attributed to a reduction in notch signalling[212]. However morphological defects are not observed in the larvae with *uxt* nonsense mutations used in this study even at 7dpf (Appendix 6) and uxt mutant larvae had empirically normal circulation (data

not shown). This discrepancy may be related to morpholino off-target effects or potentially as a consequence of UXT maternal RNA translation in the mutants used in this study relieving early developmental phenotypes.

While UXT is involved in a variety of cellular processes, the extent to which the aforementioned functions of UXT are dependent on the wider PFDL is generally unclear. However, siRNA mediated URI1 depletion in LNCaP prostate cancer cells in vitro results in increased degradation of UXT (and vice versa) with abrogation of UXT/URI1 mediated regulation of androgen receptor signalling[208]. This illustrates that at least some aspects of UXT functionality are dependent on other PFDL monomers. Given the importance of *uxt* in immunity against mycobacteria has been demonstrated we next sought to establish whether other prefoldins share this role.

5.2 Disruption of *uri1* and *pfdn6* is associated with mycobacterial cording

To ascertain whether other members of the PFDL complex were required for antimycobacterial immunity Δ*pfdn2*, *Δpfdn6*, *Δuri1*, *Δpdrg1* G0 crispant larvae were generated (see methods) and infected with *M. marinum*. *Δuri1* and *Δpfdn6* larvae were hypersusceptible to infection with extensive bacterial cording at 5dpi (Figure 11A, B), whereas *Δpdrg1* and *Δpfdn2* larvae were non-phenotypic (Figure11C, D).

5.3 Uri1 deficient larvae show increased susceptibility to infection relative to *uxt* mutants

As *Δuri1* larvae showed increased susceptibility to infection and URI1 and UXT have previously been shown to stabilise each other in vitro, we next sought to compare the infection phenotypes associated Uri1 with Uxt deficiency. *Δuri1* crispant

uxt$^{+/-}$ incross larvae where generated and then infected with *M. marinum*. This showed that Uri1 deficient larvae showed increased susceptibility to infection relative to *uxt* mutant siblings (Figure 12A, B). *uxt*$^{-/-}$ *Δuri* double knockout larvae showed no additive increase in bacterial burden or the portion of larvae with bacterial cording relative to *Δuri* single mutants (Figure 12A, B).

5.4 Uri1 deficiency reverses baseline macrophage increase of *uxt* mutants

To further investigate whether *uri1* deficiency phenocopies *uxt* mutants, we next assessed baseline macrophage number and morphology in *Δuri1* crispant *uxt*$^{+/-}$ incross larvae. *Δuri* larvae had normal numbers of macrophages which displayed normal morphology at 5dpf, whereas *uxt* mutant *larvae* showed increased numbers of abnormal macrophages as previously observed (Figure 12C, D). *uxt*$^{-/-}$ *Δuri* double mutant larvae showed normal macrophage numbers and sphericity (Figure 12C, D).

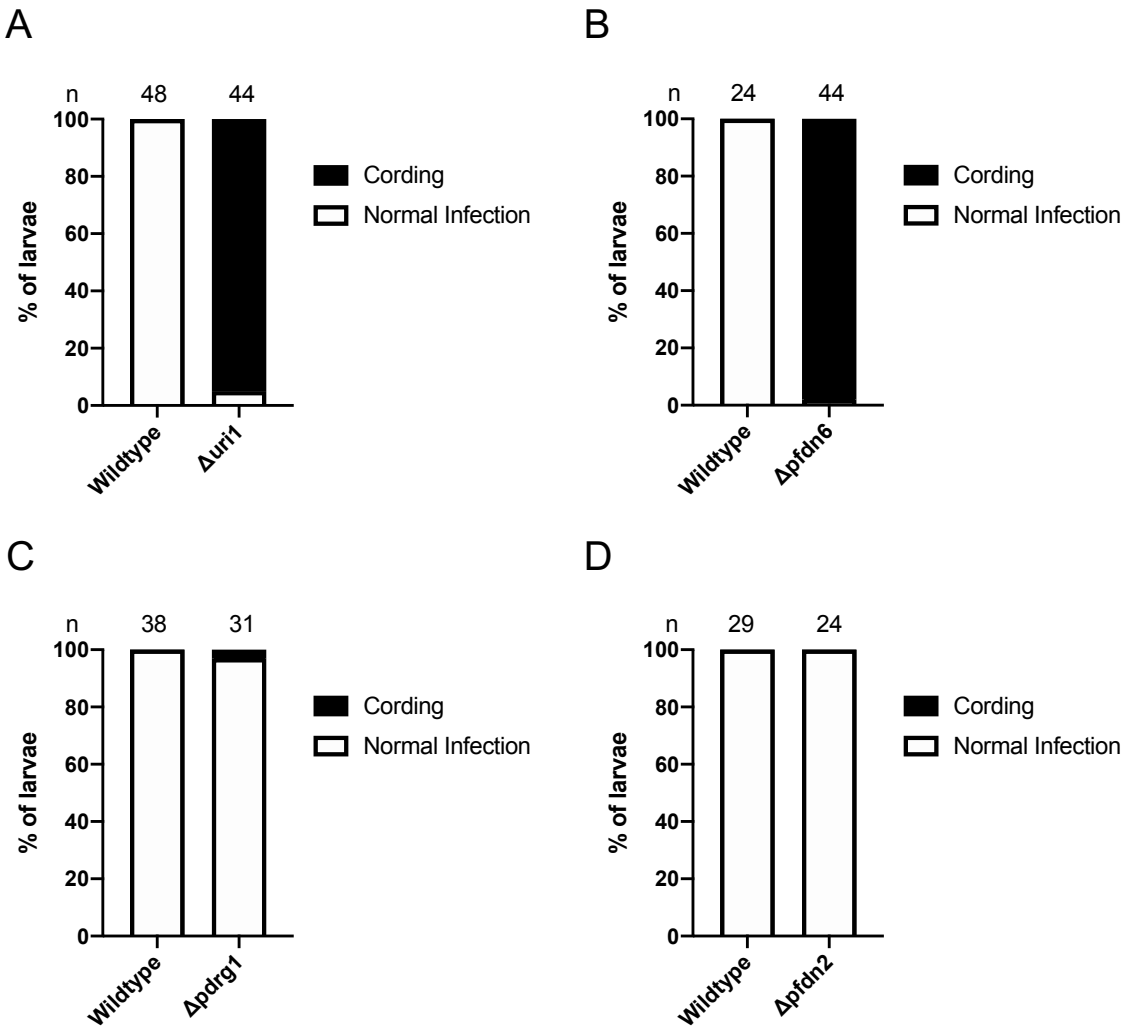

Figure 11
Δpfdn2 and *Δuri1 l*arvae are hypersusceptible to *M. marinum*

(A) Quantification of bacterial cording in Δ*uri1* crispant larvae and sibling controls at 5dpi with ~150 CFU of *M. marinum.*

(**B**) Quantification of bacterial cording in Δ*pfdn6* crispant larvae and sibling controls at 5dpi with ~180 CFU of *M. marinum.*

(C) Quantification of bacterial cording in Δ*pdrg1* crispant larvae and sibling controls at 5dpi with ~200 CFU of *M. marinum.*

(D) Quantification of bacterial cording in Δ*pfdn2* crispant larvae and sibling controls at 5dpi with ~200 CFU of *M. marinum.*

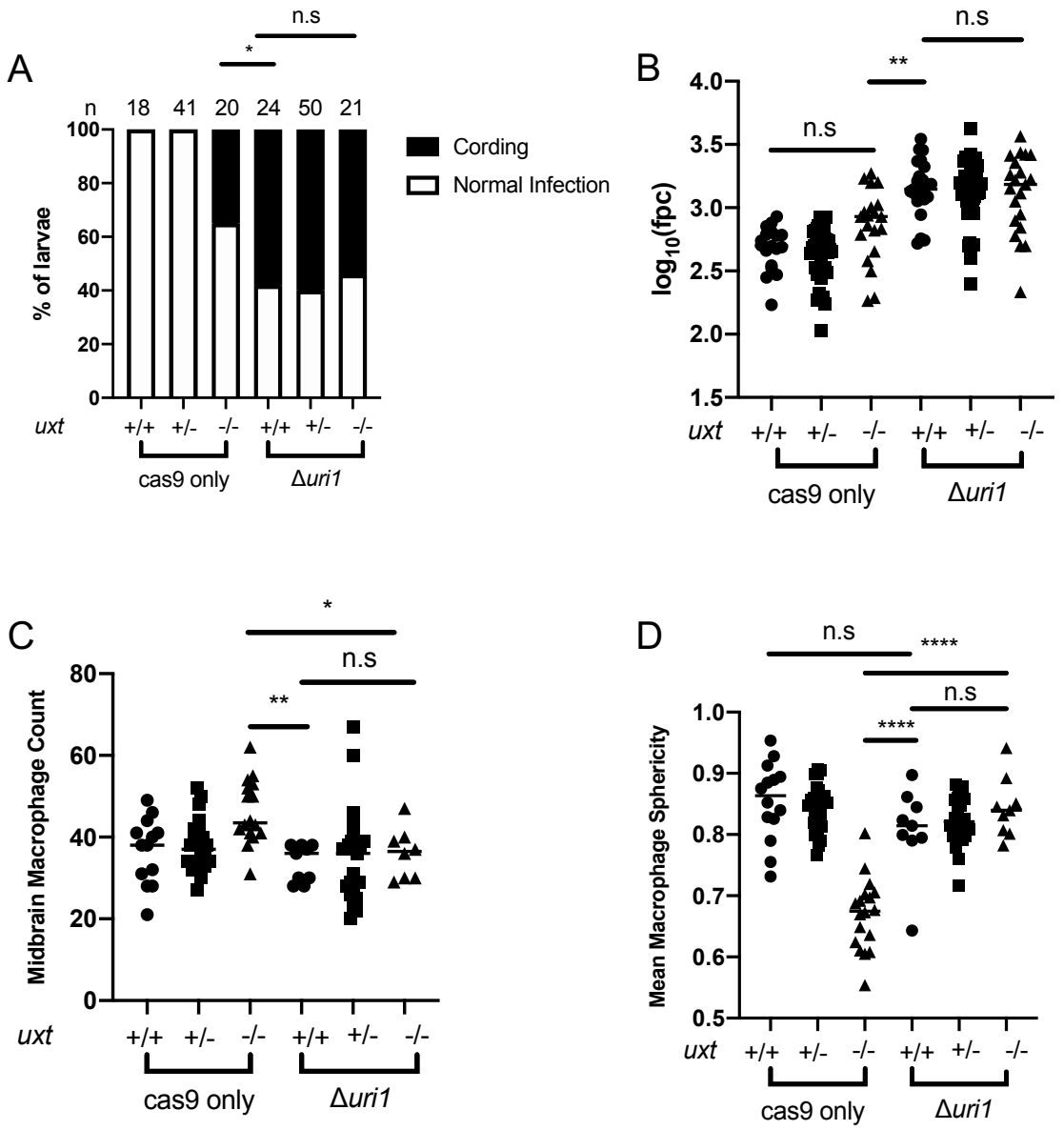

Figure 12
Δuri1 larvae show greater susceptibility to infection relative to *uxt* mutants. Uri1 depletion reverses baseline *uxt* macrophage phenotypes.

(**A**) Quantification of bacterial cording in *Δuri1 crispant uxt*$^{+/-}$ in cross larvae and sibling controls injected with unconjugated cas9 at 5dpi with ~70 CFU of *M. marinum.*

(**B**) Quantification of *M. marinum* burden measured by fluorescent pixel count (fpc) in *Δuri1 uxt*$^{+/-}$ incross larvae and sibling controls injected with unconjugated cas9.

(**C** and **D**) Mean volume (**C**) and sphericity (**D**) of macrophages in the midbrain of uninfected *mpeg1:Brainbow*, *Δuri1 uxt*$^{+/-}$ incross larvae at 5dpf and sibling controls injected with unconjugated cas9. Volume and sphericity quantification performed on confocal image stacks.

5.5 Discussion

The study of larvae with disruptive mutations in other members of the PFDL, attempted to resolve the molecular basis of susceptibility in *uxt* mutants, but has instead added additional complexity. I have demonstrated a differential requirement of PFDL components in immunity and in so doing have identified two novel genes required for immunity against mycobacteria, *pfdn6* and *uri1.*

The finding that Uri1 deficiency reverses the baseline macrophage phenotypes in *uxt* mutants is perplexing and suggests that the abnormal macrophage morphology observed in Uxt deficient animals may be disassociated from their susceptibility to infection.

A potential explanation as to why Uri1 depletion 'rescues' baseline macrophage phenotypes in *uxt* mutants could be that Uxt inhibits a hitherto unknown function of Uri1 at baseline. Uxt deficiency could then result in increased Uri1 activity leading to abnormal macrophage morphology which can then be rescued by Uri1 depletion, though there is no published evidence to support such a mechanism.

The finding that Uri1 deficient animals show increased susceptibility to infection relative to *uxt* mutants, may indicate that Uxt mediated protection of macrophages is exerted through the actions of other PFDL monomers.
As previously mentioned, depletion of URI1 in vitro is associated with increased cellular degradation of UXT and vice versa presumably reflecting the role of these proteins in the stability of the PFDL[203,208]. This is perhaps unsurprising given that Uxt and Uri1 are both α-class prefoldins, and that in the canonical prefoldin complex a dimer of α-class prefoldins forms the structural core to which β class prefoldins adhere[195]. It is notable that disruption of only one β class prefoldin (Pfdn6) resulted

in infection susceptibility. This indicates Pfdn6 either has a role in stabilising the PFDL not shared by other β class prefoldins, or a specific interaction required for immunity.

It remains possible that the observed phenotypes following disruption of PFDL monomers are independent but the finding that *uxt* deficiency does not lead to increased bacterial burden in Δ*uri* larvae suggests that they confer susceptibility due to the same biological pathway. It is unknown if any components of the PFDL are biologically active as monomers or form part of another cellular complex (besides the canonical prefoldin complex). This could be further investigated by designing and expressing modified forms of PFDL monomers which are unable to oligomerize. Substrate specificity of canonical prefoldins is determined by their coiled coil whereas oligomerization with other prefoldins is mediated β-hairpins, which could potentially be perturbed in PFDL monomers.

Lastly, the early embryonic lethality associated with depletion of Pfnd1,3,4,5 is notable as these proteins are monomers of the prefoldin complex but are not found in the PFDL, whereas disruption of monomers presents in both complexes (Pfdn2,6) was associated with minimal toxicity. This could potentially be due to off target cas9 mediated DNA cleavage, as prior studies have shown that Pfdn1 and Pfdn5 germline mutants survived to term in mice[200,201]. Alternatively, this could indicate monomers exclusive to the canonical prefoldin complex have additional (or at least non-redundant) activity in the zebrafish relative to mammalian orthologs.

Chapter 6

Future Directions

There remain many outstanding questions regarding the role of Uxt which warrant further investigation. The modality of cell death in *uxt* deficient macrophages during infection remains unclear (as discussed in Chapter 4.5) but characterisation of the mechanism is likely to have implications beyond mycobacterial immunity in understanding determinants of macrophage homeostasis and survival.

Prior characterisation of UXT indicates three main means by which Uxt deficiency may influence macrophage survival during infection. Firstly, UXT has been found to regulate apoptosis by direct interaction with cell death mediators (reviewed in Chapter 5.1) [169,175]. While apoptosis does not appear to be the cause of infection susceptibility in *uxt* deficient larvae, Uxt may directly regulate other mediators of cell death. Identification of the modality of cell death could guide immunoprecipitation or protein-proximity labelling based approaches in macrophages to identify UXT interaction partners associated with cell death for further study.

Secondly, UXT has been shown to influence transcription through interaction with various transcription factors and nuclear receptors, including NF-κB which has previously been shown to influence immunity and cell survival[166,167,209,210,213]. Loss of Uxt may result in dysregulation of an unknown transcription factor and a downstream effector resulting in cell death. Investigating a mechanism of *uxt*$^{-/-}$ susceptibility secondary to dysregulation of a transcription factor could be facilitated by performing RNA-seq on sorted infected macrophages from *uxt*$^{-/-}$ larvae followed by identification of dysregulated pathways. Additionally, the potential contribution of NF-κB signalling to the *uxt* mutant phenotype could initially be assessed through the use of a NF-κB zebrafish reporter line or genetic disruption of NF-κB signalling components[214]. While

the disruption of a transcription factor resulting in a downstream macrophage specific infection phenotype may seem improbable, this has been demonstrated in a mutant isolated from the previous genetic screen conducted in Seattle (reviewed in Chapter 2.9.1)[117].

Lastly, the PFDL to which UXT belongs regulates assembly and function of RNA polymerase II and further modulates transcription at a basic level through interaction with TFIIF[190,205,206]. Whole animal RNA-seq shows broad transcriptional changes in *uxt*$^{-/-}$ larvae with differential regulation of 2445 genes relative to wildtype siblings at 7dpf, corresponding to around 10% of all coding genes in zebrafish (Appendix 4)[215]. While this may simply be indicative of a 'sick fish', or partly due to other ENU induced mutations, *uxt*$^{-/-}$ larvae appear to be morphologically normal at 7dpf (Appendix 6) and remain viable until around 30dpf. Functional enrichment analysis of genes consistently upregulated at 3,5 and 7dpf in *uxt*$^{-/-}$ larvae shows overrepresentation of factors associated with RNA-metabolism (Appendix 7), with particularly robust expression of *pol2ra*, a subunit of RNA polymerase II (Appendix 4). Susceptibility secondary to a loss of PFDL mediated RNA polymerase complex II regulation could be investigated through the generation of a zebrafish line expressing Uri1 lacking the motifs required for Pol2re and Tfii2 interaction through transgenesis or using CRISPR homology directed repair[206]. However, it is difficult to envision how regulation of a fundamental cellular process at a basic level could indirectly result in the infection phenotype observed in this study.

While the amino acid sequence of UXT is well conserved across vertebrates, zebrafish and mice both have a single UXT isoform, whereas humans have two isoforms that appear to have distinct cellular roles[165]. The two human isoforms differ

by the inclusion of a small exon at the 5' end of the transcript encoding a 12 amino acid sequence which appears to function as both a TRAF binding motif as well as determining cellular localisation[168]. The longer UXT isoform is localised to the cytosol where it regulates both TNF mediated apoptosis as well as a serving as a component of the MAVS signalosome through interactions with TRAF2 and TRAF3 respectively[168,169]. All other studies of UXT function pertain to the shorter isoform which is localised to the nucleus[169,198]. The cellular localisation of zebrafish Uxt is not known and understanding this may provide clues into the mechanism by which Uxt regulates macrophage survival. This could be investigated through the generation of a transgenic zebrafish line expressing a fluorescently tagged form of Uxt. A complementary approach is to attempt rescue of the infection phenotype in *uxt*$^{-/-}$ larvae through exogenous expression of the different human UXT isoforms. Rescue by the cytosolic UXT isoform may indicate that the protective role of Uxt is dependent on interaction with TRAF proteins, which have been shown to regulate cell death in a variety of contexts[216]. Alternatively, rescue by the nuclear UXT isoform suggests the phenotype is due to a lack of Uxt mediated transcriptional regulation. Rescue by either isoform would provide important evidence that human UXT is functioning similarly to the zebrafish ortholog in promoting macrophage survival during mycobacterial infection.

It remains a possibility that the mechanism of susceptibility in Uxt deficient zebrafish macrophages is not operant in mammalian cells regardless of whether human UXT can rescue a phenotypic fish. This could be addressed through depletion of UXT in a human monocytic cell line such as THP-1, or in macrophages derived from peripheral blood monocular cells followed by infection and phenotyping.

If UXT deficiency also results in susceptibility to mycobacteria in human cells, subsequent rescue by expression of the zebrafish *uxt* ortholog would provide compelling evidence that UXT is fulfilling the same protective role during infection in both humans and zebrafish. Additionally, infection of UXT deficient human cells *with M. tuberculosis* would also be important in confirming whether UXT is relevant in immunity against tuberculosis.

While germline UXT deficiency is embryonic lethal in mice, the mammalian in vivo relevance of UXT in infection could be investigated through generation of a macrophage specific UXT knockout mouse line. This would also enable the application of anti-mouse antibodies and other immunological reagents in the profiling of *uxt* deficient macrophages in future studies. Furthermore, an inducible UXT knockout mouse could be used to investigate the importance of Uxt at different stages of infection, including following the onset of adaptive immunity which is not possible in the zebrafish larval model.

The in vivo relevance of human UXT, URI1 and PFN6 variants is not understood in any context. While overexpression of *UXT* in tumour cells has been variously associated with both positive and negative outcomes in cancer patients, mechanistic characterisation is lacking though is attributed to UXT mediated transcriptional regulation of androgen and oestrogen receptor signalling[167,198,208]. Germline variants in PFDL monomers have not yet been associated with pathology in individual patient studies or in GWAS studies[62,198]. However, this does not exclude a potential role for prefoldins in immunity and the 100 genome project has identified both common variants in regulatory regions as well as rare missense variants in *UXT*[217]. To investigate the importance of *UXT*, *URI1* and *PFDN6* alleles, patients

with tuberculosis could be genotyped along with healthy controls, followed by determination of whether variants are associated with infection acquisition or outcome.

This study was conducted with the aim of identifying novel determinants of tuberculosis outcome and has remained somewhat myopic in this task. As well as determining susceptibility to mycobacteria, *uxt* also appears to be required for immunity against *S. enterica* and there is also in vitro evidence that UXT is involved in signal transduction following infection with *Vesicular stomatitis virus (VSV)*[168]. It is currently unknown if *uxt* is required for immunity against other pathogens. Both *S enterica* and *M. marinum* (and *VSV*) are intracellular pathogens, it would be interesting to determine whether Uxt is also required for macrophage survival following infection with bacteria which preferentially remain extracellular or virulent fungi. Even more broadly, Uxt function may also be required for macrophage survival in response to non-infectious noxious stimuli. This could be tested by exposing *uxt*$^{-/-}$ larvae stimuli such as heat or nutrient deprivation followed by quantification of macrophage survival.

This study has focused exclusively on the role of Uxt in macrophages, despite the fact that *uxt* is a 'ubiquitously expressed transcript'. While susceptibility to mycobacterial infection appears to be due to macrophage death, *uxt* deficiency may impact function of other leucocyte populations during infection. This could be initially investigated by infecting *uxt* $^{-/-}$ larvae with Staphylococcus aureus, a pathogen which largely relies upon an effective neutrophil response for clearance, potentially followed by the creation of a neutrophil specific *uxt* knockout[218]. Using zebrafish larvae to characterise the role of *uxt* in leucocyte populations beyond macrophages

and neutrophils is complicated by a lack of characterisation of zebrafish leucocyte subsets (as well as a lack of adaptive immunity). Such studies however may be well be better suited for mouse studies due to their well characterised leucocyte subsets and tools for conditional mutagenesis.

In conclusion this study has identified a novel role for *uxt*, *uri1* and *pfdn6* in immunity against mycobacteria and provides the first in vivo evidence that prefoldins influence infection outcome and may represent a largely overlooked class of immune determinants. There remain however outstanding questions regarding the mechanism by which Uxt is able to protect macrophages during mycobacterial infection, and the broader relevance of Uxt and other PFDL components in immunity which are the subject of ongoing investigation.

.

Chapter 7

Methods

Zebrafish Husbandry

Zebrafish husbandry was performed in accordance with guidelines on the operation of the animals (scientific procedures) act issued by the UK home office. Embryos were initially maintained in fish water (reverse osmosis water supplemented with 0.18 g/l Instant Ocean) containing 0.25 µg/ml methylene blue. At 1dpf, larvae were then transferred to fish water containing 0.003% PTU (1-phenyl-2-thiourea, Sigma). Throughout development larvae were incubated at 28.5^{o}C.

Bacterial Strains and preparation

Wildtype *M. marinum* M strain (ATCC BAA-535) and its growth attenuated Δ*erp* derivative expressing either tdTomato or blue fluorescent protein under the control of the msp12 promoter were grown under hygromycin B (Formedium) selection in 7H9 Middlebrook's medium (Difco) supplemented with oleic acid, dextrose tween80 (Sigma) and albumin as previously described[98]. Single cell suspensions of *M. marinum* were prepared as previously described, this involved growing cultures to mid-log phase in 7H9OADC medium followed by repeated passage through a syringe and filtration[96]. Filtrate was then pelleted and resuspended in 7H9OADC before being divided into aliquots which were stored at -80^{o}C. *M. marinum* CFU/µl of aliquots was calculated by enumerating colony numbers following inculcation of diluted sample onto 7H10 plates supplemented with hygromycin.

Salmonella enterica var. Typhimurium (SL1344) was grown on the day of infection in Nutrient Broth (Merck) at 37^{o}C in a shaking incubator until OD_{600}1.0 was

reached and were harvested by centrifugation and re-suspended in PBS prior to infection.

Microscopy

Fluorescence microscopy was performed as previously described[96,170]. Assessment of *M. marinum* cording and burden in larvae was performed using a Nikon Eclipse Ti-E inverted microscope equipped with a 10x objective. Enumeration of macrophages in the CHT and trunk of larvae was performed on Nikon eclipse upright microscope using a 20x objective unless otherwise stated. Confocal microscopy was performed on larvae anesthetised with 0.025% MS222 and mounted in 1% agarose on optical bottom plates (MatTek Corporation) and imaged with a Nikon A1 confocal microscope. All confocal images were taken using a 20xPlan Apo 0.7 NA objective, acquired using a Galvano scanner and recorded with NIS elements software v4.3 (Nikon). Confocal still images were acquired as 35-50µm z stacks with optical sections taken at 2µm intervals. Tracking of macrophages in uninfected and infected animals was performed on confocal time-lapse microscopy images taken at 90 second intervals over 2 hours, consisting of 36µm z stacks with optical sections taken at 2µm intervals. Macrophage tracking, volumetric analysis and sphericity quantification was performed using surface rendering and tracking features of Imaris v8.0 (Bitplane Scientific Software). Enumeration of macrophages in confocal images performed using FIJI v2.0.0 (NIH).

Larval infection

Larval zebrafish infections were performed as previously described[98]. Infections were performed at 2dpf by first anesthetising larvae in 0.025% MS222 (Sigma) followed by microinjection of single cell suspensions of *M. marinum* or *Salmonella* Typhimurium in PBS supplemented with 1.5% phenol red into either the caudal artery or hindbrain ventricle[96]. When attempting to isolate or confirm a mutant phenotype during the forward genetic screen, a minimum of 60 fish per clutch were infected.

Mycobacterial cording analysis

At 5dpi infected larvae were arrayed on 96 well half area plates and then anesthetised in 0.025% MS222 and by cooling on ice for 30 minutes. The presence or absence of mycobacterial cording was then empirically assessed by fluorescence light microscopy.

When assessing mycobacterial cording during the forward genetic screen, cording analysis was performed by two independent operators and mapping only performed on larvae in which there was agreement over phenotypic status. This was done to minimise disruption of mapping due to mis-phenotyped animals.

Exome mapping and linkage analysis

At least 30 phenotypic and non-phenotypic sibling larvae were collected at 7dpf following phenotyping and fixed in 100% methanol. Nucleic acid extraction and exome sequencing were then performed as previously described[110]. Firstly, fixed larvae were incubated at 80 °C for 15 minutes to evaporate methanol, DNA extraction

was then performed by addition of lysis buffer (25 mM NaOH, 0.2 mM EDTA) and incubated for 95 °C for 30 minutes followed neutralization with 40 mM Tris-HCl. 150- to 200-bp insert Ilumina libraries were then prepared by Sanger Institute Sequencing pipelines using DNA bulked from phenotype sorted larvae. Libraries were then hybridised to predesigned 120-base biotinylated RNA oligonucleotide whole exome baits that were captured using streptavidin coated magnetic beads as previously described[110]. RNA baits were then digested, and DNA libraries were amplified for 10 cycles using standard Illumina primers. Amplified libraries were then processed on HiSeq2500 machines to perform 75-bp paired-end sequencing. Sequencing reads were then mapped to the GRCz10 zebrafish genome assembly using BWA-MEM[219].

MMAPPR was then used on aligned sequences to estimate the location of the causative mutation as previously described[220]. MMAPPR analysis first involves identification of polymorphic loci across the genome of wildtype animals. This is followed by assessment of differences in allelic frequency at polymorphic loci between phenotypic and non-phenotypic animals. Differences in allelic frequency are measured by Euclidian distance which is calculated for each identified polymorphic locus across the genome[220]. Finally, loess regression analysis was used to generate a mapping peak spanning the genomic region harbouring the causative mutation as depicted in Figure 3.

Independently, SNPs were called using GATK, and SNPs represented in mutants and located within regions bound by exome mapping peaks were used to develop KASP-based genotyping assays to rapidly distinguish between relevant alleles[221,222]. Following infection and identification of additional mutant larvae, linkage

analysis was performed by genotyping individual phenotypic larvae for SNPs present within the mapping interval. As all isolated mutants show autosomal recessive inheritance, the mapping interval was further resolved through identification of genomic regions with conserved homozygosity across all recombinant phenotypic animals.

KASP Genotyping

KASP-based genotyping has been extensively used in this study for SNP based linkage analysis as well as for genotyping *uxt*$^{+/-}$ in cross larvae. Following phenotyping of larvae arrayed in a 96 well plate, genomic DNA was extracted through the addition of 75µl lysis buffer (25 mM NaOH with 0.2 mM EDTA) and incubated at 4^{o}C overnight. Subsequently samples were incubated at 95^{o}C for 30 minutes, followed by 12^{o}c for 10 minutes in a thermocycler. 75µl neutralisation buffer (40mM Tris-HCl) was then added to each sample. 5µl of each neutralised sample was then transferred to hard-shell 96 well PCR plates (Bio-Rad) followed by addition of primers and PCR mix according to manufacturer protocol (Biosearch). Plates were read on CFX connect (BioRad) machine and analysed using CFX manager (BioRad) and genotype of larvae documented.

RNA-seq

60 uninfected *Guaguancó*$^{+/-}$ incross larvae from a timed mating of a single breeding pair were collected in 9ul of nuclease free water at 3,5 and 7dpf and frozen on dry ice. Frozen larvae were lysed in 110 µl RLT buffer (Qiagen) supplemented with beta mercaptoethanol (Sigma). Total nucleic acid extraction was then performed

by adding lysate to 180µl of Agencourt RNAClean XP (Beckman Coulter) magnetic beads and elution of nucleic acid performed as per manufacturer's instructions. RNA concentration was then quantified using Quant-iT RNA assay (Invitrogen). Genotype of each collected larvae was determined using KASP genotyping using SNPs linked to the *Guaguancó* mutation. For each time point 12 *Guaguancó*$^{-/-}$, 6 *Guaguancó*$^{+/-}$ and 6 *Guaguanco*$^{+/+}$ replicate larvae were selected for further processing. Total nucleic acid was then treated with DNAseI (NEB) and followed by preparation of sequencing libraries conducted by the Sanger Institute Sequencing pipelines using a TruSeq Stranded mRNA Sample Prep Kit (Illumina). Libraries were then pooled and sequenced on Illumina HiSeq 2500 in 75 bp paired-end mode by Sanger Institute mapping pipelines. Sequencing quality was then assessed with FastQC (v0.11.8) followed by alignment of sequencing data to the GRCz11 zebrafish genome assembly using TopHat2(v2.0.13)[223]. Read counts per gene were assessed using htseq-count (v0.6.1) and Ensembl 98 annotation used as input for DESeq2 differential expression analysis[224,225]. Functional enrichment analysis performed using G:Profiler online tool[226].

Morpholino and RNA injections

0.32 mM *tnfr1* splice-blocking morpholino (5′- CTGCATTGTGACTTACTTATCGCAC -3′) (Gene Tools) and in vitro-transcribed 200ng/µl *bcl2* mRNA were prepared in 1× Buffer Tango (Thermo Scientific) containing 2% phenol red (Sigma) and injected into 1 cell stage embryos as previously described[164] .

G0 CRISPR- overview

To facilitate rapid reverse genetic investigation in the zebrafish, we developed a protocol based on previous studies to induce null phenotypes in G0 larvae via CRISPR/cas9 mediated gene knockout[111,227]. This approach has been used in this study to rapidly generate double mutant larvae without the need for time-consuming backcrossing or raising of additional mutant families to adulthood. This approach was also useful in generating large numbers mutant larvae for complex phenotypic assays, which would otherwise require a heterozygous incross which result in clutches in which only quarter of the are homozygous mutants. Lastly, the ability to produce null alleles in G0 animals has also facilitated rapid screening of compelling candidate genes from the forward genetic study.

G0 CRISPR- gRNA design

4 non-overlapping CRISPR RNA (crRNA) oligonucleotides per target gene were designed to target APPRIS principle isoforms according to annotation in the Grcz11 zebrafish assembly. Sequences were selected based on predicted on-target efficacy and likelihood of off-target effects as predicted by IDT Custom Alt-R® CRISPR-Cas9 guide RNA online design tool, whilst avoiding regions with documented polymorphisms[228].

G0 CRISPR- sgRNA preparation and assembly of ribonucleotide complexes

Pre-synthesised Alt-R CRISPR-Cas9 crRNAs (IDT) as previously designed were obtained and diluted to 200μM in nuclease-free duplex buffer (IDT). Trans-activating crRNA (tracrRNA) (IDT) was diluted in TE buffer to a concentration of

200µM. 6µl of crRNA solution was then added to 6µl tracrRNA in 8µl duplex buffer followed by incubation at 95°C for five minutes in a thermocycler to yield a 60µM signal guide (sg)RNA solution. 2µl aliquots of sgRNA were then frozen at -80°C.

On the day of injection, Alt-R® S.p. Cas9 Nuclease V3 (IDT) protein was diluted to 10µM in cas9 buffer (20mM HEPES; 150mM KCl, pH 7.5). 1.5µl of each sgRNA solution for a given gene was then combined in a single PCR tube followed by addition of an equivalent volume of cas9 solution, to yield a 5µM cas9, 30µM sgRNA solution as previously described[111]. Samples were then incubated at 37°C for 5 minutes to complete assembly of sgRNA/cas9 complexes followed by addition of 1.5% phenol red to aid visualisation of infection volume.

G0 CRISPR- Microinjection

3nl of sgRNA/cas9 complex solution were then delivered to embryos by microinjection of 3nl of solution into 1 cell stage stages embryos derived from timed zebrafish mating. Injected embryos were checked for toxicity at 4, 24- and 48-hours post injection, with removal of dysmorphic animals.

G0 CRISPR- Genotyping

It has previously been shown that redundant targeting of a single gene at 4 loci with CRISPR/cas9 reliably results in null phenotypes in G0 zebrafish[111]. To rapidly verify disruption of targeted loci, high resolution melt (HRM) PCR genotyping assays were developed to yield ~100bp amplicons encompassing the predicted site of cas9 mediated DNA cleavage.

To perform HRM PCR, genomic DNA was first extracted through the addition of 75µl lysis buffer (25 mM NaOH with 0.2 mM EDTA) and incubated at 4°C overnight. Subsequently, samples were incubated at 95°C for 30 minutes, followed by 12°c for 10 minutes in a thermocycler. 75µl neutralisation buffer (40mM Tris-HCl) was then added to each sample. 1µl of extracted nucleic acid was added to HRM primers and precision melt supermix (Bio-rad) according to manufactures instructions. HRM PCR was conducted using Bio-Rad HRM parameters as per manufactures instructions. Analysis was performed using Precision Melt Analysis Software v1.2 (Bio-Rad)

Appendix 1

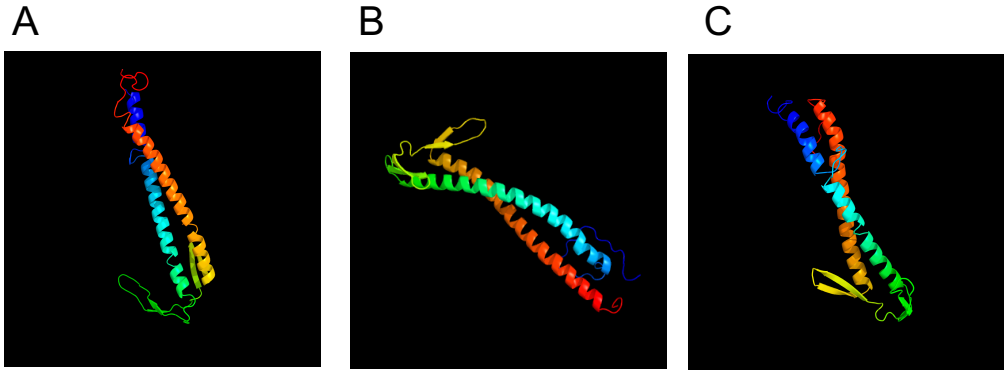

D

Consensus

1. Danio_rerio_uxt_201_
2. Homo_sapiens_UXT_201
3. Mus_musculus_Uxt_202_

```
MATPPKRRAXXXXGEKVLRYETFISDVLQRDLQKVLDHRDKVYEQLAXYLQLRNVIERLQEXXHSELYMQ
1 -----MTSGTSVINDKVLQYETFISEVLRRDLQKVLEQRDAVYEKIAQYLQLKNTIQSIQESGSKELKTD 65
2 MATPPKRRAVEATGEKVLRYETFISDVLQRDLRKVLDHRDKVYEQLAKYLQLRNVIERLQEAKHSELYMQ 70
3 MATPPKRRALDTVGEKVLRYETFISDVLQRDLQKVLDHRDKVYEQLSVYLQLRNVIERLQETNHSELYMQ 70

VDLGCNFFVDTVVPDTSRIYVALGYGFFLELTLAEALKFIDRKSSLLTELSXSLTKDSMNIKAHIHMXLE
1 VDLGCNFYVQAHVPDASRIYVAVGYGFFVEFTHAEALKFIEKKTNQLTEYTEVLTKDAAKIKANIRMVLE 135
2 VDLGCNFFVDTVVPDTSRIYVALGYGFFLELTLAEALKFIDRKSSLLTELSNSLTKDSMNIKAHIHMLLE 140
3 VDLGCNFFVDTVVPDTSRIYVALGYGFFLELTLAEALKFIDRKSSLLTELSDSLTKDSMNIKAHIHMMLE 140

GLRELQGLQNFPEXXXH---
1 GLRELQGLKDLPEDRRREVF 155
2 GLRELQGLQNFPEKPHH--- 157
3 GLRELQGLQNFPEPSPH--- 157
```

Appendix 1
UXT is conserved across vertebrates

(A-C) Phyre[2] predicted structures of zebrafish (A) human (B) and murine (C) orthologs of UXT protein[229].

(D) Amino acid alignment of zebrafish, human and murine UXT orthologs.

Appendix 2

source	term_name	term_id	adjusted_p_. value	negative_log10_of _adjusted_p_value
GO:BP	immune system process	GO:0002376	2.54E-40	39.59446594
GO:BP	immune response	GO:0006955	1.12E-27	26.94931223
GO:BP	response to biotic stimulus	GO:0009607	2.62E-17	16.58226553
GO:BP	response to other organism	GO:0051707	5.68E-17	16.2453159
GO:BP	response to external biotic stimulus	GO:0043207	5.68E-17	16.2453159
GO:BP	cytokine-mediated signaling pathway	GO:0019221	5.45E-14	13.26338332
GO:BP	cellular response to cytokine stimulus	GO:0071345	9.12E-14	13.03977127
GO:BP	response to cytokine	GO:0034097	1.31E-13	12.88366095
GO:BP	defense response	GO:0006952	4.28E-13	12.36858737
GO:BP	cell chemotaxis	GO:0060326	1.60E-12	11.79705749
GO:BP	leukocyte migration	GO:0050900	2.33E-12	11.63346166
GO:BP	defense response to other organism	GO:0098542	1.04E-11	10.9830711
GO:BP	proteasomal ubiquitin-independent protein catabolic process	GO:0010499	1.42E-11	10.84661357
GO:BP	regulation of immune system process	GO:0002682	4.94E-11	10.30613805
GO:BP	response to stress	GO:0006950	5.43E-10	9.265034097
GO:BP	chemokine-mediated signaling pathway	GO:0070098	7.81E-10	9.107414145
GO:BP	leukocyte chemotaxis	GO:0030595	1.13E-09	8.946058218
GO:BP	response to chemokine	GO:1990868	1.28E-09	8.893248968
GO:BP	cellular response to chemokine	GO:1990869	1.28E-09	8.893248968
GO:BP	multi-organism process	GO:0051704	1.43E-09	8.843908564
GO:BP	response to external stimulus	GO:0009605	1.75E-09	8.755994633
GO:BP	cell division	GO:0051301	4.59E-09	8.337888216
GO:BP	myeloid leukocyte migration	GO:0097529	1.03E-08	7.986304314
GO:BP	cell cycle process	GO:0022402	2.54E-08	7.594928721
GO:BP	cell migration	GO:0016477	4.51E-08	7.346020176
GO:BP	proteolysis involved in cellular protein catabolic process	GO:0051603	4.85E-08	7.314103444
GO:BP	antigen processing and presentation of peptide antigen via MHC class I	GO:0002474	6.68E-08	7.175308494
GO:BP	cellular protein catabolic process	GO:0044257	6.78E-08	7.1689633
GO:BP	neutrophil migration	GO:1990266	1.28E-07	6.892928016
GO:BP	neutrophil chemotaxis	GO:0030593	2.20E-07	6.657739553
GO:BP	mitotic cell cycle process	GO:1903047	2.38E-07	6.623536844
GO:BP	granulocyte migration	GO:0097530	2.88E-07	6.540170286
GO:BP	antigen processing and presentation	GO:0019882	3.72E-07	6.429546083
GO:BP	localization of cell	GO:0051674	5.09E-07	6.293122342
GO:BP	cell motility	GO:0048870	5.09E-07	6.293122342
GO:BP	granulocyte chemotaxis	GO:0071621	5.42E-07	6.265683559
GO:BP	protein catabolic process	GO:0030163	6.77E-07	6.169434982
GO:BP	proteolysis	GO:0006508	8.19E-07	6.086606673
GO:BP	cellular macromolecule catabolic process	GO:0044265	2.69268E-06	5.569814551
GO:BP	antigen processing and presentation of peptide antigen	GO:0048002	4.0951E-06	5.387735691
GO:BP	regulation of immune response	GO:0050776	5.6477E-06	5.248128728
GO:BP	chromosome segregation	GO:0007059	6.90766E-06	5.160669198
GO:BP	macromolecule catabolic process	GO:0009057	1.2533E-05	4.901945184
GO:BP	T cell activation	GO:0042110	1.56511E-05	4.805454224
GO:BP	organonitrogen compound catabolic process	GO:1901565	1.98006E-05	4.703322607
GO:BP	modification-dependent protein catabolic process	GO:0019941	3.47595E-05	4.458926692
GO:BP	ubiquitin-dependent protein catabolic process	GO:0006511	6.28333E-05	4.201810096
GO:BP	modification-dependent macromolecule catabolic process	GO:0043632	6.72199E-05	4.172502292
GO:BP	organelle fission	GO:0048285	7.26627E-05	4.13868842

source	term_name	term_id	adjusted_p_.value	negative_log10_of_adjusted_p_value
GO:BP	cellular catabolic process	GO:0044248	9.75343E-05	4.010842824
GO:BP	chemotaxis	GO:0006935	0.000111904	3.951156309
GO:BP	response to bacterium	GO:0009617	0.000203654	3.691108104
GO:BP	immune effector process	GO:0002252	0.000234585	3.629699121
GO:BP	mitotic nuclear division	GO:0140014	0.000245008	3.610819567
GO:BP	proteasomal protein catabolic process	GO:0010498	0.000256841	3.590335577
GO:BP	locomotion	GO:0040011	0.00027603	3.559044341
GO:BP	lymphocyte migration	GO:0072676	0.000290334	3.537101906
GO:BP	innate immune response	GO:0045087	0.000298784	3.524643166
GO:BP	organic substance catabolic process	GO:1901575	0.000305462	3.515042184
GO:BP	negative regulation of immune system process	GO:0002683	0.000339043	3.469744986
GO:BP	movement of cell or subcellular component	GO:0006928	0.000350085	3.455826059
GO:BP	Arp2/3 complex-mediated actin nucleation	GO:0034314	0.000428376	3.368175072
GO:BP	positive regulation of immune system process	GO:0002684	0.000432224	3.364291393
GO:BP	taxis	GO:0042330	0.000439362	3.35717769
GO:BP	catabolic process	GO:0009056	0.000612825	3.212663203
GO:BP	inflammatory response	GO:0006954	0.000715585	3.145338854
GO:BP	leukocyte activation	GO:0045321	0.001546181	2.810739671
GO:BP	nuclear chromosome segregation	GO:0098813	0.001753603	2.756068666
GO:BP	response to interferon-gamma	GO:0034341	0.001843134	2.734443128
GO:BP	cellular response to interferon-gamma	GO:0071346	0.001843134	2.734443128
GO:BP	positive regulation of immune response	GO:0050778	0.00356473	2.447973381
GO:BP	leukocyte differentiation	GO:0002521	0.003836365	2.41608006
GO:BP	cytokinesis	GO:0000910	0.003878612	2.411323634
GO:BP	regulation of leukocyte migration	GO:0002685	0.005452141	2.263432892
GO:BP	macrophage chemotaxis	GO:0048246	0.005509148	2.258915579
GO:BP	regulation of cell cycle process	GO:0010564	0.005663721	2.246898139
GO:BP	nuclear division	GO:0000280	0.006428645	2.191880557
GO:BP	cellular response to chemical stimulus	GO:0070887	0.006673259	2.17566205
GO:BP	actin nucleation	GO:0045010	0.006957765	2.157530237
GO:BP	cell activation	GO:0001775	0.008543656	2.068356236
GO:BP	lymphocyte activation	GO:0046649	0.008869794	2.05208647
GO:BP	positive regulation of response to stimulus	GO:0048584	0.010531262	1.977519597
GO:BP	reactive oxygen species metabolic process	GO:0072593	0.01153959	1.937809621
GO:BP	response to virus	GO:0009615	0.011936673	1.923116688
GO:BP	response to stimulus	GO:0050896	0.012564384	1.90085879
GO:BP	proteasome-mediated ubiquitin-dependent protein catabolic process	GO:0043161	0.012634004	1.898458985
GO:BP	peptidyl-tyrosine autophosphorylation	GO:0038083	0.013146983	1.881173885
GO:BP	cell cycle	GO:0007049	0.014009406	1.853580285
GO:BP	positive regulation of cytokine production involved in immune response	GO:0002720	0.014790521	1.830016534
GO:BP	response to tumor necrosis factor	GO:0034612	0.016637295	1.778917292
GO:BP	endoplasmic reticulum to Golgi vesicle-mediated transport	GO:0006888	0.017609333	1.754257084
GO:BP	sister chromatid segregation	GO:0000819	0.018407739	1.734999548
GO:BP	mitotic sister chromatid segregation	GO:0000070	0.026558091	1.57580314
GO:BP	macrophage migration	GO:1905517	0.026905115	1.570165153
GO:BP	positive regulation of ERK1 and ERK2 cascade	GO:0070374	0.028995934	1.537662898
GO:BP	regulation of immune effector process	GO:0002697	0.030014942	1.52266249
GO:BP	positive regulation of biological process	GO:0048518	0.035403011	1.450959805
GO:BP	lymphocyte chemotaxis	GO:0048247	0.037752674	1.423052281
GO:BP	cortical cytoskeleton organization	GO:0030865	0.044086392	1.355695438
GO:BP	regulation of cell population proliferation	GO:0042127	0.046038348	1.336880267
GO:BP	alpha-beta T cell proliferation	GO:0046633	0.04984732	1.30235819
GO:BP	regulation of alpha-beta T cell proliferation	GO:0046640	0.04984732	1.30235819
GO:BP	negative regulation of alpha-beta T cell proliferation	GO:0046642	0.04984732	1.30235819

Appendix 2

Functional enrichment analysis of all genes downregulated in 7dpf uninfected *uxt* mutant larvae relative to wildtype controls as determined by RNA-seq using Biological Process (BP) Gene Ontology database

Appendix 3

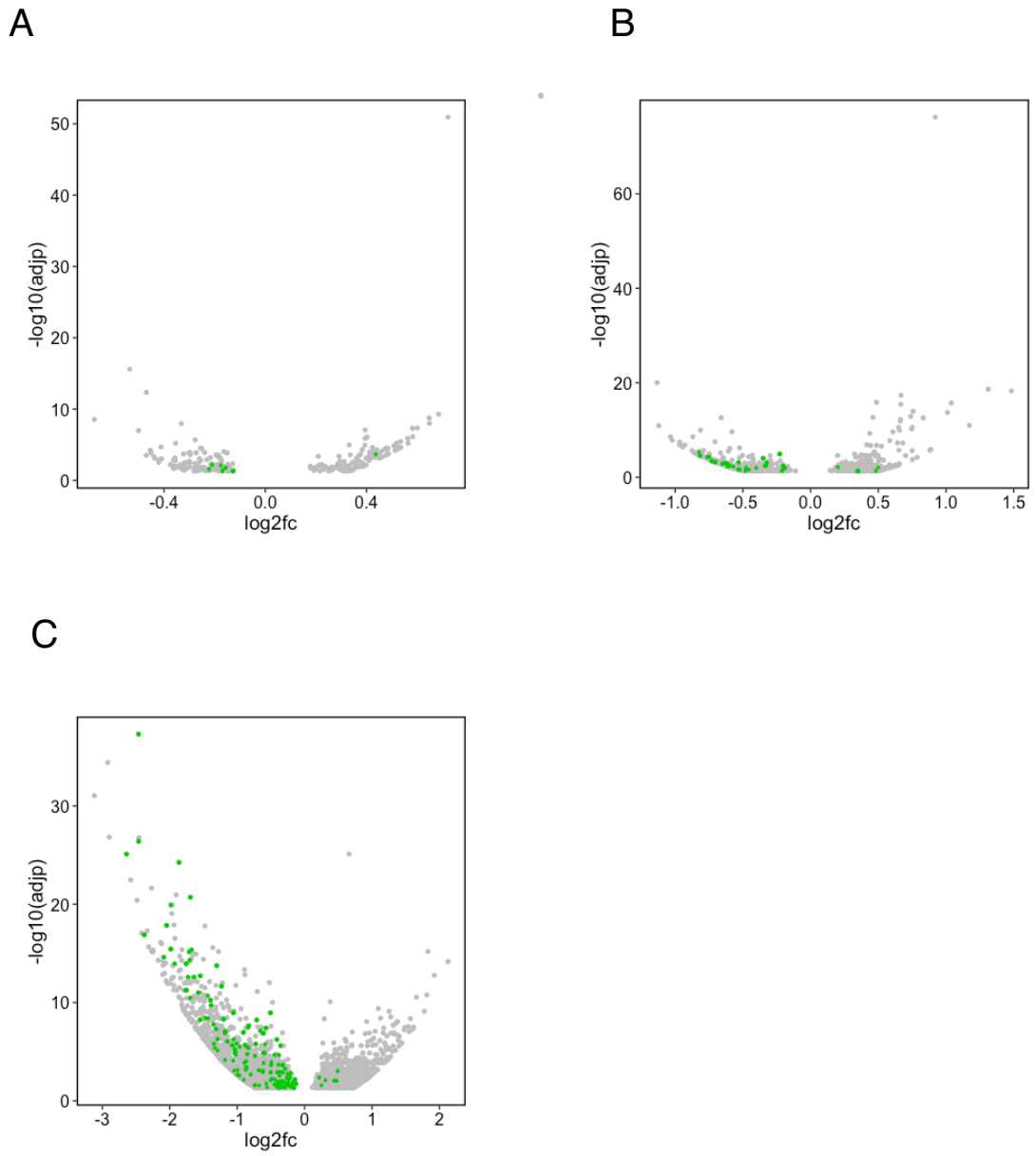

Appendix 3
Volcano plot displaying differential expression of genes between uxt$^{-/-}$ mutant larvae relative to wildtype sibling controls at 3 (A), 5(B) and 7dpf (C). Vertical axis corresponds to -$\log_{10}$ of adjusted p value, horizontal axis displays $\log_2$ fold change. Green dots represent zebrafish macrophage associated genes as previously defined by transcriptional profiling of zebrafish leucocytes[230]. Grey dots represent all other differentially regulated genes.

Appendix 4

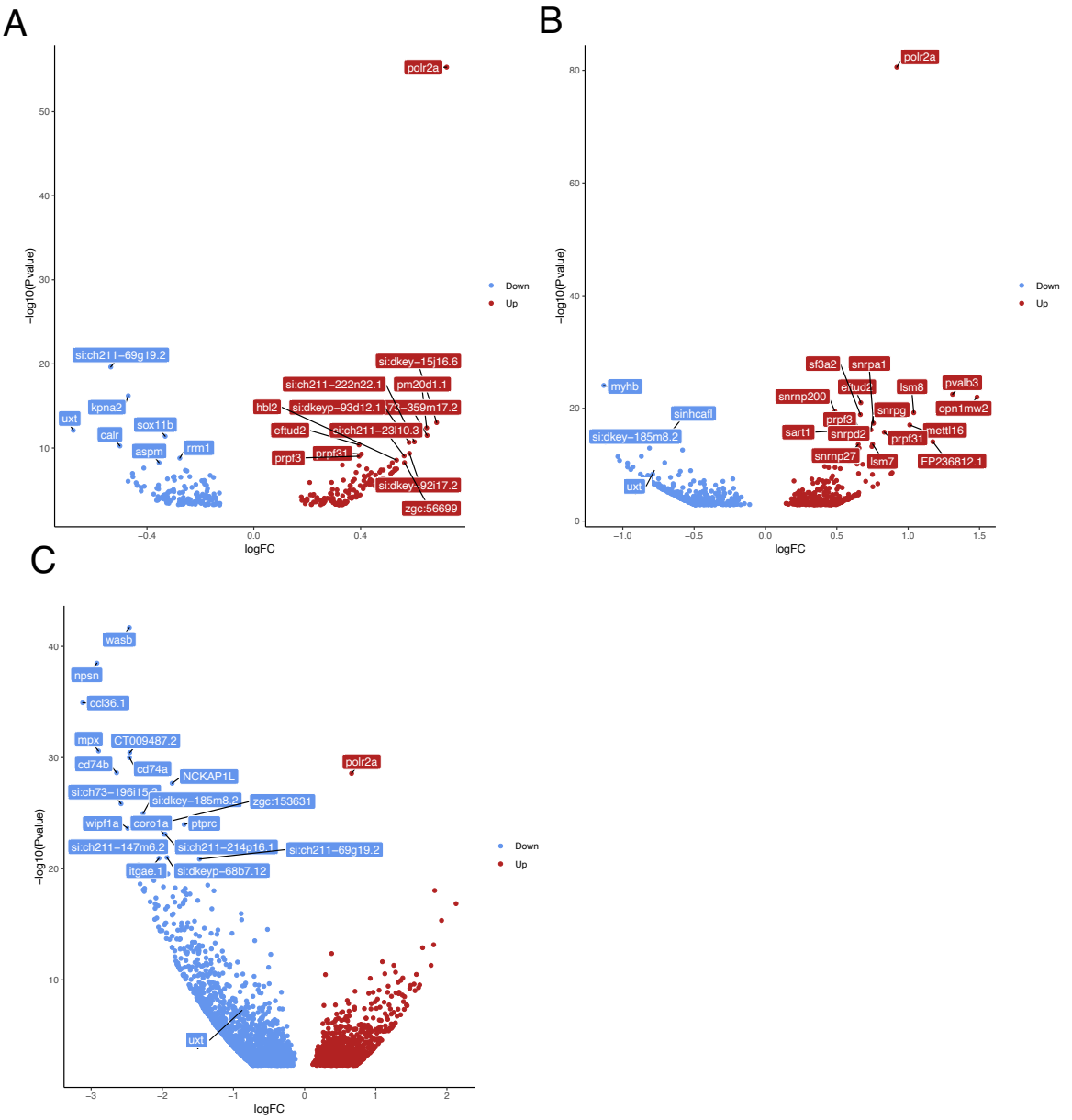

Appendix 4

Volcano plot displaying differential expression of genes between uxt$^{-/-}$ mutant larvae relative to wildtype sibling controls at 3 (A), 5(B) and 7dpf (C). Vertical axis corresponds to -$\log_{10}$ of adjusted p value, horizontal axis displays $\log_2$ fold change. Red dots represent upregulated genes, and blue dots represent down regulated genes. For each time point 20 most significantly differentially regulated genes labelled.

Appendix 5

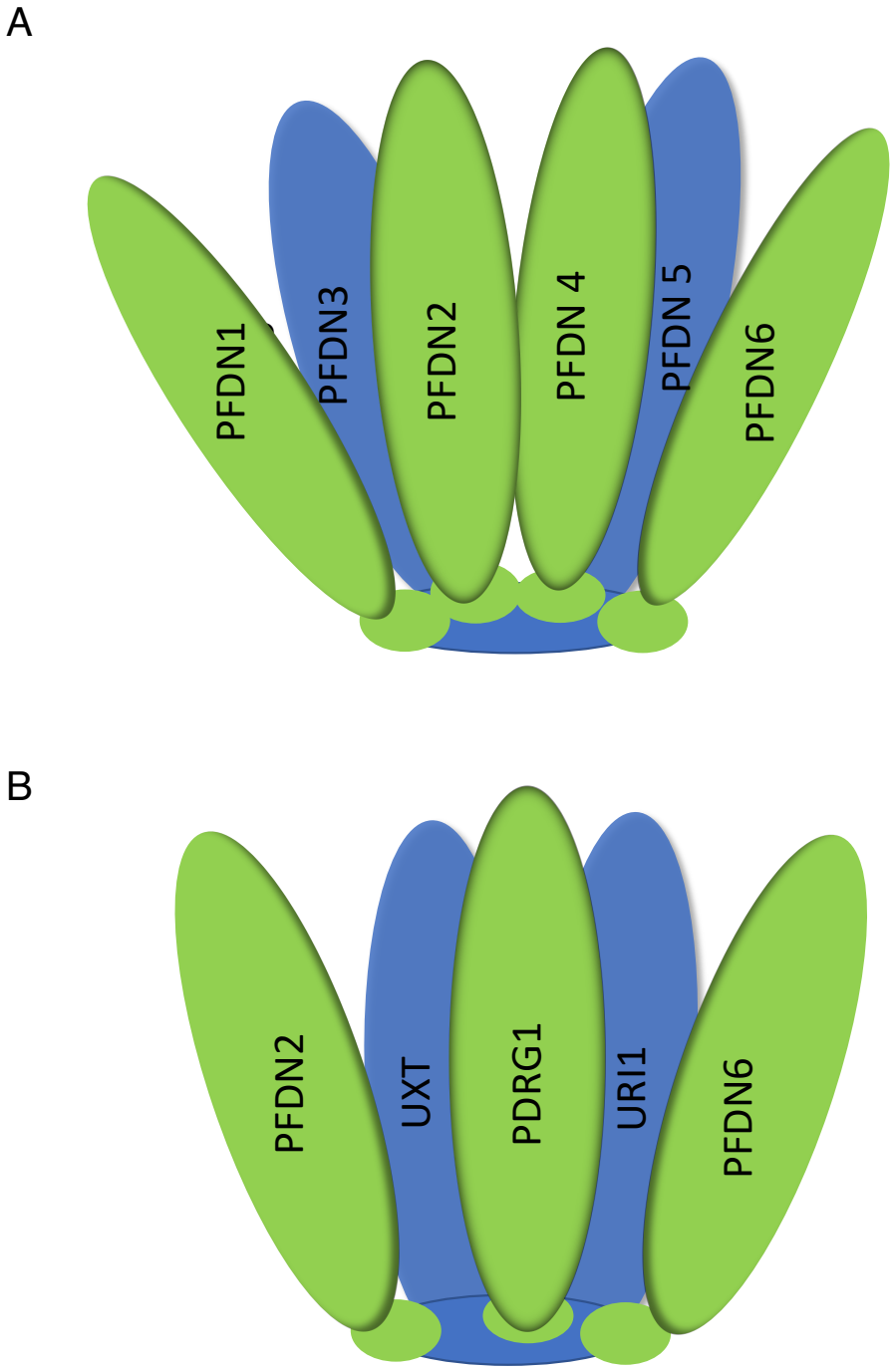

Appendix 5
Schematic of prefoldin complex[195,199] (A) and presumed structure of prefoldin like complex (B) α-prefoldins depicted in blue, β-prefoldins depicted in green

Appendix 6

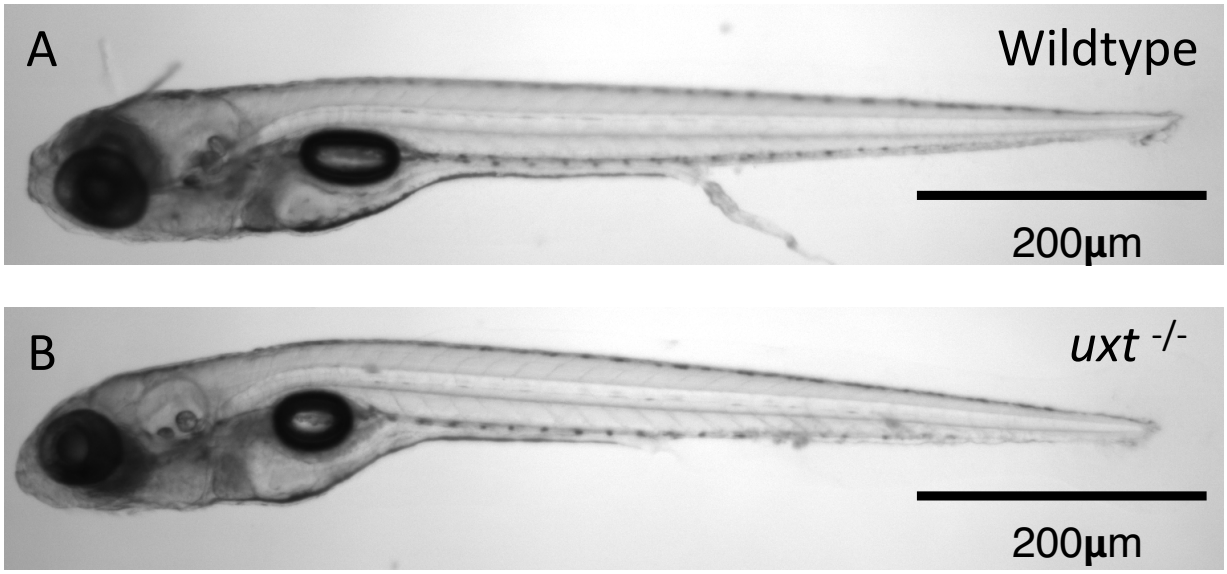

Appendix 6
4x Brightfield micrographs of wildtype (A) and uxt$^{-/-}$ (B) sibling larvae at 7dpf

Appendix 7

source	term_name	term_id	adjusted_p_value	negative_log10_of_adjusted_p_value
GO:MF	snRNA binding	GO:0017069	0.000707905	3.150025079
GO:BP	mRNA splicing, via spliceosome	GO:0000398	2.12E-07	6.6729234
GO:BP	RNA splicing, via transesterification reactions with bulged adenosine as nucleophile	GO:0000377	2.12E-07	6.6729234
GO:BP	RNA splicing, via transesterification reactions	GO:0000375	2.12E-07	6.6729234
GO:BP	RNA splicing	GO:0008380	1.04024E-06	5.982864517
GO:BP	mRNA processing	GO:0006397	4.39316E-05	4.357223312
GO:BP	mRNA metabolic process	GO:0016071	0.00019491	3.710166458
GO:BP	RNA processing	GO:0006396	0.000237473	3.624386332
GO:BP	nucleic acid metabolic process	GO:0090304	0.00142899	2.844970853
GO:BP	nucleobase-containing compound metabolic process	GO:0006139	0.006291306	2.201259176
GO:BP	heterocycle metabolic process	GO:0046483	0.009158566	2.038172509
GO:BP	cellular aromatic compound metabolic process	GO:0006725	0.00962915	2.016412065
GO:BP	organic cyclic compound metabolic process	GO:1901360	0.013320739	1.875471692
GO:BP	ribonucleoprotein complex biogenesis	GO:0022613	0.040266862	1.395052219
GO:BP	cellular nitrogen compound metabolic process	GO:0034641	0.04437001	1.352910474
GO:CC	spliceosomal snRNP complex	GO:0097525	4.64E-13	12.33335088
GO:CC	small nuclear ribonucleoprotein complex	GO:0030532	5.27E-13	12.27841927
GO:CC	spliceosomal tri-snRNP complex	GO:0097526	1.30E-12	11.88686429
GO:CC	Sm-like protein family complex	GO:0120114	1.36E-12	11.86801177
GO:CC	U4/U6 x U5 tri-snRNP complex	GO:0046540	7.24E-11	10.14010006
GO:CC	ribonucleoprotein complex	GO:1990904	6.82E-07	6.166522784
GO:CC	catalytic step 2 spliceosome	GO:0071013	3.02512E-05	4.519257955
GO:CC	spliceosomal complex	GO:0005681	3.35302E-05	4.474564021
GO:CC	U2-type spliceosomal complex	GO:0005684	0.001668151	2.777764764
GO:CC	nucleus	GO:0005634	0.009786589	2.009368662
GO:CC	U5 snRNP	GO:0005682	0.021878744	1.659977615
GO:CC	U2 snRNP	GO:0005686	0.029967616	1.523347805

Appendix 7

Functional enrichment analysis of genes consistently upregulated at 3,5 and 7 dpf in uninfected *uxt* mutant larvae relative to wildtype controls as determined by RNA-seq using Molecular Function (MF), Biological Process (BP) and Cellular Compartment (CC) Gene Ontology database

References

1. Pai, M. *et al.* Tuberculosis. *Nat. Rev. Dis. Prim.* **2**, 16076 (2016).
2. Waller, J. F. Davidson's Principles and Practice of Medicine. *Postgrad. Med. J.* (2008). doi:10.1136/pgmj.68.797.232
3. Tiemersma, E. W., van der Werf, M. J., Borgdorff, M. W., Williams, B. G. & Nagelkerke, N. J. D. Natural history of tuberculosis: Duration and fatality of untreated pulmonary tuberculosis in HIV negative patients: A systematic review. *PLoS ONE* (2011). doi:10.1371/journal.pone.0017601
4. Hershkovitz, I. *et al.* Detection and Molecular Characterization of 9000-Year-Old Mycobacterium tuberculosis from a Neolithic Settlement in the Eastern Mediterranean. *PLoS One* **3**, e3426 (2008).
5. Adams, F. The Genuine Works of Hippocrates. *South. Med. J.* (1922). doi:10.1097/00007611-192206000-00025
6. Karamanou, M. & Androutsos, G. *The masterful description of pulmonary tuberculosis by Soranus of Ephesus (c. 98-138 A.D.)*. *American Journal of Respiratory and Critical Care Medicine* **186**, 571–571 (American Thoracic Society, 2012).
7. Barberis, I., Bragazzi, N. L., Galluzzo, L. & Martini, M. The history of tuberculosis: from the first historical records to the isolation of Koch's bacillus. *J. Prev. Med. Hyg.* **58**, E9–E12 (2017).
8. Chalke, H. D. D. Some historical aspects of tuberculosis. *Public Health* **74**, 83–95 (1959).
9. Glaziou, P., Floyd, K. & Raviglione, M. Trends in tuberculosis in the UK. doi:10.1136/thoraxjnl-2018-211537

10. Frith, J. History of tuberculosis. Part 1 - Phthisis, consumption and the white plague. *J. Mil. Veterans. Health* (2014).

11. Lissant Cox, G. Sanatorium treatment contrasted with home treatment. *Br. J. Tuberc.* **17**, 27–30 (1923).

12. Koch, R. Die Ätiologie der Tuberkulose (1884). in (2018). doi:10.1007/978-3-662-56454-7_5

13. Daniel, T. M. The history of tuberculosis. *Respir. Med.* **100**, 1862–1870 (2006).

14. Calmette, A. On preventive vaccination of the new-born against tuberculosis by B.C.G. *Br. J. Tuberc.* **22**, 161–165 (1928).

15. STREPTOMYCIN treatment of pulmonary tuberculosis. *Br. Med. J.* **2**, 769–82 (1948).

16. Lienhardt, C. *et al.* Global tuberculosis control: lessons learnt and future prospects. *Nat. Rev. Microbiol.* **10**, 407–416 (2012).

17. WHO. *WHO Global Tuberculosis Report 2018*. *Pharmacological Reports* (2018). doi:10.1016/j.pharep.2017.02.021

18. Connolly, L. E., Edelstein, P. H. & Ramakrishnan, L. Why Is Long-Term Therapy Required to Cure Tuberculosis? *PLoS Med.* **4**, e120 (2007).

19. Centers for Disease Control and Prevention (CDC). Emergence of Mycobacterium tuberculosis with extensive resistance to second-line drugs--worldwide, 2000-2004. *MMWR. Morb. Mortal. Wkly. Rep.* **55**, 301–5 (2006).

20. Sacchettini, J. C., Rubin, E. J. & Freundlich, J. S. Drugs versus bugs: in pursuit of the persistent predator Mycobacterium tuberculosis. *Nat. Rev. Microbiol.* **6**, 41–52 (2008).

21. Pietersen, E. *et al.* Long-term outcomes of patients with extensively drug-resistant tuberculosis in South Africa: a cohort study. *Lancet* **383**, 1230–1239 (2014).

22. Cox, H. S. *et al.* Epidemic Levels of Drug Resistant Tuberculosis (MDR and XDR-TB) in a High HIV Prevalence Setting in Khayelitsha, South Africa. *PLoS One* **5**, e13901 (2010).

23. Fine, P. E. M. Variation in protection by BCG: implications of and for heterologous immunity. *Lancet* **346**, 1339–1345 (1995).

24. Wells, W. F., Ratcliffe, H. L. & Grumb, C. On the mechanics of droplet nuclei infection; quantitative experimental air-borne tuberculosis in rabbits. *Am J Hyg* **47**, 11–28 (1948).

25. Cambier, C. J., Falkow, S. & Ramakrishnan, L. Host evasion and exploitation schemes of Mycobacterium tuberculosis. *Cell* **159**, 1497–1509 (2014).

26. Liu, P. T. *et al.* Toll-like receptor triggering of a vitamin D-mediated human antimicrobial response. *Science (80-.).* **311**, 1770–1773 (2006).

27. North, R. J. & Jung, Y.-J. Immunity to Tuberculosis . *Annu. Rev. Immunol.* **22**, 599–623 (2004).

28. Charlson, E. S. *et al.* Topographical Continuity of Bacterial Populations in the Healthy Human Respiratory Tract. *atsjournals.org* **184**, 957–963 (2011).

29. Cambier, C. J. *et al.* Mycobacteria manipulate macrophage recruitment through coordinated use of membrane lipids. *Nature* **505**, 218–222 (2014).

30. Cambier, C. J., O'Leary, S. M., O'Sullivan, M. P., Keane, J. & Ramakrishnan, L. Phenolic Glycolipid Facilitates Mycobacterial Escape from Microbicidal Tissue-Resident Macrophages. *Immunity* **47**, 552-565.e4 (2017).

31. Levitte, S. *et al.* Mycobacterial Acid Tolerance Enables Phagolysosomal Survival and Establishment of Tuberculous Infection In Vivo. *Cell Host Microbe* **20**, 250–258 (2016).

32. Walburger, A. *et al.* Protein kinase G from pathogenic mycobacteria promotes survival within macrophages. *Science (80-.).* **304**, 1800–1804 (2004).

33. Ramakrishnan, L. Revisiting the role of the granuloma in tuberculosis. *Nat. Rev. Immunol.* **12**, 352–366 (2012).

34. Dannenberg, A. M. Immunopathogenesis of Pulmonary Tuberculosis. *Hosp. Pract.* **28**, 51–58 (1993).

35. Flynn, J. L. & Chan, J. IMMUNOLOGY OF TUBERCULOSIS. *Annu. Rev. Immunol.* **19**, 93–129 (2001).

36. Cooper, A. M. Cell-Mediated Immune Responses in Tuberculosis. *Annu. Rev. Immunol.* **27**, 393–422 (2009).

37. Wolf, A. J. *et al.* Initiation of the adaptive immune response to Mycobacterium tuberculosis depends on antigen production in the local lymph node, not the lungs. *J. Exp. Med.* **205**, 105–115 (2008).

38. Roberts, L. L. & Robinson, C. M. Mycobacterium tuberculosis infection of human dendritic cells decreases integrin expression, adhesion and migration to chemokines. *Immunology* **141**, 39–51 (2014).

39. Banaiee, N., Kincaid, E. Z., Buchwald, U., Jacobs, W. R. & Ernst, J. D. Potent Inhibition of Macrophage Responses to IFN-γ by Live Virulent Mycobacterium tuberculosis Is Independent of Mature Mycobacterial Lipoproteins but Dependent on TLR2 . *J. Immunol.* **176**, 3019–3027 (2006).

40. Fortune, S. M. *et al.* Mycobacterium tuberculosis Inhibits Macrophage Responses to IFN-γ through Myeloid Differentiation Factor 88-Dependent and -Independent Mechanisms . *J. Immunol.* **172**, 6272–6280 (2004).

41. Salgame, P. MMPs in tuberculosis: Granuloma creators and tissue destroyers. *Journal of Clinical Investigation* **121**, 1686–1688 (2011).

42. Vynnycky, E. & Fine, P. E. M. The natural history of tuberculosis: The implications of age-dependent risks of disease and the role of reinfection. *Epidemiol. Infect.* **119**, 183–201 (1997).

43. Abel, L., El-Baghdadi, J., Bousfiha, A. A., Casanova, J. L. & Schurr, E. Human genetics of tuberculosis: A long and winding road. *Philosophical Transactions of the Royal Society B: Biological Sciences* **369**, (2014).

44. WHO | Global tuberculosis report 2019. *WHO* (2019).

45. Carter, D. J. *et al.* The impact of social protection and poverty elimination on global tuberculosis incidence: a statistical modelling analysis of Sustainable Development Goal 1. *Lancet Glob. Heal.* **6**, e514–e522 (2018).

46. Narasimhan, P., Wood, J., Macintyre, C. R. & Mathai, D. Risk Factors for Tuberculosis. **2013**, 11 (2013).

47. Blas, E. & Kurup, A. S. *Equity, social determinants and public health programmes*. (World Health Organization, 2010).

48. Zhang, Z. *et al.* Risk of tuberculosis in patients treated with TNF-α antagonists: a systematic review and meta-analysis of randomised controlled trials. *BMJ Open* **7**, e012567 (2017).

49. Fox, G. J., Orlova, M. & Schurr, E. Tuberculosis in Newborns: The Lessons of the “Lübeck Disaster” (1929–1933). *PLOS Pathog.* **12**, e1005271 (2016).

50. Comstock, G. Tuberculosis in twins: a re-analysis of the Prophit survey. *Am. Rev. Respir. Dis.* (1978).

51. Kallmann, F., Tuberculosis, D. R.-A. R. of & 1943, undefined. Twin Studies on the Significance of Genetic Factors in Tuberculosis,. *atsjournals.org*

52. Fischer, A. Primary immunodeficiency diseases: An experimental model for molecular medicine. *Lancet* **357**, 1863–1869 (2001).

53. Buckley, R. H. MOLECULAR DEFECTS IN HUMAN SEVERE COMBINED IMMUNODEFICIENCY AND APPROACHES TO IMMUNE RECONSTITUTION. *Annu. Rev. Immunol* **22**, 625–55 (2004).

54. Marciano, B. E. *et al.* BCG vaccination in patients with severe combined immunodeficiency: Complications, risks, and vaccination policies. *J. Allergy Clin. Immunol.* **133**, 1134–1141 (2014).

55. Jennifer, D. E. A. & Heimall, R. A Review of Chronic Granulomatous Disease. doi:10.1007/s12325-017-0636-2

56. Lee, P. P. W. *et al.* Susceptibility to mycobacterial infections in children with X-linked chronic granulomatous disease: a review of 17 patients living in a region endemic for tuberculosis. *Pediatr. Infect. Dis. J.* **27**, 224–30 (2008).

57. Conti, F. *et al.* Mycobacterial disease in patients with chronic granulomatous disease: A retrospective analysis of 71 cases. *J. Allergy Clin. Immunol.* **138**, 241-248.e3 (2016).

58. Al-Muhsen, S. & Casanova, J.-L. The genetic heterogeneity of mendelian susceptibility to mycobacterial diseases. *J. Allergy Clin. Immunol.* **122**, 1043–51; quiz 1052–3 (2008).

59. Rosain, J. *et al.* Mendelian susceptibility to mycobacterial disease: 2014-2018 update. *Immunol. Cell Biol.* **97**, 360–367 (2019).

60. Bustamante, J., Boisson-Dupuis, S., Abel, L. & Casanova, J. L. Mendelian susceptibility to mycobacterial disease: Genetic, immunological, and clinical features of inborn errors of IFN-γ immunity. *Seminars in Immunology* **26**, 454–470 (2014).

61. Curtis, J. *et al.* Susceptibility to tuberculosis is associated with variants in the ASAP1 gene encoding a regulator of dendritic cell migration. *Nat. Genet.* **47**, 523–527 (2015).

62. Buniello, A. *et al.* The NHGRI-EBI GWAS Catalog of published genome-wide association studies, targeted arrays and summary statistics 2019. *Nucleic Acids Res.* **47**, D1005–D1012 (2019).

63. van Tong, H., Velavan, T. P., Thye, T. & Meyer, C. G. Human genetic factors in tuberculosis: an update. *Trop. Med. Int. Heal.* **22**, 1063–1071 (2017).

64. Hu, X. *et al.* No significant effect of ASAP1 gene variants on the susceptibility to tuberculosis in Chinese population. *ncbi.nlm.nih.gov*

65. Hong, E. P., Go, M. J., Kim, H.-L. & Park, J. W. Risk prediction of pulmonary tuberculosis using genetic and conventional risk factors in adult Korean population. *PLoS One* **12**, e0174642 (2017).

66. Uren, C. *et al.* A post-GWAS analysis of predicted regulatory variants and tuberculosis susceptibility. *PLoS One* **12**, e0174738 (2017).

67. McClellan, J. & King, M. C. Genetic heterogeneity in human disease. *Cell* **141**, 210–217 (2010).

68. VanderVen, B. C., Huang, L., Rohde, K. H. & Russell, D. G. The Minimal Unit of Infection: Mycobacterium tuberculosis in the Macrophage. *Microbiol. Spectr.* **4**, 10.1128/microbiolspec.TBTB2-0025–2016 (2016).

69. Jayaswal, S. *et al.* Identification of host-dependent survival factors for intracellular Mycobacterium tuberculosis through an siRNA screen. *PLoS Pathog.* **6**, 1–15 (2010).

70. Cronan, M. R. & Tobin, D. M. Fit for consumption: zebrafish as a model for tuberculosis. *Dis. Model. & Mech.* **7**, 777 LP – 784 (2014).

71. Dharmadhikari, A. S. & Nardell, E. A. What Animal Models Teach Humans about Tuberculosis. *Am. J. Respir. Cell Mol. Biol.* **39**, 503–508 (2008).

72. Clark, S., Hall, Y. & Williams, A. Animal Models of Tuberculosis: Guinea Pigs. *Cold Spring Harb. Perspect. Med.* **5**, (2015).

73. RILEY, R. L. *et al.* AERIAL DISSEMINATION OF PULMONARY TUBERCULOSIS A TWO-YEAR STUDY OF CONTAGION IN A TUBERCULOSIS WARD1. *Am. J. Epidemiol.* **70**, 185–196 (1959).

74. Lewis, P. A. & Loomis, D. ULCERATIVE TYPES AS DETERMINED BY INHERITANCE AND AS RELATED TO NATURAL RESISTANCE AGAINST TUBERCULOSIS: AN EXPERIMENTAL STUDY ON INBRED GUINEA PIGS. *J. Exp. Med.* **47**, 449–68 (1928).

75. Peñ, J. C. & Ho, W. Z. Monkey models of tuberculosis: Lessons learned. *Infection and Immunity* **83**, 852–862 (2015).

76. Flynn, J. A. L. Lessons from experimental Mycobacterium tuberculosis infections. *Microbes and Infection* **8**, 1179–1188 (2006).

77. Zhan, L., Tang, J., Sun, M. & Qin, C. Animal models for tuberculosis in translational and precision medicine. *Frontiers in Microbiology* **8**, (2017).

78. Pagán, A. J. & Ramakrishnan, L. Immunity and immunopathology in the tuberculous granuloma. *Cold Spring Harb. Perspect. Med.* **5**, (2015).

79. Fonseca, K. L., Rodrigues, P. N. S., Olsson, I. A. S. & Saraiva, M. Experimental study of tuberculosis: From animal models to complex cell systems and organoids. *PLOS Pathog.* **13**, e1006421 (2017).

80. Flynn, J. A. L. *et al.* Tumor necrosis factor-α is required in the protective immune response against mycobacterium tuberculosis in mice. *Immunity* **2**, 561–572 (1995).

81. Bean, A. G. *et al.* Structural deficiencies in granuloma formation in TNF gene-targeted mice underlie the heightened susceptibility to aerosol Mycobacterium tuberculosis infection, which is not compensated for by lymphotoxin. *J. Immunol.* **162**, 3504–11 (1999).

82. Cooper, A. M., Magram, J., Ferrante, J. & Orme, I. M. Interleukin 12 (IL-12) is crucial to the development of protective immunity in mice intravenously infected with mycobacterium tuberculosis. *J. Exp. Med.* **186**, 39–45 (1997).

83. Cooper, A. M. *et al.* Disseminated tuberculosis in interferon γ Gene-disrupted mice. *J. Exp. Med.* **178**, 2243–2247 (1993).

84. Caruso, A. M. *et al.* Mice deficient in CD4 T cells have only transiently diminished levels of IFN-gamma, yet succumb to tuberculosis. *J. Immunol.* **162**, 5407–16 (1999).

85. Kramnik, I., Dietrich, W. F., Demant, P. & Bloom, B. R. Genetic control of resistance to experimental infection with virulent Mycobacterium tuberculosis. *Proc. Natl. Acad. Sci. U. S. A.* **97**, 8560–8565 (2000).

86. Driver, E. R. *et al.* Evaluation of mouse model forming necrotic granulomas using C3HeB/FeJ mice, for the testing of M. tuberculosis drugs. *Antimicrob. Agents Chemother.* **56**, 3181–3195 (2012).

87. Stinear, T. P. *et al.* Insights from the complete genome sequence of Mycobacterium marinum on the evolution of Mycobacterium tuberculosis. *Genome Res.* **18**, 729–741 (2008).

88. Lewis, F. M. T., Marsh, B. J. & von Reyn, C. F. Fish Tank Exposure and Cutaneous Infections Due to Mycobacterium marinum: Tuberculin Skin Testing, Treatment, and Prevention. *Clin. Infect. Dis.* **37**, 390–397 (2003).

89. Tobin, D. M. & Ramakrishnan, L. Comparative pathogenesis of Mycobacterium marinum and Mycobacterium tuberculosis. *Cell. Microbiol.* **10**, 1027–1039 (2008).

90. Swaim, L. E. *et al.* Mycobacterium marinum infection of adult zebrafish causes caseating granulomatous tuberculosis and is moderated by adaptive immunity. *Infect. Immun.* **74**, 6108–6117 (2006).

91. Davis, J. M. *et al.* Real-time visualization of Mycobacterium-macrophage interactions leading to initiation of granuloma formation in zebrafish embryos. *Immunity* **17**, 693–702 (2002).

92. Herbomel, P. & Levraud, J.-P. Imaging early macrophage differentiation, migration, and behaviors in live zebrafish embryos. *Methods Mol. Med.* **105**, 199–214 (2005).

93. Herbomel, P., Thisse, B. & Thisse, C. Ontogeny and behaviour of early macrophages in the zebrafish embryo. *Development* **126**, 3735 LP – 3745 (1999).

94. Ellett, F., Pase, L., Hayman, J. W., Andrianopoulos, A. & Lieschke, G. J. mpeg1 promoter transgenes direct macrophage-lineage expression in zebrafish. *Blood* **117**, e49-56 (2011).

95. Renshaw, S. A. *et al.* A transgenic zebrafish model of neutrophilic inflammation. *Blood* **108**, 3976–3978 (2006).

96. Takaki, K., Davis, J. M., Winglee, K. & Ramakrishnan, L. Evaluation of the pathogenesis and treatment of Mycobacterium marinum infection in zebrafish. *Nat. Protoc.* **8**, 1114–1124 (2013).

97. Ramakrishnan, L. The zebrafish guide to tuberculosis immunity and treatment. *Cold Spring Harb. Symp. Quant. Biol.* **78**, 179–192 (2013).

98. Takaki, K., Cosma, C. L., Troll, M. A. & Ramakrishnan, L. An in vivo platform for rapid high-throughput antitubercular drug discovery. *Cell Rep.* **2**, 175–84 (2012).

99. Ordas, A. *et al.* Testing tuberculosis drug efficacy in a zebrafish high-throughput translational medicine screen. *Antimicrob. Agents Chemother.* **59**, 753–62 (2015).

100. Tobin, D. M. *et al.* The lta4h Locus Modulates Susceptibility to Mycobacterial Infection in Zebrafish and Humans. *Cell* **140**, 717–730 (2010).

101. Feldman, W. H. & Baggenstoss, A. H. The residual infectivity of the primary complex of tuberculosis. *Am. J. Pathol.* **14**, 473-490.3 (1938).

102. Volkman, H. E. *et al.* Tuberculous granuloma formation is enhanced by a Mycobacterium virulence determinant. *PLoS Biol.* **2**, e367 (2004).

103. Abdallah, A. M. *et al.* Type VII secretion — mycobacteria show the way. *Nat. Rev. Microbiol.* **5**, 883–891 (2007).

104. Volkman, H. E. *et al.* Tuberculous Granuloma Induction via Interaction of a Bacterial Secreted Protein with Host Epithelium. *Science* **327**, 466 (2010).

105. Davis, J. M. & Ramakrishnan, L. The Role of the Granuloma in Expansion and Dissemination of Early Tuberculous Infection. *Cell* **136**, 37–49 (2009).

106. Clay, H. *et al.* Dichotomous Role of the Macrophage in Early Mycobacterium marinum Infection of the Zebrafish. *Cell Host Microbe* **2**, 29–39 (2007).

107. Hashish, E. *et al.* Mycobacterium marinum infection in fish and man: epidemiology, pathophysiology and management; a review. *Vet. Q.* **38**, 35–46 (2018).

108. Carradice, D. & Lieschke, G. J. Zebrafish in hematology: sushi or science? *Blood* **111**, 3331 LP – 3342 (2008).

109. Hernández, P. P. *et al.* Single-cell transcriptional analysis reveals ILC-like cells in zebrafish. *Sci. Immunol.* **3**, eaau5265 (2018).

110. Kettleborough, R. N. W. *et al.* A systematic genome-wide analysis of zebrafish protein-coding gene function. *Nature* **496**, 494–497 (2013).

111. Wu, R. S. *et al.* A Rapid Method for Directed Gene Knockout for Screening in G0 Zebrafish. *Dev. Cell* **46**, 112-125.e4 (2018).

112. Demy, D. Lou *et al.* Generating parabiotic zebrafish embryos for cell migration and homing studies. *Nat. Methods* **10**, 256–258 (2013).

113. Nguyen-Chi, M. *et al.* TNF signaling and macrophages govern fin regeneration in zebrafish larvae. *Cell Death Dis.* **8**, e2979 (2017).

114. Burg, L. *et al.* Conditional mutagenesis by oligonucleotide-mediated integration of loxP sites in zebrafish. *PLOS Genet.* **14**, e1007754 (2018).

115. Kim, H., Kim, M., Im, S.-K. & Fang, S. Mouse Cre-LoxP system: general principles to determine tissue-specific roles of target genes. *Lab. Anim. Res.* **34**, 147 (2018).

116. Ablain, J., Durand, E. M., Yang, S., Zhou, Y. & Zon, L. I. A CRISPR/Cas9 vector system for tissue-specific gene disruption in zebrafish. *Dev. Cell* **32**, 756–764 (2015).

117. Berg, R. D. *et al.* Lysosomal Disorders Drive Susceptibility to Tuberculosis by Compromising Macrophage Migration. *Cell* **165**, 139–152 (2016).

118. Lawson, N. D. & Wolfe, S. A. Forward and Reverse Genetic Approaches for the Analysis of Vertebrate Development in the Zebrafish. *Developmental Cell* **21**, 48–64 (2011).

119. Kutscher, L. M. & Shaham, S. Forward and reverse mutagenesis in C. elegans. *WormBook : the online review of C. elegans biology* 1–26 (2014). doi:10.1895/wormbook.1.167.1

120. Golling, G. *et al.* Insertional mutagenesis in zebrafish rapidly identifies genes essential for early vertebrate development. **31**, 135 (2002).

121. Amsterdam, A. *et al.* A large-scale insertional mutagenesis screen in zebrafish. *Genes Dev.* **13**, 2713–2724 (1999).

122. Talbot, W. S. & Hopkins, N. Zebrafish mutations and functional analysis of the vertebrate genome. *Genes and Development* **14**, 755–762 (2000).

123. Schneeberger, K. Using next-generation sequencing to isolate mutant genes from forward genetic screens. *Nature Reviews Genetics* **15**, 662–676 (2014).

124. Michelmore, R. W., Paran, I. & Kesseli, R. V. Identification of markers linked to disease-resistance genes by bulked segregant analysis: A rapid method to detect markers in specific genomic regions by using segregating populations. *Proc. Natl. Acad. Sci. U. S. A.* **88**, 9828–9832 (1991).

125. Shimoda, N. *et al.* Zebrafish genetic map with 2000 microsatellite markers. *Genomics* **58**, 219–232 (1999).

126. Geisler, R. *et al.* Large-scale mapping of mutations affecting zebrafish development. *BMC Genomics* **8**, (2007).

127. Davis, M. W. & Hammarlund, M. Single-nucleotide polymorphism mapping. *Methods Mol. Biol.* **351**, 75–92 (2006).

128. Chen, D. *et al.* High-resolution, high-throughput SNP mapping in Drosophila melanogaster. *Nat. Methods* **5**, 323–329 (2008).

129. Stickney, H. L. *et al.* Rapid mapping of zebrafish mutations with SNPs and oligonucleotide microarrays. *Genome Research* **12**, 1929–1934 (2002).

130. Candela, H., Casanova-Sáez, R. & Micol, J. L. Getting started in mapping-by-sequencing. *J. Integr. Plant Biol.* **57**, 606–12 (2015).

131. Henke, K., Bowen, M. E. & Harris, M. P. Perspectives for identification of mutations in the zebrafish: Making use of next-generation sequencing technologies for forward genetic approaches. *Methods* **62**, 185–196 (2013).

132. Sohn, J.-I. & Nam, J.-W. The present and future of de novo whole-genome assembly. *Brief. Bioinform.* **19**, 23–40 (2018).

133. Ellis, T. H. N., Hofer, J. M. I., Timmerman-Vaughan, G. M., Coyne, C. J. & Hellens, R. P. Mendel, 150 years on. *Trends in Plant Science* **16**, 590–596 (2011).

134. Muller, H. J. The Production of Mutations by X-Rays. *Proc. Natl. Acad. Sci.* **14**, 714–726 (1928).

135. Beadle, G. W. & Tatum, E. L. Genetic Control of Biochemical Reactions in Neurospora. *Proc. Natl. Acad. Sci.* **27**, (1941).

136. Crick, F. H. C., Barnett, L., Brenner, S. & Watts-Tobin, R. J. General nature of the genetic code for proteins. *Nature* **192**, 1227–1232 (1961).

137. Benzer, S. BEHAVIORAL MUTANTS OF Drosophila ISOLATED BY COUNTERCURRENT DISTRIBUTION. *Proc. Natl. Acad. Sci. U. S. A.* **58**, 1112–9 (1967).

138. Brenner, S. THE GENETICS OF CAENORHABDITIS ELEGANS. *Genetics* **77**, (1974).

139. Nüsslein-Volhard, C. & Wieschaus, E. Mutations affecting segment number and polarity in Drosophila. *Nature* **287**, 795–801 (1980).

140. Bradbury, J. Small fish, big science. *PLoS Biology* **2**, (2004).

141. Nüsslein-Volhard, C. The zebrafish issue of development. *Dev.* **139**, 4099–4103 (2012).

142. Poltorak, A. *et al.* Defective LPS signaling in C3H/HeJ and C57BL/10ScCr mice: Mutations in Tlr4 gene. *Science (80-.).* **282**, 2085–2088 (1998).

143. Murdock, J. L. & Núñez, G. TLR4: The Winding Road to the Discovery of the LPS Receptor. *J. Immunol.* **197**, 2561–2562 (2016).

144. Beutler, B. Innate immunity and the new forward genetics. *Best Pract. Res. Clin. Haematol.* **29**, 379–387 (2016).

145. Altshuler, D., Daly, M. J. & Lander, E. S. Genetic mapping in human disease. *Science* **322**, 881–888 (2008).

146. Botstein, D., White, R. L., Skolnick, M. & Davis, R. W. Construction of a genetic linkage map in man using restriction fragment length polymorphisms. *American Journal of Human Genetics* **32**, 314–331 (1980).

147. Gusella, J. F. *et al.* A polymorphic DNA marker genetically linked to Huntington's disease. *Nature* **306**, 234–238 (1983).

148. Raffan, E. & Semple, R. K. Next generation sequencingimplications for clinical practice. *Br. Med. Bull.* **99**, 53–71 (2011).

149. Neehus, A.-L. *et al.* Impaired IFNγ-Signaling and Mycobacterial Clearance in IFNγR1-Deficient Human iPSC-Derived Macrophages. *Stem Cell Reports* **10**, 7–16 (2018).

150. Flynn, J. L. *et al.* An essential role for interferon gamma in resistance to Mycobacterium tuberculosis infection. *J. Exp. Med.* **178**, 2249 LP – 2254 (1993).

151. Govoni, G. & Gros, P. *Review Macrophage NRAMP1 and its role in resistance to microbial infections*.

152. Vidal, S. M., Malo, D., Vogan, K., Skamene, E. & Gros, P. Natural resistance to infection with intracellular parasites: Isolation of a candidate for Bcg. *Cell* **73**, 469–485 (1993).

153. Vidal, S. M., Malo, D., Marquis, J.-F. & Gros, P. Forward Genetic Dissection of Immunity to Infection in the Mouse. (2008). doi:10.1146/annurev.immunol.26.021607.090304

154. Bellamy, R. *et al.* Variations in the *NRAMP1* Gene and Susceptibility to Tuberculosis in West Africans. *N. Engl. J. Med.* **338**, 640–644 (1998).

155. Abel, L. *et al.* Susceptibility to Leprosy Is Linked to the Human *NRAMP1* Gene. *J. Infect. Dis.* **177**, 133–145 (1998).

156. Stienstra, Y. *et al.* Susceptibility to Buruli ulcer is associated with the SLC11A1 (NRAMP1) D543N polymorphism. *Genes Immun.* **7**, 185–189 (2006).

157. Turcotte, K. *et al.* A mutation in the Icsbp1 gene causes susceptibility to infection and a chronic myeloid leukemia-like syndrome in BXH-2 mice. *J. Exp. Med.* **201**, 881–90 (2005).

158. Shiau, C. E., Kaufman, Z., Meireles, A. M. & Talbot, W. S. Differential requirement for irf8 in formation of embryonic and adult macrophages in zebrafish. *PLoS One* **10**, (2015).

159. Marquis, J.-F., LaCourse, R., Ryan, L., North, R. J. & Gros, P. Disseminated and Rapidly Fatal Tuberculosis in Mice Bearing a Defective Allele at IFN Regulatory Factor 8. *J. Immunol.* **182**, 3008–3015 (2009).

160. Hambleton, S. *et al.* IRF8 mutations and human dendritic-cell immunodeficiency. *N. Engl. J. Med.* **365**, 127–138 (2011).

161. Tobin, D. M. *et al.* Host genotype-specific therapies can optimize the inflammatory response to mycobacterial infections. *Cell* **148**, 434–446 (2012).

162. Roca, F. J. & Ramakrishnan, L. TNF dually mediates resistance and susceptibility to mycobacteria via mitochondrial reactive oxygen species. *Cell* **153**, 521–534 (2013).

163. Roca, F. J., Whitworth, L. J., Redmond, S. & Jones, A. A. TNF Induces Pathogenic Programmed Macrophage Necrosis in Tuberculosis through a Mitochondrial-Lysosomal-Endoplasmic Reticulum Circuit. *Cell* **178**, (2019).

164. Clay, H., Volkman, H. E. & Ramakrishnan, L. Tumor Necrosis Factor Signaling Mediates Resistance to Mycobacteria by Inhibiting Bacterial Growth and Macrophage Death. *Immunity* **29**, 283–294 (2008).

165. Yates, A. D. *et al.* Ensembl 2020. *Nucleic Acids Res.* **48**, D682–D688 (2019).

166. Sun, S. *et al.* UXT is a novel and essential cofactor in the NF-κB transcriptional enhanceosome. *J. Cell Biol.* **178**, 231–244 (2007).

167. Sánchez-Morgan, N., Kirsch, K. H., Trackman, P. C. & Sonenshein, G. E. UXT Is a LOX-PP Interacting Protein That Modulates Estrogen Receptor Alpha Activity in Breast Cancer Cells. *J. Cell. Biochem.* **118**, 2347–2356 (2017).

168. Huang, Y. *et al.* UXT-V1 Facilitates the Formation of MAVS Antiviral Signalosome on Mitochondria. *J. Immunol.* **188**, 358–366 (2012).

169. Huang, Y. *et al.* UXT-V1 protects cells against TNF-induced apoptosis through modulating complex II formation. *Mol. Biol. Cell* **22**, 1389–1397 (2011).

170. Pagan, A. J. *et al.* Myeloid growth factors promote resistance to mycobacterial infection by curtailing granuloma necrosis through macrophage replenishment. *Cell Host Microbe* **18**, 15–26 (2015).

171. Clements, W. K. & Traver, D. Signalling pathways that control vertebrate haematopoietic stem cell specification. *Nature Reviews Immunology* **13**, 336–348 (2013).

172. Ferrero, G., Mahony, C. B., Traver, D., Bertrand, J. Y. & Rie Wittamer, V. Embryonic Microglia Derive from Primitive Macrophages and Are Replaced by cmyb-Dependent Definitive Microglia in Zebrafish. *CellReports* **24**, 130–141 (2018).

173. Potts, K. S. & Bowman, T. V. Modeling Myeloid Malignancies Using Zebrafish. *Front. Oncol.* **7**, 297 (2017).

174. Svahn, A. J. *et al.* Development of ramified microglia from early macrophages in the zebrafish optic tectum. *Dev. Neurobiol.* **73**, 60–71 (2013).

175. Sethurathinam, S., Singh, L. P., Panneerselvam, P., Byrne, B. & Ding, J. L. UXT plays dual opposing roles on SARM-induced apoptosis. *FEBS Lett.* **587**, 3296–3302 (2013).

176. Qi, M. *et al.* UXT, a novel MDMX-binding protein, promotes glycolysis by mitigating p53-mediated restriction of NF-κB activity. *Oncotarget* **6**, 17584–17593 (2015).

177. Vaseva, A. V. *et al.* P53 opens the mitochondrial permeability transition pore to trigger necrosis. *Cell* **149**, 1536–1548 (2012).

178. Galluzzi, L. *et al.* Molecular mechanisms of cell death: Recommendations of the Nomenclature Committee on Cell Death 2018. *Cell Death and Differentiation* **25**, 486–541 (2018).

179. Amaral, E. P. *et al.* A major role for ferroptosis in Mycobacterium tuberculosis–induced cell death and tissue necrosis. *J. Exp. Med.* **216**, 556–570 (2019).

180. Robinson, N. *et al.* Programmed necrotic cell death of macrophages: Focus on pyroptosis, necroptosis, and parthanatos. *Redox Biology* **26**, (2019).

181. Zingarelli, B., O'Connor, M., Wong, H., Salzman, A. L. & Szabó, C. Peroxynitrite-mediated DNA strand breakage activates poly-adenosine diphosphate ribosyl synthetase and causes cellular energy depletion in macrophages stimulated with bacterial lipopolysaccharide. *J. Immunol.* **156**, 350–8 (1996).

182. Feldstein, A. E., Werneburg, N. W., Li, Z., Bronk, S. F. & Gores, G. J. Bax inhibition protects against free fatty acid-induced lysosomal permeabilization. *Am. J. Physiol. - Gastrointest. Liver Physiol.* **290**, (2006).

183. Yang, C. T. *et al.* Neutrophils exert protection in the early tuberculous granuloma by oxidative killing of mycobacteria phagocytosed from infected macrophages. *Cell Host Microbe* **12**, 301–312 (2012).

184. Tsujimoto, Y. Role of Bcl-2 family proteins in apoptosis: apoptosomes or mitochondria? *Genes to Cells* **3**, 697–707 (1998).

185. McIlwain, D. R., Berger, T. & Mak, T. W. Caspase Functions in Cell Death and Disease. *Cold Spring Harb. Perspect. Biol.* **5**, (2013).

186. Walters, K. B. *et al.* Muscle degeneration and leukocyte infiltration caused by mutation of zebrafish fad24. *Dev. Dyn.* **238**, 86–99 (2009).

187. Viringipurampeer, I. A. *et al.* Rip3 knockdown rescues photoreceptor cell death in blind pde6c zebrafish. *Cell Death Differ.* **21**, 665–675 (2014).

188. Mocelin, R. *et al.* N-Acetylcysteine Reverses Anxiety and Oxidative Damage Induced by Unpredictable Chronic Stress in Zebrafish. *Mol. Neurobiol.* **56**, 1188–1195 (2019).

189. Schröer, A., Schneider, S., Ropers, H.-H. & Nothwang, H. G. Cloning and Characterization of UXT, a Novel Gene in Human Xp11, which Is Widely and Abundantly Expressed in Tumor Tissue. *Genomics* **56**, 340–343 (1999).

190. Chávez, S. & Puerto-Camacho, P. Prefoldins. *eLS* 1–8 (2016). doi:doi:10.1002/9780470015902.a0026334

191. Geissler, S., Siegers, K. & Schiebel, E. A novel protein complex promoting formation of functional α- and γ-tubulin. *EMBO J.* **17**, 952–966 (1998).

192. Vainberg, I. E. *et al.* Prefoldin, a Chaperone that Delivers Unfolded Proteins to Cytosolic Chaperonin. *Cell* **93**, 863–873 (1998).

193. Rodríguez-Milla, M. A. & Salinas, J. Prefoldins 3 and 5 Play an Essential Role in Arabidopsis Tolerance to Salt Stress. *Mol. Plant* **2**, 526–534 (2009).

194. Abe, A. *et al.* Prefoldin plays a role as a clearance factor in preventing proteasome inhibitor-induced protein aggregation. *J. Biol. Chem.* **288**, 27764–27776 (2013).

195. Siegert, R., Leroux, M. R., Scheufler, C., Hartl, F. U. & Moarefi, I. Structure of the Molecular Chaperone Prefoldin: Unique Interaction of Multiple Coiled Coil Tentacles with Unfolded Proteins. *Cell* **103**, 621–632 (2000).

196. Leroux, M. R. *et al.* MtGimC, a novel archaeal chaperone related to the eukaryotic chaperonin cofactor GimC/prefoldin. *EMBO J.* **18**, 6730–6743 (1999).

197. Martín-Benito, J. *et al.* Divergent Substrate-Binding Mechanisms Reveal an Evolutionary Specialization of Eukaryotic Prefoldin Compared to Its Archaeal Counterpart. *Structure* **15**, 101–110 (2007).

198. Djouder, N. *Prefoldins: the new chaperones*. **1106**, (Advances in Experimental Medicine and Biology 1106, 2018).

199. Martín-Benito, J. *et al.* Structure of eukaryotic prefoldin and of its complexes with unfolded actin and the cytosolic chaperonin CCT. *EMBO J.* **21**, 6377–6386 (2002).

200. Cao, S. *et al.* Subunit 1 of the Prefoldin Chaperone Complex Is Required for Lymphocyte Development and Function. *J. Immunol.* **181**, 476 LP – 484 (2008).

201. Lee, Y. *et al.* Prefoldin 5 is required for normal sensory and neuronal development in a murine model. *J. Biol. Chem.* **286**, 726–736 (2011).

202. Gstaiger, M. *et al.* Control of Nutrient-Sensitive Transcription Programs by the Unconventional Prefoldin URI. *Science (80-.).* **302**, 1208–1212 (2003).

203. Mita, P. *et al.* Analysis of URI Nuclear Interaction with RPB5 and Components of the R2TP/Prefoldin-Like Complex. *PLoS One* **8**, e63879 (2013).

204. Boulon, S. *et al.* HSP90 and its R2TP/Prefoldin-like cochaperone are involved in the cytoplasmic assembly of RNA polymerase II. *Mol. Cell* **39**, 912–924 (2010).

205. Dorjsuren, D. *et al.* RMP, a Novel RNA Polymerase II Subunit 5-Interacting Protein, Counteracts Transactivation by Hepatitis B Virus X Protein. *Mol. Cell. Biol.* **18**, 7546 LP – 7555 (1998).

206. WEI, W. *et al.* Interaction with general transcription factor IIF (TFIIF) is required for the suppression of activated transcription by RPB5-mediating protein (RMP). *Cell Res.* **13**, 111–120 (2003).

207. Hořejší, Z. *et al.* CK2 Phospho-Dependent Binding of R2TP Complex to TEL2 Is Essential for mTOR and SMG1 Stability. *Mol. Cell* **39**, 839–850 (2010).

208. Mita, P. *et al.* Regulation of androgen receptor-mediated transcription by RPB5 binding protein URI/RMP. *Mol. Cell. Biol.* **31**, 3639–52 (2011).

209. Markus, S. M. *et al.* Identification and characterization of ART-27, a novel coactivator for the androgen receptor N terminus. *Mol. Biol. Cell* **13**, 670–682 (2002).

210. McGilvray, R., Walker, M. & Bartholomew, C. UXT interacts with the transcriptional repressor protein EVI1 and suppresses cell transformation. *FEBS J.* **274**, 3960–3971 (2007).

211. Schafler, E. D. *et al.* UXT is required for spermatogenesis in mice. *PLoS One* **13**, e0195747–e0195747 (2018).

212. Zhou, Y. *et al.* UXT potentiates angiogenesis by attenuating Notch signaling. *Development* **142**, 774–786 (2015).

213. Hayden, M. S. & Ghosh, S. NF-κB, the first quarter-century: remarkable progress and outstanding questions. *Genes Dev.* **26**, 203–234 (2012).

214. Karra, R., Knecht, A. K., Kikuchi, K. & Poss, K. D. Myocardial NF-κB activation is essential for zebrafish heart regeneration. *Proc. Natl. Acad. Sci.* **112**, 13255 LP – 13260 (2015).

215. Howe, K. *et al.* The zebrafish reference genome sequence and its relationship to the human genome. *Nature* **496**, 498–503 (2013).

216. Xie, P. TRAF molecules in cell signaling and in human diseases. *J. Mol. Signal.* **8**, 7 (2013).

217. Auton, A. *et al.* A global reference for human genetic variation. *Nature* **526**, 68–74 (2015).

218. Rigby, K. M. & DeLeo, F. R. Neutrophils in innate host defense against Staphylococcus aureus infections. *Semin. Immunopathol.* **34**, 237–259 (2012).

219. Li, H. Aligning sequence reads, clone sequences and assembly contigs with BWA-MEM. (2013).

220. Hill, J. T. *et al.* MMAPPR: Mutation Mapping Analysis Pipeline for Pooled RNA-seq. *Genome Res.* **23**, 687–697 (2013).

221. McKenna, A. *et al.* The genome analysis toolkit: A MapReduce framework for analyzing next-generation DNA sequencing data. *Genome Res.* **20**, 1297–1303 (2010).

222. Semagn, K., Babu, R., Hearne, S. & Olsen, M. Single nucleotide polymorphism genotyping using Kompetitive Allele Specific PCR (KASP): Overview of the technology and its application in crop improvement. *Molecular Breeding* **33**, 1–14 (2014).

223. Kim, D. *et al.* TopHat2: accurate alignment of transcriptomes in the presence of insertions, deletions and gene fusions. *Genome Biol.* **14**, R36 (2013).

224. Love, M. I., Huber, W. & Anders, S. Moderated estimation of fold change and dispersion for RNA-seq data with DESeq2. *Genome Biol.* **15**, 550 (2014).

225. Anders, S., Pyl, P. T. & Huber, W. HTSeq-A Python framework to work with high-throughput sequencing data. *Bioinformatics* **31**, 166–169 (2015).

226. Reimand, J., Kull, M., Peterson, H., Hansen, J. & Vilo, J. G:Profiler-a web-based toolset for functional profiling of gene lists from large-scale experiments. *Nucleic Acids Res.* **35**, (2007).

227. Burger, A. *et al.* Maximizing mutagenesis with solubilized CRISPR-Cas9 ribonucleoprotein complexes. *Dev.* **143**, 2025–2037 (2016).

228. Rodriguez, J. M. *et al.* APPRIS 2017: principal isoforms for multiple gene sets. *Nucleic Acids Res.* **46**, D213–D217 (2018).

229. Kelley, L. A., Mezulis, S., Yates, C. M., Wass, M. N. & Sternberg, M. J. E. The Phyre2 web portal for protein modeling, prediction and analysis. *Nat. Protoc.* **10**, 845–858 (2015).

230. Athanasiadis, E. I. *et al.* Single-cell RNA-sequencing uncovers transcriptional states and fate decisions in haematopoiesis. *Nat. Commun.* **8**, 2045 (2017).